Sputtering of Inorganic Insulators

By R.E. Johnson
Engineering Physics, Thornton Hall,
University of Virginia, Charlottesville, VA 22903, U.S.A.
and
J. Schou
Association Euratom-Risø National Laboratory,
Physics Department, DK-4000 Roskilde, Denmark

Synopsis

Results for knock-on and electronic sputtering of inorganic insulators are summarized. Knock-on sputtering of room-temperature insulators can be treated using standard sputtering theory at low fluences. Since these materials are mostly chemical compounds, the treatment is roughly analogous to that for alloy sputtering. Whereas data are available only for one elemental room-temperature insulator, sulfur, a number of studies have been performed for low-temperature condensed gases for which nonlinear effects are observed even at low excitation densities.

The impressive development in electronic sputtering of inorganic insulators during the last decade is also described. Solid-state electronic transport and relaxation processes, which occur following the production of electronic excitations in a solid by charged particles and photons, can be studied by sputtering and luminescence measurements combined with molecular dynamics calculations. For the rare-gas solids the dynamics of exciton transport, trapping, and relaxation are reasonably well described, with the primary energizing process being a repulsive interaction of an atom within an excimer or with the lattice. Aspects of the nonradiative electronic transitions leading to electronic sputtering for solid nitrogen and oxygen are similarly understood, since the sputtering yields are linear in excitation density at low excitation densities. These yields, like those for other low-temperature condensed gases, become quadratic at higher excitation densities, consistent with the 'thermal spike' ejection. Because of the richness of possible electronic relaxation processes, there is no universal mechanism in electronic sputtering. However, for incident charged particles the efficiency of electronic sputtering of all inorganic insulators is determined both by the size of the nonradiative relaxation energy released compared to the surface binding energy and by the size of the excitation density deposited, with nonlinear dependencies on excitation density predominating.

Contents

1 Introduction

Inorganic insulators comprise a class of materials with widely differing properties. This includes highly refractory materials, some metallic oxides, as well as the most volatile materials, the frozen gases, which are solids only at very low temperatures. In addition, the electrical conductivity can differ by many orders of magnitude throughout this class of insulators, and the composition varies from simple structures of pure elements to complicated chemical compounds.

The physical processes leading to the sputtering of insulators are knock-on collisions and electronic excitations. For knock-on sputtering a comprehensive data base and a number of theoretical treatments exist for elemental metals, alloys, and refractory solids (Andersen & Bay, 1981; Sigmund, 1981; Betz & Wehner, 1983; Townsend, 1983; Kelly, 1984a,b; Lam, 1990; Falcone, 1990; Sigmund & Oliva, 1993). Therefore, to extend knock-on sputtering to inorganic insulators means

that the sputtering of multicomponent and of volatile solids must be described. The treatment of electronic sputtering is different as it is induced by incident electrons and photons as well as by ions and does not occur in metals, except, possibly, at very high excitation density when a significant density of inner shell excitations is created.

The emphasis in this article is on electronic sputtering of inorganic insulators for which the most dramatic advances have occurred over the last fifteen years, particularly for the low-temperature condensed gases. The interest in such solids was stimulated in part by the first systematic studies of sputtering of water ice by W.L. Brown, L.J. Lanzerotti and coworkers which gave unexpectedly large sputtering yields (Brown et al., 1978). These experiments were performed in response to the Voyager spacecraft observations, which showed that the icy objects in the outer solar system were exposed to energetic plasma-ion bombardment (Brown et al., 1982; Johnson, 1990).

The low-temperature condensed gases are also ideal systems for basic studies of the differences in electronic relaxation processes between gases and solids. Because the lattice binding energies vary over an order of magnitude, such solids provide a means for exploring the efficiency of processes leading to sputtering and the dependence on excitation density. Electronic sputtering of these solids is closely related to photon, electron, and ion-stimulated desorption of adsorbed species (DIET, 1983-1993). Therefore, the classical MGR-desorption mechanism (Menzel & Gomer,1964; Redhead, 1964) has often been invoked to describe the non-radiative, electronic transitions leading to sputtering.

Immediate applications of electronic sputtering are the particle release from cryopanels during bombardment by stray particles in accelerators (Benvenuti et al., 1987), and lithography by radiation-induced alterations of solids (Brown, 1984). Knock-on sputtering of insulators has been studied much less systematically than electronic sputtering, but is also of considerable interest for planetary science (Johnson, 1990). This trend contrasts with the rapid developments occurring in sputter deposition, which was the dominant production method for epitaxial thin films of metal oxides and other refractory solids up to 1990 (Harper, 1990; McClanahan & Laegreid, 1991; Geerk et al., 1989). In spite of the wide use of sputter deposition, almost no systematic data are available at present for many oxides including high T_c-superconductors.

The content of this chapter has overlap with that in a number of other chapters in this issue, particularly the chapters on desorption/sputtering of biomolecules by heavy-ion beams and laser pulses (Reimann, 1993; Håkansson, 1993) and the chapter on sputtering of alkali-halides (Szymonski, 1993). We first review the concepts behind knock-on sputtering of inorganic insulators. This includes consideration of both linear and nonlinear sputtering processes. Although this discussion

is brief, it lays the ground work for the discussion of electronically-induced sputtering and the resulting material alterations. Alterations occur because of the lack of stoichiometry in sputtering of room-temperature insulators, which are mostly chemical compounds (Betz & Wehner, 1983), and because chemical processes can be induced in such materials (Roth, 1983). We then describe sputtering in response to electronic excitations produced by fast ions, electrons, or photons, with the emphasis on ion-induced sputtering, and we include the results of relevant molecular dynamics calculations. This is followed by a brief review of the experimental methods used to study electronic sputtering. Finally, recent experimental results are presented for both knock-on and electronic sputtering of inorganic insulators.

Before proceeding we note that sputtering can be separated into three, roughly separate physical processes. First, the incident radiation produces a distributed source of momentum transfer events. An event may be a direct momentum transfer to a target atom, by an incident ion or by a nuclear fragment from a radioactive decay, or it may be momentum produced by a non-radiative relaxation process following an electronic excitation. Second, for excitations of species at some depth into the solid, the possibility of momentum transport to the surface can be described by an approximation to the Boltzmann transport equations, such as the linear collision cascade, diffusion or hydrodynamic equations. Finally, either for an excitation at the surface or for momentum transported to the surface, escape is determined by the binding of atoms and molecules to the solid.

2 Stopping Power Concepts

Since sputtering is determined by the local energy density deposited in the solid, for incident fast ions and electrons an important quantity is the stopping power dE/dx, the energy loss per unit path length. This quantity is described in reviews by Sigmund (1975a) and Ziegler et al. (1985) for ions and by Inokuti (1971) and Schou (1988) for electrons.

The total stopping power for fast ions is usually expressed as a sum of the electronic and nuclear-elastic contributions,

$$dE/dx = (dE/dx)_{\mathrm{e}} + (dE/dx)_{\mathrm{n}}.$$

The second term gives the energy deposited which is known to lead to knock-on sputtering, whereas the first term gives the contribution that in some materials can lead to electronic sputtering. Although there can be synergism between electronic and knock-on processes for ions with keV/amu energies (e.g., Matsunami, 1990; Varga et al., 1991), we ignore this here. A quantity that, to first order, is

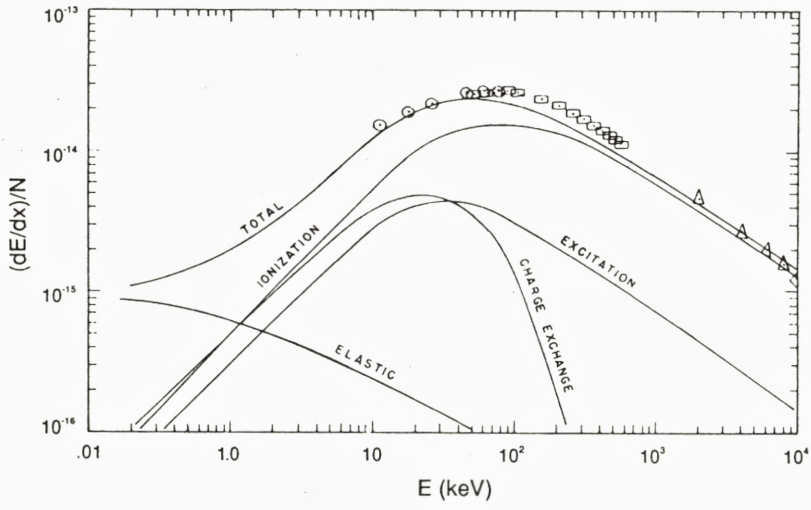

Figure 1a. Semi-empirical stopping cross sections, S, for water vapour where $dE/dx = N_{\mathrm{mol}}S$ with N_{mol} the molecular density. S is given as a sum of its constituents S_{n} (elastic or knock-on) and S_{e} (a sum of ionization, excitation and the charge exchange cycle); data points and curves from Miller and Green (1973).

independent of the material density N is also used,

$$S(E) = \frac{1}{N}\frac{dE}{dx}$$

called the stopping cross section, shown for water in fig. 1a. The yield of molecules ejected per incident ion by these two processes is also assumed to be roughly additive, as suggested by the structure of the measured sputtering yields for protons incident on low temperature solid H_2O in fig. 1b. The electronic component of the stopping power in fig. 1a. is, in turn, a sum of different excitation processes, making electronic sputtering of insulators a richer and more complex phenomenon.

In the description of measured yields, stopping powers obtained directly or extrapolated from measurements are used. Since sputtering is a surface process, it is important to remember that the value of the stopping power at the entrance surface can differ from the value measured: the average stopping power after passage through a thin sample, called the 'equilibrium charge state' stopping power. This fact has often hampered comparisons of measured yields to models. Ion beams can be prepared in a variety of charge states, but the effective charge state of the ions moving inside the material can change from that of the incident ions. This change occurs over a distance determined by the electron capture and loss cross sections

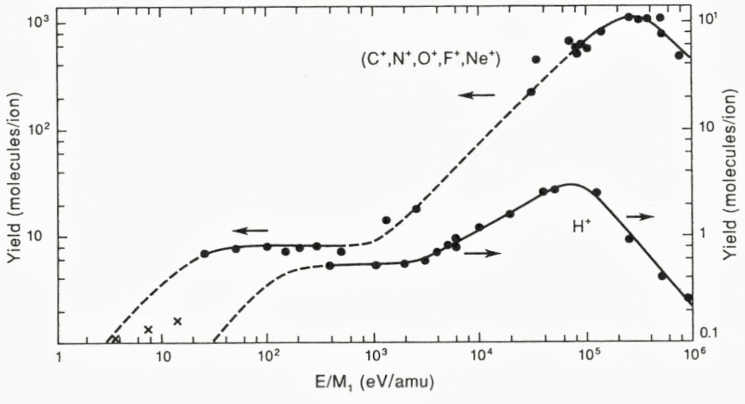

Figure 1b. The sputtering yield of water ice (< 77 K) vs. E/M_1 (ion energy/ion mass) by incident H^+ and medium mass ions (C^+, N^+, O^+, F^+, Ne^+): experimental points •, and molecular dynamics calculations, ×, from Johnson (1990).

(Allison, 1958; Maynard & Deutsch, 1987). Although the electronic sputtering yield is found to be sensitive to the incident ion charge state, few attempts have been made to use a non-equilibrium charge state stopping power for interpreting sputtering (e.g., Johnson & Brown, 1982; Nieschler et al., 1984; Wien et al., 1987). Therefore, to facilitate comparisons with theory, equilibrium charge state beams can be prepared for fast ions by having the beam first penetrate a thin carbon foil, since the equilibrium charge is expected to be roughly independent of the material penetrated. Use of molecular projectiles provides an additional control over the energy deposition near the surface (Andersen & Bay, 1974; Oliva-Florio et al., 1979; Brown et al., 1980b; Ellegaard et al., 1993a) by creating overlapping regions of excitation. Because the components of the incident molecule gradually scatter, the overlap decreases with distance into the solid, allowing a test of the effective depth for energy deposition leading to ejection.

3 Theory: Knock-on Sputtering

When an incident particle strikes a target particle in the surface or in the near surface layers of a solid, the struck particle may have sufficient momentum and the appropriate direction to overcome the binding forces. It can escape either directly or after scattering from a neighbor, as in fig. 2a. If it does not escape directly, the struck particle will collide with another target particle setting up a cascade of collisions which can transport momentum to the surface and lead to particle

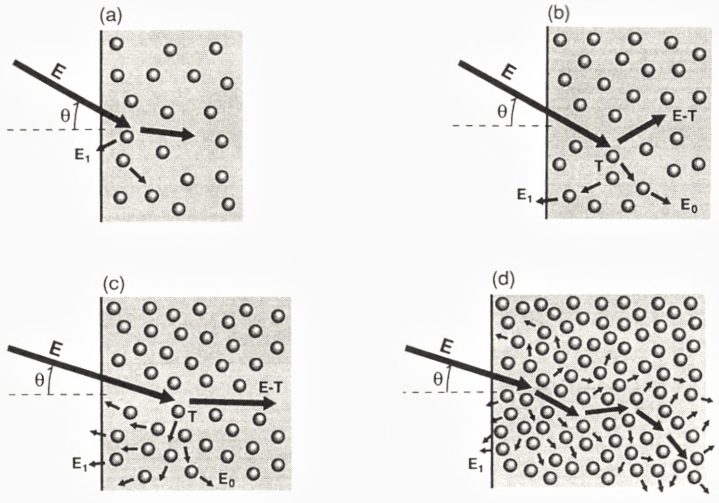

Figure 2. a) Incident ion ejects an atom from the solid in a direct knock-on; b) incident ion strikes an atom and initiates a cascade which leads to an ejected atom; c) a cascade in a volatile solid; d) a high density of cascades giving a cylindrically energized region and a nonlinear sputtering yield.

ejection.

An important aspect in sputtering is the density of atoms set in motion near the surface as indicated in figs. 2a-d. It affects both the description of the momentum transport in the solid and whether species in a molecular insulator are ejected as atoms or molecules. In addition, the cascades produced act separately when the number per unit volume is small (linear sputtering regime), as in fig. 2b or 2c, or cooperatively when the density of cascades is high (nonlinear sputtering regime) as in fig. 2d. Finally, if the energy deposited does not dissipate sufficiently fast, the ambient temperature of the target can increase, leading to beam-induced sublimation. In the following, we treat each of these contributions separately.

3.1 Single-Collision Ejection

The probability of direct ejection by a knock-on event is calculated from the collision cross section $d\sigma(\vec{p};\vec{p}_1,\vec{p}_2)$, where $\vec{p}$ is the momentum of the incident ion, with the direction generally given relative to the surface normal, and $\vec{p}_1$ and $\vec{p}_2$ are the momenta of the incident and recoiling target particle after the collision. The probability per unit path length for a collision is obtained from $Nd\sigma$, where N is the number of atoms per volume. We write $P_{\rm es}(\vec{p}_2,x)$ as the probability of a target

particle of momentum $\vec{p}_2$ to escape from a depth x where it is set in motion by the collision (Oliva et al., 1987; Sigmund et al., 1989). If the mean free path for an energetic collision, λ_c, determined from $N d\sigma$, is much greater than the average thickness of a monolayer, ℓ, then the single collision sputtering yield is calculated as a product of the probability of producing an energetic recoil and the escape probability,

$$Y^s = \int\int P_{es}(\vec{p}_2, x) \frac{N d\sigma}{\cos\theta} dx \tag{1}$$

where θ is the angle of incidence with respect to the surface normal. Y^s varies steeply with θ near $\theta = 0$, but for large θ it becomes $\sim \ell/(2\lambda_c \cos\theta)$, since ejection occurs predominantly from the surface layer, and since roughly half the directions are outward. λ_c^{-1} can be estimated by integrating $N d\sigma$ over energy transfers greater than the displacement energy of the solid. For sputtering of refractory solids at large θ, Y^s is an important or even dominant fraction of the total sputtering yield evaluated below.

3.2 Collision Cascades

In addition to direct ejection, a primary recoil set in motion below the surface can initiate a cascade of collisions which can transport momentum to the surface, as in fig. 2b (Sigmund, 1969, 1972, 1981; Kelly, 1984b). The Boltzmann transport equation for moving particles colliding with nearly stationary particles provides the energy distributions of recoils, which only weakly depend on the interaction forces (Sigmund, 1969). In a solid composed of identical atoms, the number of recoils set in motion with energy between E_0 and $E_0 + dE_0$ by a primary recoil of energy T is

$$G(T, E_0) dE_0 \approx \Gamma \frac{T}{E_0^2} dE_0 \text{ for } T \gg E_0. \tag{2}$$

When recoil energy is also lost to electronic and vibrational excitation, that amount of energy is removed from T in eq. (2). Only the quantity Γ in eq. (2) is determined by the interatomic potential, and it is of the order of unity. Calculating the angular distribution is more complicated, but in the limit $T \gg E_0$, i. e., after a number of generations of recoils, it approaches an isotropic distribution.

The probability of escape for a recoil approaching the surface is $P_{es}(\vec{p}_0, x)$, where $E_0 = p_0^2/2M$. Since the production of secondary recoils is determined by the quantity $N d\sigma$, the cascade contribution to sputtering has a form like that in eq. (1), but includes momentum transport,

$$Y^c \approx \alpha \int\int\int\int P_{es}(\vec{p}_0, x) G(T, E_0) dE_0 \frac{d\Omega}{4\pi} N d\sigma dx. \tag{3}$$

Here $d\Omega/4\pi$ comes from the assumed isotropic production of recoils, and the transport coefficient α, which corrects for this, includes the dependence on incident angle θ (Sigmund, 1969). The total yield, to which experiment is compared, is $Y = Y^{\mathrm{s}} + Y^{\mathrm{c}}$; near threshold Y^{s} dominates. For isotropically produced primary recoils, resulting from radioactive decay or electronic excitations, the transport correction is not needed and it is possible to replace $G(T, E_0)$ in eq. (3) by $G(T, E_0) + \delta(T - E_0)$, so that eqs. (1) and (3) can be combined.

The variables in eq. (3) can be separated and the integrals carried out. At energies much larger than the threshold energy for initiating sputtering (Andersen & Bay, 1981), the resulting yield is often written

$$Y = Y^{\mathrm{s}} + Y^{\mathrm{c}} \approx \Lambda_{\mathrm{c}} F_{\mathrm{D}}(E, 0). \tag{4}$$

The quantity $F_{\mathrm{D}}(E, x)$, which depends also on θ, is the distribution of recoil energy per unit depth as obtained from a Boltzmann transport equation. Because $F_{\mathrm{D}}(E, x)$ is not uniform with depth the surface value, $F_{\mathrm{D}}(E, 0)$, is used in eq. (4). This includes the source function and transport (Sigmund, 1969), whereas Λ_{c} is an ejection efficiency, which contains the averaged escape probability.

To relate the discussion above to electronically stimulated sputtering we note that, if the spatial dependence of the cascade is known, a yield, $Y(T, x)$, can be constructed for a primary recoil produced at a depth x with energy T. A sputter-weighted depth describing transport and escape for a uniform excitation density (Cui et al., 1988) can be defined[1]:

$$\overline{\Delta x}(T) = \int Y(T, x) dx. \tag{5a}$$

The total yield $(Y^{\mathrm{s}} + Y^{\mathrm{c}})$ is obtained by integrating over the primary recoil distribution $N d\sigma$,

$$Y = \int \overline{\Delta x}(T) \frac{N d\sigma}{\cos\theta} dx \approx \frac{\overline{\Delta x_{\mathrm{c}}}}{\lambda_{\mathrm{c}} \cos\theta}. \tag{5b}$$

This is equivalent to the result in eq. (4), and can be written using the mean depth $\lambda_{\mathrm{c}} \cos\theta$ between the production events of two energetic primary recoils and $\overline{\Delta x_{\mathrm{c}}}$, a sputter-weighted depth.

Sigmund (1969) approximately solved the transport equations for a steeply varying, Born-Mayer-like, interaction, giving $\Gamma \approx 6/\pi^2$ in eq. (2), and determining the dependence of α on the ion/target atom mass ratio. He treated both planar and spherical surface binding. For atomic ejection subject to planar binding of

[1] $\overline{\Delta x}(T)$, as defined by eq. (5a), may considerably exceed the maximum depth of origin of sputtered particles, i.e., the depth range over which $Y(T, x)$ is nonvanishing.

magnitude U,

$$\Lambda_c = \frac{\Gamma/4}{N\overline{\sigma}_d U} \tag{6a}$$

where $(N\overline{\sigma}_d)^{-1}$ is the effective mean-free-path for escape, and $\overline{\sigma}_d$ is the diffusion (momentum-transfer) cross section averaged over the spectrum of escape energies[2]. Since particles are predominantly ejected from the surface layer (Sigmund et al., 1989), $(N\overline{\sigma}_d)^{-1}$ is approximately the thickness of a monolayer

$$\ell = N^{-1/3}. \tag{6b}$$

Then, the quantity in eq. (4) becomes

$$\Lambda_c = \frac{\Gamma}{4}\frac{\ell}{U}. \tag{6c}$$

In addition, the sputtering yield in eq. (4) is often written using

$$F_D(E,0) = \alpha(dE/dx)_n \approx \alpha(0)\frac{NS_n}{\cos^q\theta}, \tag{7}$$

applicable at small angles, where S_n is the nuclear stopping cross section (fig. 1a) and the exponent q depends weakly on the incident ion to target atom mass ratio (Sigmund, 1969; Oliva-Florio et al., 1979). For normal incidence, Andersen & Bay (1981) have determined the quantity $\alpha\Gamma/4\overline{\sigma}_d$. Although the traditionally assumed values of Γ and $\overline{\sigma}_d$ have to be altered (Vicanek et al., 1989), the value typically used for $\alpha\Gamma/4\overline{\sigma}_d$ at normal incidence is close to that derived experimentally by Andersen & Bay.

From the recoil distribution G in eq. (2), the energy spectrum of the ejecta for planar binding can be obtained. A particle escapes when the component of energy normal to the surface is greater than that of the barrier U. This gives

$$\frac{1}{Y}\frac{dY}{dE_1} = \frac{2UE_1}{(U+E_1)^3}, \tag{8a}$$

where E_1 is the energy of the ejected particle. For spherical binding the energy of the escaping particle must be greater than U and the direction outward. This gives

$$\frac{1}{Y}\frac{dY}{dE_1} = \frac{U}{(U+E_1)^2}, \tag{8b}$$

and the yield parameter in eq. (6a) doubles in size. The quantity U typically used for comparison with data is the cohesive energy, equal to the average sublimation energy. This is appropriate for experiments in which a number of layers of material are removed. For crystalline surfaces and sub-monolayer yields, the actual surface binding energy is appropriate.

[2] $\overline{\sigma}_d = 2C_0 = \pi\lambda_0 a_{BM}^2$ in Sigmund's (1969) notation.

4 Theory: Nonlinear Effects

In the above it was assumed that a recoil always struck a nearly stationary atom and the collisions were binary. A breakdown in the latter assumption does not affect the above expressions significantly (Cui et al. 1988, 1989a,b,c). However, when the first assumption breaks down and recoils strike atoms already set in motion, nonlinear effects occur in sputtering. For instance, the energy spectrum of a primary recoil cascade is not proportional to the energy transfer, T, generating the cascade, as in eq. (2), and the energy spectrum of the ejecta will exhibit an enhancement at low energies over that in eq. (8a). Such a cascade is often referred to as a 'thermal spike', or just a 'recoil spike', as thermodynamic equilibrium is generally not attained. If these spikes are well separated spatially or in time then the calculated yield is still linear in the quantity λ_c^{-1} , as in eq. (5c): proportional to the number of energetic primary recoils set in motion per unit path length. However, when λ_c is of the order of or less than the cascade radius, as in fig. 2d, then recoils in one cascade can strike those in another (Andersen & Bay, 1974; Sigmund, 1974, 1975b). In this case, even if the ion flux is low, so the sample is not heated, the sputtering yield can vary faster than linearly with λ_c^{-1}, and a quasi-thermal equilibrium can occur (Sigmund, 1977). Whereas eq. (2) applies for the prompt recoils having large energies, the motion of the majority of the particles is generally calculated from the equations of continuum mechanics, often under the assumption that the local energy spectrum is nearly Maxwellian. Recent sputter results for volatile solids and the improvements in molecular dynamics calculations have led to increased interest in nonlinear sputtering.

4.1 Continuum Mechanics

Molecular dynamics calculations are useful for obtaining a quantitative description of the ejecta in this regime. The models described below can often approximate this. They are obtained by reducing the nonlinear Boltzmann transport equation (Sigmund, 1981) to the equations of continuum mechanics: the continuity, momentum, and energy equations, and an equation of state (e.g., Urbassek et al., 1993),

$$\frac{\partial N}{\partial t} + \nabla \cdot (N\vec{v}) = 0 \tag{9a}$$

$$\frac{\partial (N\vec{v})}{\partial t} + \nabla \cdot (N\vec{v}\vec{v}) = -\nabla P/M + \text{viscous terms}, \tag{9b}$$

$$\frac{\partial (NE)}{\partial t} + \nabla \cdot (N\vec{v}E) = -P\nabla \cdot \vec{v} + \nabla \cdot (\kappa N \nabla E). \tag{9c}$$

Here the atoms of mass M have a local average velocity, $\vec{v}$, and a distribution of velocities around the average, determined by a mean energy E. Also, $N\vec{v}$ is the local flux of material, $NM\vec{v}\vec{v}$ is the momentum flux of a local volume element, and $N\vec{v}E$ is the energy flux. The quantity $-\nabla P$ in eq. (9b) is the volume force, where P is the local pressure, and κ in eq. (9c) is the 'thermal' diffusivity. The mean energy per particle, E, in eq. (9c) is often written as the specific heat at constant volume times a temperature. The quantities E, N, and P are related by the equation of state of the material, which is complicated for a solid experiencing large temperature gradients (Zel'dovich & Raizer, 1967).

For a given excitation distribution, the starting point is the flux of escaping particles at the surface, Φ_s, the number per unit area per unit time crossing the surface after the time t from the ion impact. The yield produced by a single incident ion is calculated from an expression of the form,

$$Y = \int\int \Phi_s(\vec{\rho}, t) d^2\rho \, dt \tag{10}$$

where ρ is the radial distance from the point of penetration. In a yield calculation, two principal excitation geometries are considered: spherical, representing the case for which a gaussian-like distribution of energy has been deposited, and cylindrical, in which a track of atoms of initial root-mean-square radius $\overline{\rho}$ has been energized.

Although the linear cascade yield can also be calculated from eq. (10), here we apply it only to the nonlinear regime. Johnson et al. (1991) describe the statistics of the transition from low to high excitation density. Generally, this is ignored and the nonlinear yield is added to the linear yield as indicated in fig. 3. All of the nonlinear models exhibit a 'threshold' dependence at low values of the deposited energy density relative to the cohesive energy density, or $\ell(dE/dx)/U \approx 1$ in fig. 3 (Sigmund & Claussen, 1981; Johnson, 1987). The threshold dependence for the nonlinear contribution is not easily observed in atomic ejection by knock-on sputtering. It has been seen for molecular ejection from organic insulators (Håkansson, 1993) and for electronic sputtering of an inorganic insulator (Torrisi et al., 1988).

Unfortunately, calculating the sputter flux, Φ_s, from eqs. (9) is not straightforward, so that various approximations are used. Assuming diffuse transport gives the thermal spike model: i.e., flow is neglected, $\vec{v} = 0$ in eqs. (9), and eq. (9c) is solved for E. On the other hand, in most 'hydrodynamic' models diffuse transport is neglected, $\kappa = 0$, and $\vec{v}$ and E are computed from eqs. (9). For example, since the times for energy deposition and the evolution of cascades are short compared to acoustic transport times, a weak 'shock' may be generated, so that 'shock-wave' solutions to eqs. (9) have been applied (Yamamura, 1982).

To clarify the dE/dx dependence of the models, we write the yield in eq. (10)

in terms of the net volume V_s of material which is sputtered,

$$Y = NV_s = N\pi\rho_s^2 \overline{\Delta x}_s, \tag{11}$$

where ρ_s is the radial extent of the sputtered volume and $\overline{\Delta x}_s$ is the sputter depth (Johnson, 1987). Note the difference between the quantities, $\overline{\Delta x}_c$ in eq. (5b) and $\overline{\Delta x}_s$ in eq. (11). The former is determined by the depth from which the initially deposited energy contributes to ejection of surface species, whereas $\overline{\Delta x}_s$ above is the mean depth of the ejected volume. The dependence of ρ_s and $\overline{\Delta x}_s$ on dE/dx is given below for approximate solutions to eq. (9).

4.2 Thermal Spike Sputtering

The most frequently applied estimate of Φ_s is that obtained from the 'thermal spike' model. Φ_s in eq. (11) is assumed to depend on $\vec{\rho}$ and t only via the local energy at the surface, $E_s(\vec{\rho}, t)$: i.e.,

$$\Phi_s(\vec{\rho}, t) \rightarrow \Phi_s[E_s(\vec{\rho}, t)], \tag{12}$$

where E_s is obtained by solving eq. (9c) in the diffusion approximation ($v = 0$). Analytic forms for the yield are obtained for thermal diffusivity, $\kappa \propto E^n$ (Johnson & Evatt, 1980), assuming that molecules individually make the transition to the gas phase, by analogy with normal sublimation. This is well understood for $E_s \ll U$, however, the model is occasionally applied at high dE/dx, $E_s \gg U$, to describe situations in which flow must occur. To account for this, the surface at which Φ_s and E are described can be allowed to evolve, forming a crater, and the energy transported away by the sputter flux accounted for in eq. (9c) (Urbassek & Sigmund, 1984).

Generally, the vapor pressure–flux relationship is used for the surface flux in eq. (12),

$$\Phi_s \approx \frac{P_s(kT_s/U)}{\sqrt{2\pi MkT_s}}, \tag{13a}$$

where $c_v kT_s = E_s$, with c_v the specific heat at constant volume (dimensionless here). The effective vapor pressure is often written,

$$P_s\left(\frac{kT_s}{U}\right) \approx P_s^0 \left(\frac{kT_s}{U}\right)^m \exp\left(-\frac{U}{kT_s}\right),$$

explicitly indicating the effect of the barrier to escape, U. Using this and analytic expressions for E_s, sputtering yields are obtained [Mozumder, 1969; Vineyard, 1976; Johnson & Evatt, 1980; Sigmund & Claussen, 1981; Claussen, 1982; Sigmund

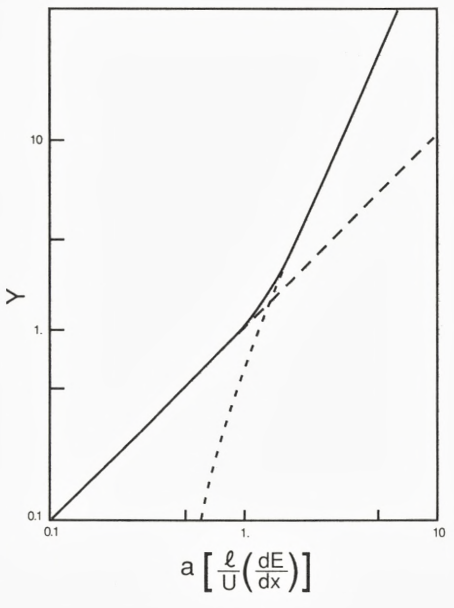

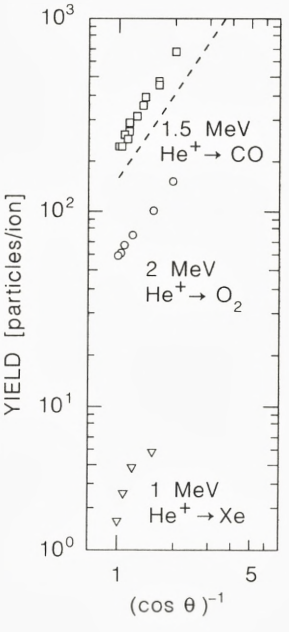

Figure 3. Schematic drawing of a yield versus scaled energy deposition: linear yield at low dE/dx and nonlinear at high dE/dx [here a quadratic yield based on cylindrical thermal spike model in eq. (14) at high dE/dx]. The parameter a is of the order of $(\ell/\overline{\rho})^2$ in this model, where $\overline{\rho}$ is the root mean square width of the cylindrical region and ℓ taken from eq. (6b).

Figure 4. The yield as a function of the reciprocal cosine of the angle of incidence, θ: (squares) Brown et al. (1984); (circles) Gibbs et al. (1988); (triangles) Ollerhead et al. (1980); (dashed-line) $(\cos\theta)^{-1.64}$ in eq. (16a).

& Szymonski, 1984]. Since sputtering is not sublimation-like and local thermal equilibrium is usually not achieved, a simpler approximation to the ejected flux is

$$\Phi_s \approx \frac{1}{4} N v_s G_s. \tag{13b}$$

Here v_s is the mean speed of surface molecules, obtained from E_s, so that $Nv_s/4$ is the flux to the surface, and G_s is a barrier function. Johnson et al. (1991) use $G_s = (1 - U/E_s)\Theta(E_s - U)$, where $\Theta(x)$ is the step function. This assumes that the molecules in the solid have a delta function distribution in energy at the mean local energy E_s.

It is found for an initially narrow cylindrical spike that the yield has the form

$$Y \approx c_s \left(\frac{\ell}{U} \frac{dE}{dx} \right)^2 g_s(\theta), \tag{14}$$

where c_s is a model-dependent constant, and the angular dependence is contained in $g_s(\theta)$ (Johnson, 1987; Johnson et al., 1991). This applies beyond the threshold region ($\ell(dE/dx)/U \gg 1$) and is obtained for Φ_s from either eq. (13a) or eq. (13b).

To clarify the dependence on dE/dx in eq. (14), we define a critical radius, $\rho_c \gg \overline{\rho}$, at which the uniformly distributed energy density equals the cohesive energy density, NU,

$$\frac{dE/dx}{\pi\rho_c^2} = NU. \tag{15}$$

First, the area $\pi\rho_c^2$ is proportional to dE/dx by eq. (15), and the area $\pi\rho_s^2$ in eq. (11) can be set equal to $\pi\rho_c^2$. Second, we assume that the sputter depth in eq. (11) can be written as the mean transport speed times the decay time of the spike, $\overline{\Delta x_s} \approx \overline{v}_s \Delta t$. For an average diffusivity $\overline{\kappa}$, the time for decay of the spike is $\Delta t \approx \pi\rho_c^2/\overline{\kappa}$. Substituting these into eq. (11), we obtain the dependence on dE/dx in eq. (14) if the ratio $\overline{v_s}/\overline{\kappa}$ is independent of the energy density. The onset of the threshold region in fig. 3 is $\overline{\rho} \approx \rho_c$.

Using a constant diffusivity, in which case the cylindrical track of energy transfer events can be treated additively, and including the truncation of the excitation region at the surface, we obtain

$$g_s(\theta) = \frac{4q}{\pi} \tan^{-1} q \text{ for } q = \cos^{-1}\theta \tag{16}$$

for $g_s(\theta)$ in eq. (14), or

$$g_s(q) \approx q^x, x = 1 + 2/\pi \text{ for } q \to 1. \tag{16a}$$

(Johnson, 1989). The approximation in eq. (16a) is in good agreement with the measured angular dependence shown in fig. 4. In addition, spike models lead to ejected particle energy distributions which peak at energies lower than and decay more rapidly at high energies than the result in eq. (5a) (Sigmund & Claussen, 1981).

When the penetration depth is comparable to the mean radial extent of the energy deposition, $\overline{\rho}$, sputtering is produced by a roughly spherical spike of total energy E. If the center of the spike is at the surface and $\overline{\rho}$ is small, so the geometry is hemispherical, then a critical radius, r_c, is obtained by spreading the energy over $(2\pi r_c^3/3)$. That is,

$$\frac{E}{2\pi r_c^3/3} = NU.$$

This gives $r_c \propto E^{1/3}$, so that $\rho_s^2 \propto E^{2/3}$ in eq. (11). Using the diffusive estimate above, $\overline{\Delta x_s} \approx \overline{v_s}\pi r_c^2/\overline{\kappa}$, one obtains the yield in eq. (11) in the form $Y \propto E^{4/3}$ (Vineyard, 1976; Johnson & Evatt, 1980; Claussen, 1982).

An incident ion with a large mean-free path for collisions may create recoil spikes which are well separated along the track of the ion, as in fig. 2c. Ellegaard et al. (1990, 1992) called these subspikes, since for a small mean-free path, λ_c, they can merge to a cylindrical spike, as in fig. 2d. As stated earlier, the yield for non-overlapping recoil spikes is linear in λ_c^{-1}, but the expression in eq. (5a) becomes $\overline{\Delta x}(T) \propto T^{5/3}$ (Johnson & Brown, 1982; Johnson et al., 1991) for spherical 'subspikes' with centers randomly distributed in depth along an ion's track. In addition, the energy spectrum of the ejecta exhibits an enhancement at low energies (Claussen, 1982), which O'Shaughnessy et al. (1988a) approximated using eq. (8b).

4.3 Hydrodynamic Sputtering

In contrast to spike models, most other models based on eqs. (9) are referred to as hydrodynamic in that they roughly account for the momentum and continuity equations, as well as the energy equation. We briefly compare these models, which are also discussed in Reimann (1993), and we assume that the same effective U applies in each model.

In 'shock' models the energy left at the surface by the passing shock wave is typically considered (Yamamura, 1982; Carter, 1983). The yield is then calculated as in the spike model, giving an effective ejection area in eq. (11), $\pi\rho_s^2 \propto dE/dx$. By scaling arguments the sputter depth, $\overline{\Delta x}_s$, is also proportional to ρ_s, so that the yield in eq. (11) varies as

$$Y \approx c_{sh} \left[\frac{\ell}{U} \frac{dE}{dx} \right]^{3/2} \tag{17}$$

written in dimensionless form (Bitensky & Parilis, 1987). Similarly, $Y \propto E^{3/2}$ for a spherically excited volume (Yamamura, 1982).

Since the flux of ejecta is a momentum transport quantity it is sensible to use eq. (9b) to describe Φ_s. The outward component of the momentum transferred to a volume element in the solid can be estimated from

$$N v_x \approx -\frac{1}{M} \int \frac{\partial P}{\partial x} dt \tag{18a}$$

where P is the local pressure in eq. (9b). This applies under the assumption that the density changes are small, even for relatively large pressure gradients (Johnson et al., 1989). At the surface this momentum can couple into particle motion. The criteria for ejection are: the x-component of the momentum transferred to a particle must exceed a critical momentum, $M v_x > p_c$, where p_c is a minimum momentum for escape, and the particles between it and the surface must also escape

(Bitensky et al., 1990). A yield is then obtained (Johnson et al., 1989) using eq. (18a) and assuming the energy is deposited in a narrow cylindrical track, the energy in the overlapping cascades is treated additively, and the diffusivity in eq. (9c) is a constant. Ignoring dissipation of energy to other processes, the sputter radius and depth are found to be proportional to dE/dx. Substituting $\rho_s \propto dE/dx$ and $\overline{\Delta x_s} \propto dE/dx$ into eq. (11), one obtains

$$Y \approx c_p \left(\frac{\ell}{U} \frac{dE}{dx} \right)^3 g_p(\theta), \tag{18b}$$

where c_p is model dependent (Fenyö & Johnson, 1992). Bitensky et al. (1990) obtained a similar expression modifying the shock model to account for the momentum flux and obtained a form for $g_p(\theta)$. The threshold region was also recently described (Fenyö, 1993).

Urbassek & Michl (1987) assumed that, in a highly energized cylindrical region produced by heavy keV ions, emptying by 'gas flow' into the vacuum along the track direction occurs much faster than radial transport. Therefore, they used a flux like that in eq. (13b) with $G_s = \Theta(E_s - U)$ (Balaji et al., 1990). They assumed that the effective sputter radius in eq. (11), ρ_s, approximately equals the average initial radius of the energized, cylindrical region, $\bar{\rho}$. They then calculated the depth of ejection, $\overline{\Delta x_s}$, as in the spike model, so that $\overline{\Delta x_s} \propto dE/dx$ for $\rho_c \gg \bar{\rho}$. This results in a slower dependence of the yield on dE/dx:

$$Y = c_g \frac{\ell}{U} \frac{dE}{dx} \left(\frac{\bar{\rho}}{\ell} \right)^2 ,$$

with c_g again a model dependent constant and where U in their model is determined by the gas condensation temperature. The effective dE/dx in their calculation was obtained by considering the shape of the recoil cascade for these incident low energy ions.

Because of the difficulties in describing both the evolution of energy and momentum and the phase transformation that occurs at the surface associated with particle ejection, molecular dynamics simulations have been performed, as will be discussed. For typical dE/dx, a 'weak shock' is usually seen propagating out of the high excitation density region, but only depositing small amounts of energy across the solid (Urbassek & Waldeer, 1991; Fenyö & Johnson, 1992). This shock may be responsible for promptly ejecting weakly attached surface species. What remains is a transiently pressured volume which produces a radial compression of the material and an outward expansion (Johnson & Sundqvist, 1992). The competition between the pressurized driven flow and the radial energy transport out of the region, determines the properties of the ejecta (Urbassek & Waldeer, 1991;

Urbassek et al., 1993). This establishes an exciting connection between sputtering and hydrodynamic processes at the atomic level.

4.4 Beam Heating

For ion sputtering a large fraction of the deposited energy goes to heat the sample. For sufficiently well conducting solids, this energy is effectively dissipated. For relatively high beam fluxes, for which the cooling is too slow, an increase in the surface temperature of the sample can occur giving rise to enhanced surface loss (Sigmund & Szymonski, 1984). In this case, a heating term is added to eq. (9c); in equilibrium this heat is dissipated by sublimation, radiative cooling, and/or conduction. If ϕ is the incident ion flux then, ignoring sublimation and radiative cooling, the heating has negligible effect on the yield if the equilibrium energy density achieved is much less than the cohesive energy density

$$\phi EL/\kappa \ll NU \tag{19a}$$

where L is the penetration depth. When there is a contribution to sputtering it is characterized by a Maxwell-Boltzmann energy distribution for escaping particles (Haring et al., 1984a),

$$dY/dE_1 \propto \frac{E_1 e^{-E_1/kT_s}}{(kT_s)^2}, \tag{19b}$$

where T_s is the target surface temperature, a function of $\phi(E)$.

4.5 Overview

The events associated with erosion of a solid by the collisional (knock-on) energy deposited can be roughly ordered in time so that the contributions to the yield are treated additively (Sigmund, 1977; Kelly, 1979; Sigmund & Szymonski, 1984). Direct ejection is followed by a collision cascade in which fast particles collide with much slower particles resulting in an E_1^{-2} component to the high energy part of the energy spectrum. Subsequently, particles with similar speeds begin to collide, either in an individual cascade or in overlapping cascades. This can contribute an enhanced low energy component to the sputter ejecta. The yield and energy spectrum for this contribution are partially explained by elastic-collision spike models. Finally, an increase in the ambient temperature can produce sublimation (a late effect) which is characterized by a Maxwell-Boltzmann energy distribution. As the cascade energy degrades in a molecular solid, molecules may dominate the ejecta and, eventually, chemical effects can occur, also a late effect. We consider the latter after discussing electronically stimulated sputtering.

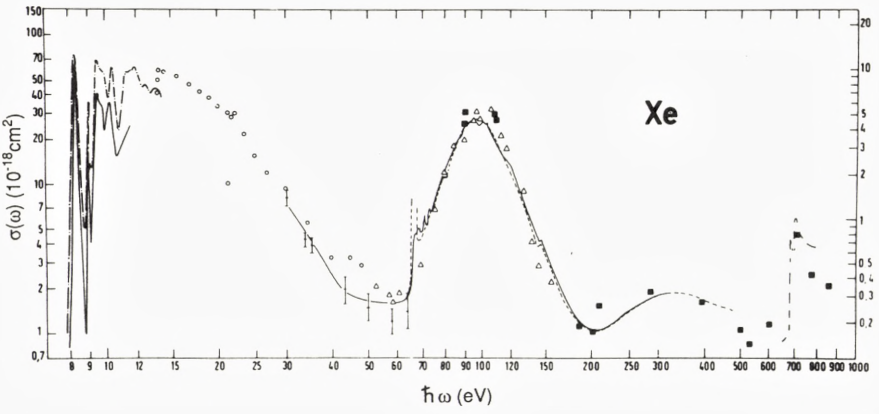

Figure 5. Absorption cross section for solid Xe versus $\hbar\omega$, photon energy. Dashed lines and symbols are for absorption in a gas; solid lines only are solid state absorption determined by reflectance. From Sonntag (1977).

5 Theory: Electronic Sputtering

The electronic energy deposited by a fast ion has also been shown to lead to sputtering. This process is closely related to photon and electron-stimulated desorption. However, that subject usually implies ejection of adsorbed species primarily as ions, whereas a description of the dominant neutral ejecta is emphasized here for bulk species. Electronic sputtering was first studied extensively for the alkali halides (Townsend, 1983; Szymonski, 1993). A parallel development for more refractory materials was stimulated by Haff (1976). He pointed out that the electronic relaxation processes, which produce tracks in dielectrics, could also produce sputtering.

Whereas the principal problems in knock-on sputtering are the description of momentum transport and escape, electronic sputtering is a more complex phenomenon, requiring also an understanding of the conversion of electronic energy into atomic motion. The incentive for understanding this is high, however, as electronically-induced ejection provides one of the few measures of the non-radiative relaxation processes occurring in solids. The unraveling of the sputtering process is complicated by the fact that, in addition to any nonlinearities in transport and ejection discussed above, the energy conversion processes themselves can change with excitation density.

In order to characterize electronic sputtering and to identify the linear and nonlinear regimes, we use the mean depth for producing an excitation, λ_e. The deposition of electronic energy is determined by the absorption spectrum of the

material $\sigma_{\rm abs}(\omega)$, given in fig. 5 for gaseous and solid xenon, and the frequency spectrum of the exciting radiation. Therefore, for absorption of an incident photon of energy $\hbar\omega$ to a sputtering precursor state,

$$\lambda_{\rm e}^{-1} = N\sigma_{\rm abs}(\omega). \tag{20a}$$

A charged particle, on the other hand, produces a track of ionizations and excitations along its path through the solid. Therefore, $\lambda_{\rm e}$ is often estimated from the electronic stopping power, fig. 1a,

$$\lambda_{\rm e}^{-1} \propto f_{\rm e}(dE/dx)_{\rm e}, \tag{20b}$$

where $f_{\rm e}$ is the fraction of the electronic energy converted into atomic motion which can lead to sputtering. The physics of transport and escape then leads to expressions for the yield like those for knock-on sputtering. That is, one replaces $(dE/dx)_{\rm n}$ or $\lambda_{\rm c}$ by $f_{\rm e}(dE/dx)_{\rm e}$ or $\lambda_{\rm e}$, respectively, in the yield expressions above. For instance, when sputtering occurs in response to individual excitations which are uniformly distributed in depth, one can write

$$Y = \frac{\overline{\Delta x_{\rm e}}}{\lambda_{\rm e}} = \Lambda_{\rm e}\left(\frac{dE}{dx}\right)_{\rm e} \tag{20c}$$

as in eqs. (5b) and (4). Similarly, the quantity $\ell f_{\rm e}(dE/dx)_{\rm e}/U$ would be used in eqs. (14), (17), and (18b).

5.1 Electronic Energy Deposition

For a fast charged particle, electronic excitations are produced in two ways. The incident particle makes a close collision with an electron in a binary encounter, transferring sufficient kinetic energy to cause ionization, or a fast charged particle passing some distance from an atom produces a time varying field. The frequency components of this field can be absorbed according to $\sigma_{\rm abs}(\omega)$, producing dipole excitations and ionizations.

For fast ions or electrons with $v \gg v_0$, where v_0 is the Bohr velocity, dipole excitations dominate, but the close collision component produces more energetic ionizations and, consequently, ionization cascades. The weighted spectrum of energy deposition is similar to $\hbar\omega\sigma_{\rm abs}(\omega)$ in fig. 5. Peaks are seen for inner shell excitations and ionization is the dominant energy deposition process for fast ions or electrons. The amount of energy exceeding the ionization energy for a shell (or band gap energy in a solid) goes into secondary electron kinetic energy. From the spectrum in fig. 5 the distribution of secondary electron energies is seen to be broad and extends to very high energies.

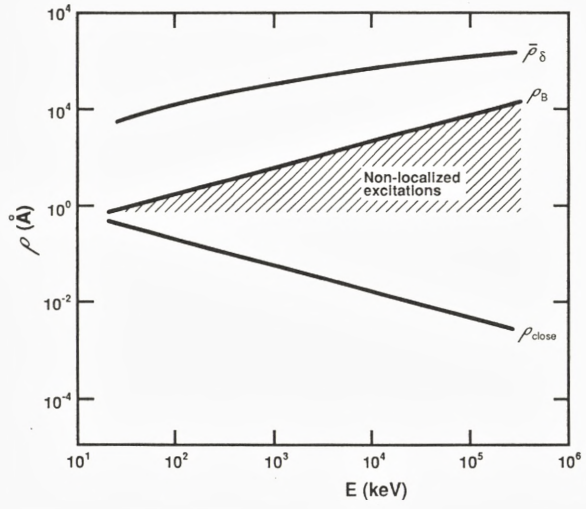

Figure 6a. The 'track' structure for a fast light ion: $\bar{\rho}_\delta$ is the average distance for secondary electron ejection perpendicular to a track, ρ_B is the Bohr adiabatic radius, ρ_{close} is the distance of closest approach in a head-on collision with an electron. Brandt & Ritchie (1974).

5.1.1 Primary Excitation

Useful quantities are the number of primary ionizations per unit path length, dJ/dx, and the electronic energy lost per unit path length $(dE/dx)_e$ in fig. 1a. For a bare ion of charge $Z_1 e$ and speed $v \gg v_0$, where v_0 corresponds to the average velocity of the electrons in the outer orbitals, incident on a target having Z_2 electrons per atom (Inokuti, 1971),

$$\frac{1}{N}\frac{dJ}{dx} = \int_{\hbar\omega > I} \sigma(v,\omega) d\omega \approx 4\pi \frac{(Z_1 e^2)^2}{m_e v^2} \frac{2m_e \overline{z^2}}{\hbar^2} \ln \frac{2m_e v^2}{I''} \qquad (21a)$$

$$\frac{1}{N}\left(\frac{dE}{dx}\right)_e = \int \hbar\omega \sigma(v,\omega) d\omega \approx 4\pi \frac{(Z_1 e^2)^2}{m_e v^2} Z_2 \ln \frac{2m_e v^2}{I'}. \qquad (21b)$$

In eq. (21a), $\sigma(v,\omega)$ is a cross section differential in ω, and $\overline{z^2}$ a ground state matrix element giving the extent of the electron cloud. The integration in eq. (21a) is over all ionizations, whereas the integration in eq. (21b) is over all excitations and is weighted by the energy of excitation $\hbar\omega$. The expressions on the right of eqs. (21) are the Bethe-Bohr expressions for fast ions, where I' and I'' are averaged 'ionization' energies determined from the energy absorption spectrum. Whereas the quantity dJ/dx is dominated by dipole excitations, the close collision contribution

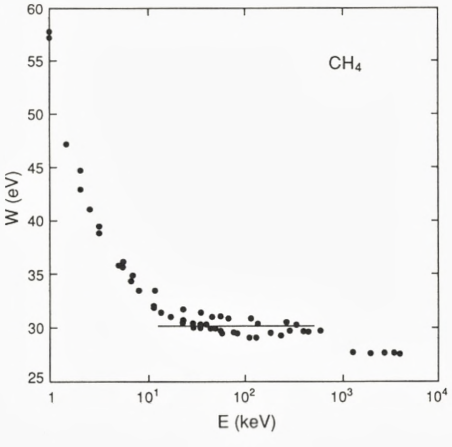

Figure 6b. W-value versus E for protons on gas phase CH_4: horizontal line is the ICRU value (30.5 $\pm$ 1.0 eV); points: data from Srdoč et al. (1993).

to $(dE/dx)_e$ is comparable to the dipole contribution because of the larger $\hbar\omega$ (e.g Lindhard & Winter, 1964; Fano, 1963). For fast ions these two contributions to $(dE/dx)_e$ have roughly the same dependence on v, a result of the Coulomb interaction between a bare ion and an electron.

The similarity in the energy dependence of the two expressions in eqs. (21a) and (21b) at large v leads to the useful result that their ratio, $(dE/dx)_e/(dJ/dx)$, is slowly varying in energy for fast particles with $v \gg v_0$. This ratio is the average energy expended per ionization produced by the incident particle, which for 1 MeV H^+ on a number of materials is $\sim$ 60 eV, increasing slowly with increasing v.

In a condensed material the same description applies but the absorption spectrum $\sigma_{abs}(\omega)$ changes. The principal change is for the outer shell electrons and is, therefore, small for the weakly bound rare-gas solids, as seen in fig. 5. When the electron clouds from neighbors overlap significantly either in the initial or final state, then the spectrum shifts and collective effects occur. In metals, the conduction band is formed and the absorption is dominated by a broad plasma-like state associated with the classical plasma frequency, $\omega_p = (4\pi e^2 N_e/m_e)^{1/2}$, where N_e is the density of free electrons in the conduction band.

5.1.2 Secondary Electrons

Those energetic electrons which are not produced by inner shell decay are forward directed and travel some average distance from the ion track, which we write as $\overline{\rho}_\delta$. The subscript comes from the often-used term delta-rays for energetic secondary

Table I

SOLIDIFIED GASES							
Species	Sublimation energy, U (meV/part.)	Ionization energy I (eV)	Density, molecule or atom (10^{22}/cm^3)	W (eV)	Bulk yield for incident 2keV e^-	6keV H_2^+	1MeV He^+
Ne	19.6	21.56	4.54	39.3	28	107	
Ar	80	15.76	2.67	26.6	2.7	26	48[b]
Kr	116	14.00	2.22	23.0		15	
Xe	164	12.13	1.73	20.5			8.1[e]
D_2	12.65	15.46	3.03	36.5[a]		209[j]	
N_2	78	15.6	2.21	37.0	1.1	12.6	32[i]
O_2	90	12.2	2.28	32.5	2.4	37	140[c]
CO	88	14.0	2.2	34.5	1.7[g]	36[f]	300[h]
H_2O	532	12.6	3.3	30.0			10[d]

W, gas phase values for fast protons; I, gas phase. a) electron value. b) Reimann et al. (1988). c) Johnson et al. (1991). d) Bøttiger et al. (1980). e) Ollerhead et al. (1980). f) Schou (unpubl.). g) Schou et al. (1985). h) Chrisey et al. (1990). i) Rook et al. (1985). j) Stenum et al. (1990). All other yields for electron and hydrogen ion bombardment from Schou (1991).

electrons. This distance is compared in fig. 6a to the maximum distance for dipole excitations, the Bohr adiabatic radius, a dynamic screening length, $\rho_B \approx v/\overline{\omega}$, where $\hbar\overline{\omega} \approx I'$ in eq. (21b) is the mean energy of the outer shell electrons. For a close collision with an electron at a target atom, a binary collision distance is shown in fig. 6a. These lengths are used to define the structure of the ionization track; the inner (infra-)track, $\rho < \rho_B$, and the outer (ultra-)track, $\rho_B < \rho < \overline{\rho}_\delta$. Because energetic secondary electrons produced near the surface can be scattered and ejected, aspects of the energy spectrum in the solid can be studied (Baragiola, 1993a). These electrons typically deposit their energy over distances $\sim$ 10-20Å, with the tail of the distribution extending to $\overline{\rho}_\delta$ (Dubus et al., 1987). The most energetic electrons efficiently produce additional ionization and excitations. In this decay process resonant excitations may produce important differences between solids (Inokuti, 1991). Measurements in the gas phase and calculations both indicate that the distribution in excitation density decays beyond the Bohr radius, ρ_B, as $\sim \rho^{-2}$ out to the radius determined by the maximum energy transfer to the electrons, $\overline{\rho}_\delta$.

The often-used quantity W is defined as the average energy expended per ionization or electron-hole pair produced by an ion or an electron stopping in a material (Table I): W is equal to the incident ion energy, E, divided by the number of ion-

electron pairs produced (ICRU, 1979). Because W is only slowly varying with v at $v \gg v_0$, the value in a given depth is approximately equal to W, except close to the surface. Therefore, the mean depth between two ionization events in eq. (20b) is

$$\lambda_e^{-1} \approx (dE/dx)_e/W. \tag{21c}$$

The value of W is about half $(dE/dx)_e/(dJ/dx)$ at high velocities, implying that for every primary ionization an additional ionization is produced (Paretzke et al., 1986). On the other hand, W increases with decreasing energy at low energies, fig. 6b, approaching the average energy per primary ionization after nuclear energy loss is accounted for. Because excitations below the ionization threshold become more important at low ion energies, W may not be the appropriate quantity to use in an estimate of λ_e from $(dE/dx)_e$ at all energies, as suggested by fig. 1a. In addition, at high velocities, secondary electron transport lowers the effective $(dE/dx)_e$ (i.e., the density of deposited energy) at the surface (Schou, 1980; Johnson et al. 1991). These differences, combined with the change in the radial distribution indicated in fig. 6a, can cause a difference in the sputtering yield measured above and below the maximum in $(dE/dx)_e$, referred to later as two branches.

W has three contributions for fast incident ions or electrons (Platzman, 1961): the fraction of the net energy deposited in the formation of electron-hole pairs, the fraction deposited in excitation, and that fraction of the secondary electron energy transfered to the lattice. The fraction of energy deposited in electron-hole pairs is (I/W) where I is the ionization energy. For an atomic material most of the energy is in electron-hole pair recombination energy ($\sim$ 65% for Ar), whereas in a molecular material it becomes $\sim$ 40% of the total, as low energy excitations are efficiently produced. Therefore, W/I is smaller for atomic ($\sim$1.5) than molecular gases ($\sim$ 2.5), Table I. Although results are sparse, W is roughly proportional to the band gap energy for a solid. In the solid state both holes and excited states (excitons) are produced by a fast incident ion. The secondary electrons produced for the most part remain in the solid, and therefore each hole has, on the average, an associated electron. Since most sputtering experiments are not able to distinguish between excitons and electron-hole pairs, we use the word exciton in the following discussion unless we are specifically referring to the behavior of holes.

5.2 Electronic Energy Conversion

Below the electronic excitation threshold, the secondary electrons can heat the lattice or cause vibrational excitations in a molecular solid. The energy so expended is of the order of 10-30% of the initial energy deposited for fast, light ions with energies above the maximum in the electronic stopping power, depending on the material. This can lead to sputtering only at very high excitation densities

Table II

Electronic Relaxation Processes		
1	$A^+ + B + M \rightarrow AB^+ + M + \Delta E$	Ion-molecule reaction
2	$A^* + B + M \rightarrow (AB)^* + \Delta E + M$	Dimerization
3	$AB^+ + e \rightarrow (AB)^* + \Delta E$	Recombination
4	$(AB)^* \rightarrow A + B + \Delta E$	Repulsive Decay
5	$A^* + \text{lattice} \rightarrow A^* + \text{lattice} + \Delta E$	Lattice Relaxation
6	$AB(v) + M \rightarrow AB(v') + M + \Delta E$	Vibrational Relaxation
7	$A^+ + B^+ \rightarrow A^+ + B^+ + \Delta E$	Coulomb Repulsion
8	$A^{++} + B \rightarrow A^+ + B^+ + \Delta E$	Charge Exchange
9	$A^+ + e + e \rightarrow A^* + e\ (\text{hot})$	Dielectronic Recombination
10	$A^{**} + e \rightarrow A^* + e\ (\text{hot})$	Collisional Deexcitation
11	$A^* + A^* \rightarrow A^* + A^+ + e\ (\text{hot})$	Excited State Fusion
12	$A + A(v) \rightarrow A + A(v') + \Delta E$	Vibrational Quenching

(Williams & Sundqvist, 1987; Ritchie & Claussen, 1982), as it occurs in small energy increments, vibrations and phonons. A large fraction of the electronic energy is tied up as electron-hole pairs or excitons, involving larger increments of energy in large band-gap materials. The relaxation (decay) of these states is discussed below following concepts outlined earlier (Johnson & Brown, 1982).

Two classes of relaxation processes are described. At low excitation density, the excitonic regime, the effects are primarily due to individual exciton decay processes. In certain frozen gases, processes analogous to gas-phase processes, not surprisingly, determine the creation of atomic or molecular motion, Table II. At high excitation density, processes (7-12) in Table II are enhanced in the track core. The latter involve multiple excitations or ionizations: pairs of electrons, holes or excitons. In addition, cooperative processes occur. This is the track regime, to be discussed later. Initially, only certain special decay routes were thought to lead to damage and sputtering. However, almost all contributions to the relaxation process lead to an effect at sufficiently high excitation density in some material (Johnson, 1993).

5.2.1 Low Excitation Density

It is seen from the excitation spectrum in fig. 5 that outer shell and inner shell excitations are produced. In both the gas and solid phase the inner shell excitations typically relax by an Auger transition, $(A^+)^* \rightarrow A^{++} + e$, in less than 10^{-13} sec, leading to a multiply ionized species and an additional, energetic secondary electron (Baragiola, 1993a, 1993b). Such processes in condensed matter are evident in the secondary electron spectrum, and can result in the transfer of an electron to a

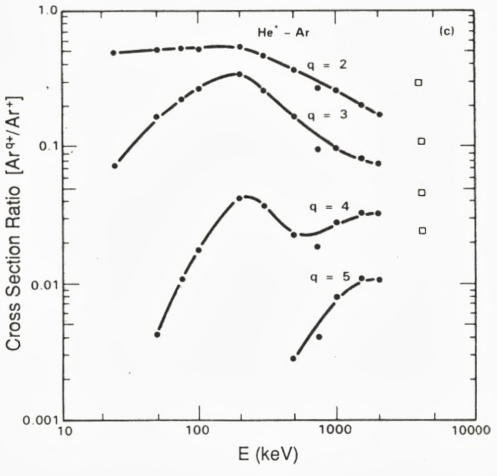

Figure 7. Ionization cross sections for gas phase Ar by He^+ vs. E: total ionization produced in multiply-ionizing processes divided by single ionization cross section

neighbor ($\sim 10^{-14}$ sec), $A^{++} + A \rightarrow A^+ + A^+$, producing two closely spaced holes. This also occurs via inner shell electron transfer from a neighbor (Knotek & Feibelman, 1978). The Coulomb repulsion of trapped, neighboring holes has been suggested to account for a number of phenomena observed in defect and track formation in dielectrics, as well as in electronic sputtering (e.g., Itoh et al., 1985).

Multiple ionization occurs also by the excitation of shallow core holes (2s electron in oxygen), shake-off, capture plus ionization, etc. (Rudd et al., 1992). These processes can have surprisingly large cross sections below the peak in the stopping cross section, as indicated for argon in fig. 7. By the above processes, low energy electrons dominate the secondary electron spectrum and excitations exceeding the band gap eventually relax to electron-hole pairs at the band gap. Because the electrons are much more mobile than the holes, the mobility of the holes controls the density of events in this regime.

For a hole at the band gap, relaxation occurs by photon emission or by a nonradiative process. In the gas phase, dissociative recombination (3 and 4 in Table II) is a dominant recombination and heating route. In a van der Waals bonded molecular solid this also occurs. A relaxation scheme for solid argon, based on the gas phase (Johnson and Inokuti, 1983) is shown in fig. 8 in terms of the pair potentials between an ion, Ar^+, or an excited argon, Ar^*, and a neighbor. A hole combines with a neighbor to form a vibrationally excited Ar_2^+. While relaxing vibrationally, this dimer can recombine with a cool electron into an electronic state

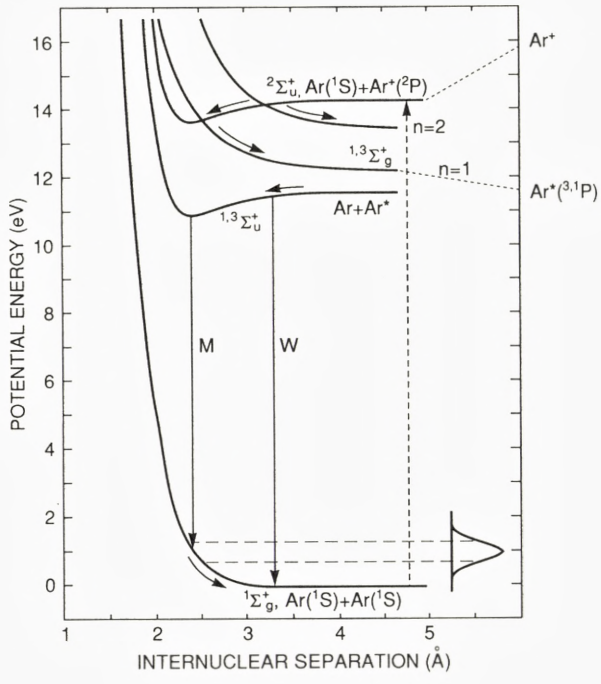

Figure 8. Potentials for Ar-pairs in solid Ar. The excited state, Ar* $n = 1$, which leads to the $[(3p)^5\ 4s)]$ state is indicated. This splits into singlet and triplet states. There is, of course, an ensemble of repulsive and attractive states associated with higher states indicated, e. g. n=2, and these are both Σ and Π states. The luminescence bands M and W are indicated. The W band is an ejected dimer (Reimann et al., 1988). Vertical dashed line indicates excitation to a hole state. Other dashed line indicates transition to gas phase on ejection. The solid arrows indicate a relaxation pathway (i.e., vibrational relaxation followed by dissociative recombination and repulsive decay).

with a repulsive interaction, causing the two argon atoms to separate energetically,

$$Ar_2^+ + e \rightarrow Ar + Ar^* + \Delta E, \quad \Delta E \approx 1eV. \tag{21c}$$

If occurring at the surface, an excited Ar may be ejected as the sublimation energy is only 0.08 eV. If the excited species is not ejected, it also can react with a neighbor forming an excimer. Since this potential energy curve does not 'cross' the ground state energy, the excimer decays by emission of a photon. Since this takes $> 10^{-9}$ sec, the excimer typically relaxes to a low vibrational state prior to photon emission, except in solid neon for which the vibrational-lattice interaction is extremely weak. Emission from the relaxed state gives the M-band luminescence indicated in fig. 8,

while unrelaxed, ejected dimers account for the W-band also indicated. Because the internuclear separation in the relaxed excimers is much smaller than that for two ground state neighbors, repulsive potential energy is again released (Reimann et al., 1988),

$$Ar_2^* \rightarrow Ar + Ar + \hbar\omega + \Delta E, \quad \Delta E \approx 1eV.$$

Repulsive decay of internal states of molecules or between excited dimers can be an important source of kinetic energy in excited insulators (Børgesen et al., 1982).

5.2.2 Exciton/Hole Dynamics

It has been pointed out often that electrons in the conduction band of a dielectric usually are mobile with a high diffusivity ($\sim$ 1000 cm^2/sec). The holes can also be mobile but much less so ($\sim$1 cm^2/sec) (Schwentner et al., 1985; Brown, 1993). Therefore, it may at first seem puzzling that electronic sputtering can occur, since the electrons and holes rapidly 'neutralize'. In a metal, neutralization is equivalent to recombination, whereas in a dielectric or a semi-conductor recombination can lead to release of the band-gap energy either radiatively or non-radiatively. Therefore, the band gap energy may be available for sputtering (Brown, 1984). The competition between hole diffusivity and the electron cooling rate (Johnson & Inokuti, 1983) determines the dilution of the energy density in the 'track' at the time of recombination and sputter ejection, affecting the efficacy of events (7-12) in Table II.

In a crystalline material the mobile holes and free excitons are waves distributed over many lattice sites. However, it is useful in the following to think of holes and excitons as localized entities which hop between the atomic or molecular constituents. This is the Frenkel picture of holes and excitons: electron exchange can occur between a hole and a neighbor

$$Ar^+ + Ar \rightarrow Ar + Ar^+$$

resulting in transport. For a typical spacing in solid argon ($\sim$ 3.4 Å), overlap integrals (Johnson, 1970) give a time for exchange with each neighbor ($\tau_{ex} \approx 10^{-14}$ sec) leading to a hole diffusivity of $\sim$ 1 cm^2/sec. For the larger atoms, Kr and Xe, the hopping times are shorter (Fugol', 1988) because of larger electron overlap. On the other hand, for the $n = 1$ state in solid argon (fig. 8) the exchange time is longer ($\sim 10^{-13}$ sec), since two electrons are involved, leading to a lower exciton diffusivity $\sim$ 0.1cm^2/sec (Schwentner et al., 1985; Tarrio & Schnatterly, 1992).

Such holes or excitons can diffuse until they trap at a defect, grain boundary, or a surface. In a carefully prepared, large, and very good crystal they may diffuse long enough to emit a photon (free exciton emission) or until a random lattice

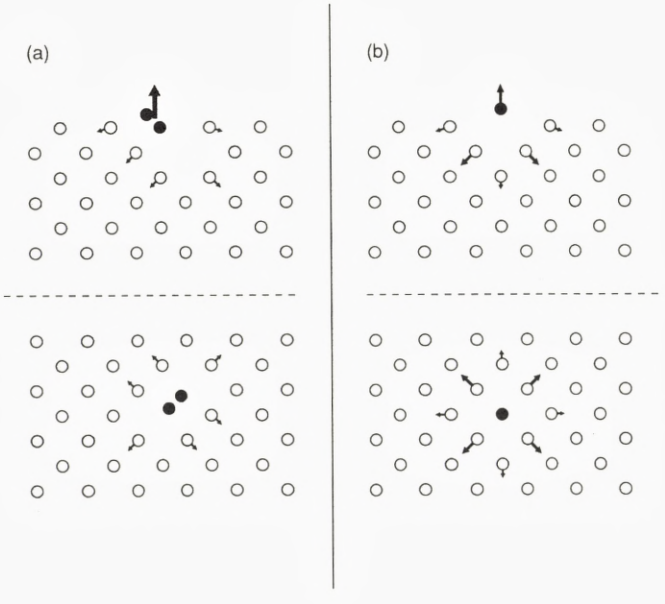

Figure 9. a) Trapped dimer (e.g. Ar_2^* in fig. 8) in bulk: leads to M-band emission in fig. 8; at surface: leads to ejection in Ne and Ar, in a vibrationally excited state; W-band in fig. 8. b) Trapped atomic exciton in bulk. At the surface it ejects an Ar (see fig. 8). In Ne it has sufficient energy to eject a number of atoms.

disturbance leads to self-trapping: the lattice distorts localizing the hole. For solid xenon a shift in the principal luminescence feature between excitons trapped at intrinsic defects and self-trapped excitons is observed (Varding et al., 1993). All trapped species formed diffuse much more slowly ($\ll 0.1 cm^2/sec$).

In atomic rare-gas solids such effects are well studied and trapping occurs to two principal end states, which are indicated schematically in fig. 9. Either the lattice distorts symmetrically forming an atomic, trapped exciton, which is dominant for solid neon, or the excited species interact strongly with a particular neighbor forming a molecular, trapped exciton (an excimer), dominant for typical laboratory samples of argon, krypton, and xenon (Schwentner et al., 1985; Zimmerer, 1987). The latter is indicated in the potential energy diagram in fig. 8. This dimerization process occurs in all the dielectrics of interest and is seen clearly by the M-band luminescence, fig. 8. Although these are typical end states, cluster-like states may occur: Ar_n^+ , for a highly damaged lattice or surface (Baba et al., 1991).

Assuming that 'recombination' awaits the trapping process, and ignoring the net field in an ion track, one may roughly describe excitation transport by a field

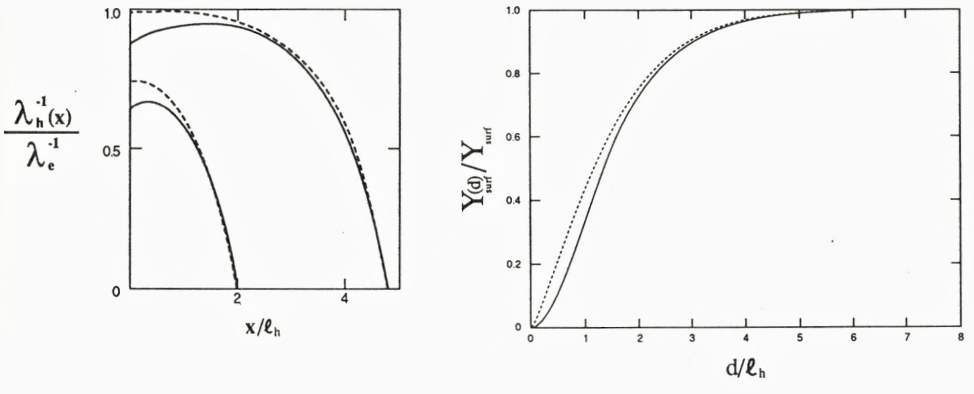

Figure 10. a) The distribution , eq. (24), of trapped excitons versus depth for two sample depths, $d = 2\ell_h$ and $5\ell_h$ and for $\Delta = 0$, dashed curves, and $\Delta = 0.1$, full curves: $\Delta = \tau_h \ell / \tau_h^s \ell_h$. For latter the increase in surface trapped species not shown. (See also, Reimann et al., 1988). b) The change in the surface layer contribution to the yield (including enhanced trapping) for $\Delta = 0.1$ and 10. The lack of sensitivity of shape to enhanced trapping allows extraction of ℓ_h from experiment.

free diffusion equation. For mobile holes with local density, N_h,

$$\frac{\partial N_\mathrm{h}}{\partial t} = D_\mathrm{h} \nabla^2 N_\mathrm{h} - \frac{1}{\tau_\mathrm{h}} N_\mathrm{h} - k_\mathrm{hh} N_\mathrm{h}^2 - k_i N_\mathrm{h}. \tag{22a}$$

Here D_h is the hole diffusivity, τ_h^{-1} is a trapping rate, k_hh describes the hole-hole interaction, and k_i represents quenching by impurities (Reimann et al., 1988). The effect of the free electrons from the background on hole transport can be roughly included in D_h, τ_h and k_hh.

Ignoring the surface effects discussed, the initial condition for a fast incident ion is approximated as a narrow cylindrical track

$$\lambda_\mathrm{e}^{-1} \frac{\exp(-\rho^2/\bar{\rho}^2)}{\pi \bar{\rho}^2}$$

with $\lambda_\mathrm{e}^{-1} \approx (dE/dx)_\mathrm{e}/W$. Under the assumption of a constant diffusivity, the holes are non-interacting ($k_\mathrm{hh} = 0$), a reflecting surface, and a solid without impurities ($k_i = 0$), the distribution of trapped holes becomes

$$N_\mathrm{h}(t \to \infty, \rho) = \lambda_\mathrm{e}^{-1} \frac{\exp(-\rho^2/\ell_\mathrm{h}^2)}{\pi \ell_\mathrm{h}^2} \tag{22b}$$

for $0 \ll x \ll d$, where d is the sample thickness, and ℓ_h is the average diffusion length: $\ell_\mathrm{h} = (D_\mathrm{h} \tau_\mathrm{h})^{1/2}$. For enhanced trapping at the vacuum interface, a term

of the form, - $(\ell/\tau_h^s)\delta(x)N_h$, can be added or appropriate boundary conditions be given (Reimann et al., 1984b, 1988). Here, the layer thickness is $\sim \ell$, eq. (6b), and $(\tau_h^s)^{-1}$ is the increase in the surface trapping rate (Reimann et al., 1988). The quantity ℓ/τ_h^s is called the recombination velocity as it gives the recombination rate at a surface. For a sample thickness $d \gg \ell_h$, the enhancement in the number of the excitons trapped in the surface layer is given by the multiplicative factor

$$R_s = \frac{1 + \Delta(\ell_h/\ell)}{1 + \Delta},$$

$$\Delta \equiv \tau_h \ell / \tau_h^s \ell_h. \tag{23}$$

Here the first part, $1/(1 + \Delta)$, accounts for the reduction of species in the layer due to diffusion (see fig. 10a), and the second part gives the increase due to surface trapping (Boring et al., 1989)[3].

Surface trapping can occur also at the substrate. For a perfectly quenching substrate (recombination velocity infinite at $x = d$) and for a vacuum interface which does not trap preferentially (recombination velocity zero at $x = 0$) the radially integrated density, $\lambda_h^{-1}(x) \equiv \int_0^\infty N_h \pi d\rho^2$, gives the mean depth between trapped holes, λ_h. From eq. (22a) this gives

$$\lambda_h^{-1}(x) = \lambda_e^{-1}\left(1 - \frac{\cosh(x/\ell_h)}{\cosh(d/\ell_h)}\right) \tag{24}$$

where λ_e^{-1} is the initial excitation density, assumed independent of depth for a fast incident ion traversing a thin sample. If $\ell_h \gg \ell$, then even for a large surface trapping efficiency the depth dependence of the trapped hole distribution, shown in fig. 10a, does not change significantly. For $\ell_h = 60\ell$, typical for fast ion or electron sputtering of argon (Reimann et al., 1988), the changes seen in fig. 10a correspond to a factor of six increment in the trapping rate in the surface layer:

$$\Delta = (\tau_h \ell / \tau_h^s \ell_h) = 0.1.$$

A hole trapped at depth x can, on recombination, lead to a yield, $Y(\Delta E, x)$, due to energy release ΔE from one or more of the repulsive decay processes in fig. 8. The subsequent energy transport and escape are determined by molecular dynamics. The total yield is obtained from the trapped hole distribution as in eq. (24). If dx/λ_h is the probability of a hole being trapped between x and $x + dx$, then the average yield is

$$Y(d) = \int Y(\Delta E, x) \frac{dx}{\lambda_h(x)}. \tag{25a}$$

[3]Note: eq. (23) differs from eq. (4.2) in Reimann et al. (1988).

Below we look at bulk and surface contributions separately. The M-band (bulk) and W-band ('surface') luminescence were treated in a similar manner (Reimann et al., 1988).

When only surface trapped species lead to ejection the yield in eq. (25a) becomes,

$$Y_{\text{surf}} = Y(\Delta E, 0)\frac{\ell}{\lambda_{\text{e}}}R_{\text{s}} \tag{25b}$$

for $d \gg \ell_h$. For a uniform excitation density, a quenching substrate, and no enhanced trapping at the surface ($R_{\text{s}} = 1$), the yield vs. thickness due to surface-trapped species is

$$\frac{Y_{\text{surf}}(d)}{Y_{\text{surf}}} = 1 - \frac{1}{\cosh(d/\ell_{\text{h}})} \tag{25c}$$

(Reimann et al., 1988; Ellegaard et al., 1988). Including even a large increase in the surface trapping rate, for example, $\Delta = 0.1$ and 10 for $\ell_{\text{h}} = 60\,\ell$, which corresponds to increases of 6 and 600 times, does not change the thickness dependence of the surface component of the yield, as seen in fig. 10b. However, it can significantly affect the size of the yield, giving $R_{\text{s}} = 6.4$ and 54.6 respectively in eqs. (23) and (25b). Finally, when the depth from which an energy release leading to ejection of an argon atom, $\overline{\Delta x}(\Delta E)$ from eq. (5a), is much smaller than the diffusion length, ℓ_h, then the bulk contribution to the yield in eq. (25a) for $R_{\text{s}} = 1$ becomes

$$\sim \lambda_{\text{e}}^{-1}\frac{\overline{\Delta x}(\Delta E)}{1+\Delta},$$

resembling the first part of eq. (23).

There are some important assumptions in the above description. We have replaced a distribution in grain boundaries and impurities by the diffusion length, ℓ_h, ignored fields, and the electron 'recombination' times are assumed to be much larger than the hole trapping times, τ_h. Grain size and quenching by impurities, k_i in eq. (22a), simply changes ℓ_h (Reimann et al., 1988). Although it is clear that interactions between excitons must play an increasingly important role in determining the electronic sputtering yield with increasing excitation density, and λ_{e}^{-1} is a few per monolayer for 1 MeV He^+ in argon, the holes are assumed to be non-interacting in eq. (22a), $k_{\text{hh}} = 0$. Itoh et al. (1985,1987) point out that holes can attract, via lattice polarization, and trap close together. A related process is the fusion of excitons to produce holes, $A^* + A^* \rightarrow A^+ + A + e$ (process 11) seen even in molecular clusters (Schriver et al., 1987). However, ionized or excited atoms interact with neighbors by both repulsive and attractive states. Typically, there are more states leading to repulsion than to attraction, producing a net, weakly-repulsive interaction. This can lead to scattering of holes, affecting the diffusion constant, D_h, or τ_{h} can be modified if this interaction enhances trapping.

5.2.3 Track Core Processes

The understanding of nonlinear yields has been a dominant aspect of electronic sputtering since the water ice measurements of Brown et al. (1978). The ejection due to Coulomb repulsion between two randomly produced ionizations near the surface gives a nonlinear yield (Haff, 1976; Johnson & Brown, 1982, 1983). In addition, as the excitation density, λ_e^{-1} , increases, the energy releases in mini-cascades from a density of randomly distributed excitations can overlap. As described for knock-on sputtering, this also can produce nonlinear yields. One replaces λ_c by λ_e, or dE/dx by $f_e(dE/dx)_e$ in eqs. (14), (17), and (18b), where f_e is the fraction of the electronic energy participating in sputtering. Therefore, above some threshold excitation density (Johnson, 1987) thermal spike sputtering gives a yield quadratic in $(dE/dx)_e$ (viz. fig. 3). Including the statistics of the transition from a linear to a quadratic sputtering regime results in a yield that differs from that obtained by addition which was used in fig. 3 (Johnson et al., 1991).

As the excitation density increases alternate electronic relaxation pathways can occur. For instance, the Coulomb explosion model of track formation (Fleischer et al., 1975) has been applied to sputtering. Counting only primary ionization, dJ/dx in eq. (21a), the repulsive energy density in a narrow track is

$$\left(\frac{dE}{dx}\right)_{\text{coul}} \propto \frac{e^2}{\epsilon}\left(\frac{dJ}{dx}\right)^2 \tag{26a}$$

where e is the electron charge and ϵ an effective dielectric constant. If $(dE/dx)_{\text{coul}}$ in eq. (20c) is used to calculate direct ejection gives $Y \propto (dJ/dx)^2$ (Haff, 1976). This can also be used to energize a thermal spike (Seiberling et al., 1980, 1982), using eq. (26a) in eq. (14), giving $Y \propto (dJ/dx)^4$, or to produce shock ejection (Bitensky & Parilis, 1987), using eq. (26a) in eq. (17), which would give $Y \propto (dJ/dx)^3$. The latter authors used $(dE/dx)_e$ for the driving energy, instead of $(dE/dx)_{\text{coul}}$. This results in a yield proportional to $(dE/dx)_e^{3/2}$ (Reimann, 1993).

The release of energy during the decay of the hot plasma in the track core can clearly lead to enhanced sputtering, but a good description is waiting. The electrons cool to the lattice, by scattering from neutrals and ions, while the high density of incompletely screened holes produces repulsion after trapping. Using the total, rather than primary ionization, the net coulomb energy can roughly be written (Johnson & Brown, 1982)

$$\left(\frac{dE}{dx}\right)_{\text{coul}} \approx \frac{e^2}{\epsilon}\left(\frac{(dE/dx)_e}{W}\right)^2 \ln\left(\frac{\overline{\rho}^2 + \overline{\rho}_-^2}{2\overline{\rho}\,\overline{\rho}_-}\right) \tag{26b}$$

which must be less than $(dE/dx)_e$. Here $\overline{\rho}$ and $\overline{\rho}_-$ are the root-mean-square radii of the hole and electron distributions during Coulomb repulsion and ejection. $\overline{\rho}_-$

is, therefore, a rapidly decaying function of time.

Watson & Tombrello (1985) treated the plasma decay and calculated an average $\overline{\rho}$. They used the net repulsive potential in the track to energize the lattice, calculating escape via eq. (13a). Recently Ritchie et al. (1989) gave a description of the hot plasma decay, including ambipolar diffusion for positive and negative charges along with the hydrodynamic equations, eqs. (9). The principal problem is the complexity of the atomic processes which determine cooling, recombination, and repulsion.

Not only can hole repulsion heat the lattice, but so can electron cooling via collisions with the neutrals and holes in the lattice. In a dense plasma, electron-electron collisions will enhance the de-excitation and recombination rates (processes 9 and 10, Table II), converting the band gap energy into secondary electron kinetic energy (Ritchie & Claussen, 1982). The energized electrons can lose their kinetic energy to lattice motion, producing a thermal spike (Klaumünzer et al. 1986; Houpert et al., 1989). In a molecular solid, the energized electrons would instead excite molecular vibrations, leading to material expansion. A sufficiently rapid expansion, due to high excitation density, has been suggested as a cause of material ejection (Williams & Sundqvist, 1987).

5.3 Molecular Dynamics

5.3.1 Solid-State Potentials

When energy is deposited in the lattice by an energetic exothermic process, it can be transported to the surface by collisions, viz. eq. (2). Therefore, energy release in the bulk as well as at the surface can lead to sputtering, eq. (5a). This transport of energy through the solid can be described by molecular dynamics, MD (Hoover, 1986; Nieminen, 1993; Robinson, 1993). In this method the interaction of each particle with all neighbors in a sample, not necessarily pair-wise, is calculated at each time step. Therefore, knowing the potentials and using the position and momentum at the beginning of the time step, new positions and momenta are obtained and the atomic motion can be followed.

Whereas ground state potentials in many solids are available, for the electronic processes occurring in Table II the interaction potentials between a localized, excited species and its neighbors are poorly known. Unlike the ground-state atoms and molecules, which are often closed-shell structures, an excited atom or molecule in the field of neighbors interact via an ensemble of potentials. For the simple case of an Ar^+ interacting with one Ar neighbor, this involves, ignoring spin-orbit splitting, two Σ states (zero angular momentum along the internuclear axis) and two doubly degenerate Π states (one unit of angular momentum) (Herzberg, 1950).

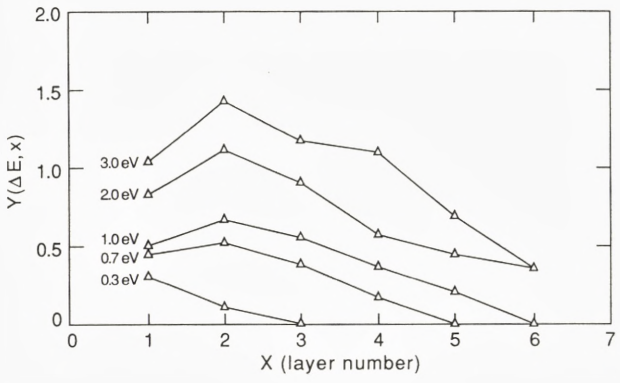

Figure 11. Yield versus depth due to energy release in crystal Ar, (100) face: ΔE indicated (Cui et al., 1988).

The differences between these interactions have to do with the shape of their electron distribution relative to the intermolecular axis. The potentials for these states evolve to the polarization potential at large separation, and the splitting between the two Σ states and that between the Π states determines the electron exchange rate with a neighbor (e.g., Johnson, 1982). Pair potentials for some Σ states are shown in fig. 8. There is, of course, an ensemble of repulsive and attractive excited states with each having a width in the solid.

When there are a number of neighbors, linear combinations of the wave functions associated with the excited argon atom can be used to diagonalize the interaction matrix. For an excited atom in a symmetric distribution of neighbors the resulting wave function has the symmetry properties of the field. Therefore, for the trapped atomic exciton in fig. 9b, the potential is approximated by a linear combination of the six potentials (Boursey et al., l977 ; Cui et al., 1989a), and the net interaction is weakly repulsive (viz. fig. 8). Using these potentials in a MD calculation, the trapping of an atomic exciton at an undamaged vacuum surface was found to lead to ejection (Cui et al., 1989a), as predicted by Coletti et al. (1985) and as indicated in fig. 9b.

For the dimer in fig. 9a, the lowest excited state is described by the attractive $^{1,3}\Sigma_u^+$ potential acting between the two atoms (Schwentner et al., 1985), as indicated in fig. 8. Each of these atoms also interacts with the neighbors by an average made up of the other five potentials (Cui et al., 1989b). Such simple schemes have, of course, limited applicability, especially as the symmetry is broken at a surface and at defects. Also, when the radius of the electron cloud exceeds the interatomic radius, the increased distortion requires many body interactions.

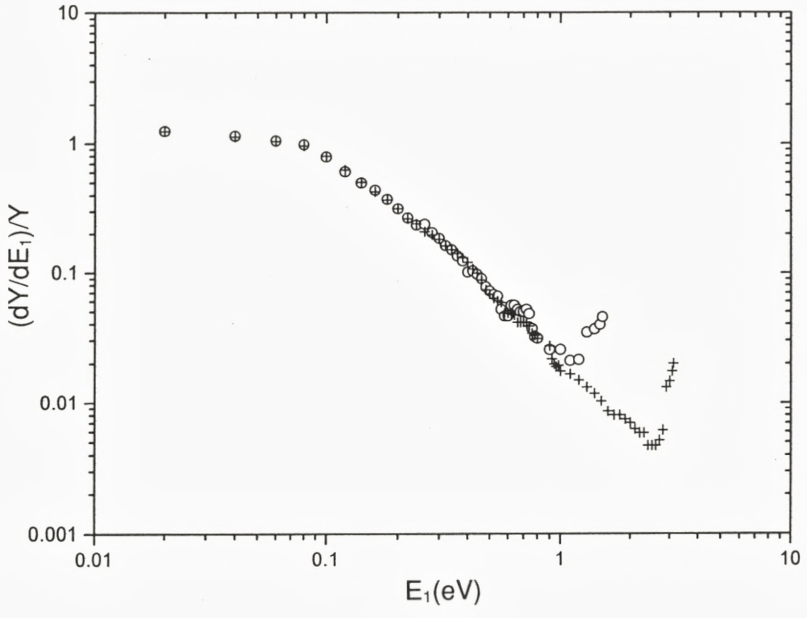

Figure 12. Energy spectra of ejected O_2 from solid amorphous O_2 for $\Delta E = 3.2$ eV (+) and 1.6 eV (○). O_2 given a kinetic energy in random direction at all depths. Decay as E_1^{-2} seen: spectra resembles eqs. (8a) and (8b) with the single event ejection added, as discussed in text. (Liu & Johnson, 1993).

5.3.2 Calculations: Single Events

To represent an energetic nonradiative relaxation event, an atom or molecule can simply be set in motion, or a pair interaction can be changed from attractive to repulsive to represent excitation to a repulsive state. In a crystal focussed collision sequences can occur (Robinson, 1981; Townsend, 1983; Cui et al., 1988), but when ΔE significantly exceeds the sublimation energy, U, the expression in eq. (2) with $T = \Delta E$ roughly applies for both crystalline and amorphous solids, even though the binary collision approximation breaks down (Garrison and Johnson, 1986; Cui et al., 1988, 1989c). $Y(\Delta E, x)$ is given in fig. 11 for a cascade in crystalline argon initiated by a randomly oriented momentum transfer event.

For sputtering by photons or when surface effects are important, eq. (25a), this is averaged over the distribution of excitations with depth. For a uniform distribution, using the definition of $\overline{\Delta x}$ in eq. (5a), the integration of $Y(\Delta E, x)$ gives

$$\overline{\Delta x}(\Delta E) \sim c\ell(\Delta E - U)/U \tag{27}$$

which is seen to be linear in ΔE. By contrast a diffusive cascade would give, $\overline{\Delta x}(\Delta E) \propto \Delta E^{5/3}$ (Johnson & Brown, 1982), as discussed earlier. Because of the linear dependence on ΔE in eq. (27)[4], the quantity f_e in eq. (20b) has the form $f_e \approx \Delta E/W$, when electron-hole pair formation is a precursor to electronic sputtering.

By application of molecular dynamics to a number of condensed gases, the quantity c in eq. (27) was found to be about 0.15 for atomic and molecular solids (Johnson et al., 1991) roughly consistent with $c \approx \Gamma/4$ and $(N\overline{\sigma}_d)^{-1} \approx \ell$ as in eq. (6c). The calculated energy spectrum of sputtered atoms directly reflects the recoil energy spectrum discussed earlier, $G(\Delta E, E_0) + \delta(\Delta E - E_0)$, as seen in fig. 12 for O_2 molecules set in motion in a random direction and at random depths in solid oxygen (Liu & Johnson, 1993). The E_1^{-2} dependence in eqs. (8a) and (8b) over a range of energies $U < E_1 < \Delta E$ is remarkably well reproduced, implying that binary collisions are not a necessary requirement for such a dependence (Cui et al., 1988). Since the statistics of the low-energy ejecta was poor, the absence of the maximum in fig. 12 like that in eq. (8a) at $U/2 \approx 0.04$ eV is not certain. The fraction of ΔE dissipated to internal degrees of freedom is $\sim 10\%$ at these energies and no dissociation occurs. Excitation to a repulsive dissociating state of O_2 leads to a similar spectrum for the O_2 ejecta without the peak at large E_1, and, of course, O atoms were also ejected (Banerjee et al., 1991b); note that O_3 could not form easily for the potentials used.

5.3.3 Calculations: Tracks

A number of molecular dynamics calculations have been carried out for a track of excitations. Cui & Johnson (1989) and Banerjee et al. (1991a) treated vibrationally excited molecules in a cylindrical track in an amorphous solid of van der Waals bonded O_2 molecules. Although the excitation was rapid, no ejection occurred unless the molecules in the track were excited above the dissociation limit because of the large average spacing between molecules. When the internal molecular well structure was artificially modified so that the atoms in the vibrating molecule experienced larger excursions, a stronger vibrational-lattice interaction was produced. The rate of transfer of the internal energy to center of mass energy of the neighboring molecules was now seen to increase with excitation density as shown in fig. 13. Therefore, the total energy transfer to lattice motion, which we will call $(dE/dx)_{\text{eff}}$, also increased. This manner of excitation resulted in a calculated yield which depended roughly on $(dE/dx)_{\text{eff}}^3$ over the narrow range of $(dE/dx)_{\text{eff}}$ studied. Earlier such a dependence was found for massive molecules, intended to represent biomolecules which were excited by vibrational expansion (Fenyö et al., 1990). Assuming $(dE/dx)_{\text{eff}} \approx f_e(dE/dx)_e$, these early MD cal-

[4]For a variety of decay routes, an average $\overline{\Delta E}$ can be used

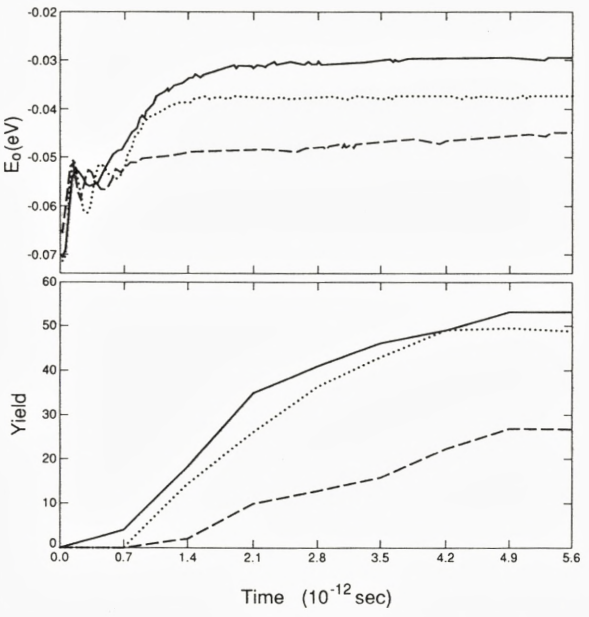

Figure 13. Time dependence of the average center-of-mass energy of molecules in a cylindrical volume of a sample of a diatomic solid: mass same as O_2, interatomic energy smaller than O_2 and separation larger. Molecules are initially excited vibrationally for three different values of internal vibrational energy per molecule. The transfer of vibrational energy to center of mass energy, E_0, is seen vs. time, as in the accumulated ejection yield, Y. From Banerjee et al. (1991a).

culations were suggestive for developing the so-called pressure pulse model given in eqs. (18a) and (18b) (Johnson et al., 1989; Reimann, 1993). Since then, MD calculations have been used to test this model (Fenyö & Johnson, 1992; Fenyö, 1993).

Recently, Urbassek et al. (1993) excited a cylindrical volume of atoms in an argon solid by giving them kinetic energy in a random direction. Such an excitation might be the result of a Coulomb explosion in the track or some other 'track' process. At the lowest $(dE/dx)_{\text{eff}}$ the yield also exhibited a cubic dependence. Surprisingly, at larger $(dE/dx)_{\text{eff}}$ the yield became nearly linear for the ejection times, up to 10^{-11} sec, and for initial energies and sample conditions studied. This result occurred because the radial diffusion of energy was slow compared to the transport by flow of gas from the transiently pressurized track.

6 Theory: Molecular Solids and Compositional Changes

6.1 Preferential Ejection

Because the sputter yield depends inversely on the cohesive energy, U, the more volatile elements of a mixed material are sputtered preferentially at low fluences. In the linear cascade regime the description of sputtering from an alloy or a chemical compound has been treated by a number of authors resulting in approximate analytic expressions for the yield of each species (Andersen & Sigmund, 1974; Haff & Switkowski, 1976; Andersen, 1984; Sigmund & Lam, 1993). For knock-on sputtering, an approximate yield ratio for two species, Y_i and Y_j, is (Sigmund, 1981)

$$\frac{Y_i}{Y_j} \approx \frac{c_i}{c_j}\left(\frac{M_j}{M_i}\right)^{2m}\left(\frac{U_j}{U_i}\right)^{1-2m}, \tag{28a}$$

where c_i is the relative concentration of species i in the surface region, U_i is the average surface binding energy of species i, and m is a number determined by the interaction potential. For a steeply repulsive potential $m \approx 0$. For thermal spike sputtering, eqs. (12) - (16), under the assumption of a cylindrical region of excitation,

$$\frac{Y_i}{Y_j} \approx \frac{c_i}{c_j}\frac{M_j}{M_i} g(U_i, U_j) \tag{28b}$$

where

$$g = \begin{cases} (U_j/U_i)^2 & \text{(Kelly, 1979)} \\ \\ \exp\left(\dfrac{U_j - U_i}{kT}\right) & \text{(Sigmund, 1981)} \end{cases}$$

At very low fluences the surface concentrations, c_i, are generally equal to the bulk concentrations, c_i^0 , but they change with fluence, since the more volatile elements are depleted more rapidly. Because diffusion occurs along the damage path of an ion, the extent of this depleted region can approach the ion penetration depth (Kelly 1984; Sigmund & Oliva, 1993). Although the sputtering is initially non-stoichiometric, the yield ratio can become stoichiometric at high fluences, $(Y_i/Y_j) \approx (c_i^0/c_j^0)$, as the concentrations in the surface region change according to either eq. (28a) or (28b). These expressions should only be used as a guide to understanding compositional alteration by sputtering.

6.2 Sputtering of Molecules

In a molecular material, atoms or molecules may be ejected. Based on the above discussion, the relative yields will depend on the relative sizes of the cohesive energy

of the molecular solid, U, the dissociation energy, E_b, and the removal energy, U_a, for a particular atomic species (Kelly, 1987).

In addition, the relative yields are extremely sensitive to the spatial extent of the momentum distribution at the surface. The likelihood of molecular ejection is enhanced if correlated events occur at the surface (Urbassek & Hofer, 1993). Therefore, molecular ejection becomes relatively more important when a volume element at the surface has a net directed momentum, figs. 2c and 2d (Johnson et al., 1989; Reimann, 1993). For a typical high excitation density, the initiating events often lead to fragmentation and fragment ejection, whereas the later, correlated energy transport can lead to molecular ejection (Bitensky & Parilis, 1987; Johnson & Sundqvist, 1992). Although it can be useful to roughly characterize the relative amounts of atomic and molecular species by an average temperature, ejection is, in general, a nonequilibrium process.

Let us consider a low-density collision cascade in a low temperature solid of condensed, homonuclear diatomic molecules (solid O_2 or N_2). If the energy transfer, T, to either atom of a molecule is much greater than $\sim 2E_b + U_a$, atomic ejection is dominant. The energy transfer to the atom must be at least $2E_b$ for dissociation since half the energy transferred to one atom goes to motion of the center-of-mass of the molecules. For lower values of binary collision energy transfer molecular ejection dominates. Because the recoil number density in eq. (2) grows at low recoil energies, a large number of molecules can be ejected as $U \ll E_b + U_a$ in these solids.

Since electronic relaxation events typically release small energies, electronic sputtering at low excitation densities leads to atomic ejection only by repulsive dissociation at the surface. Below the surface these events can lead to ejection of molecules by momentum transfer to the surface, as discussed. The residual atoms in the bulk are radicals which are difficult to sputter as they have relatively large binding energies to the solid, U_a. Therefore, with increasing fluence they accumulate and react, so that chemical processes can eventually control sputtering, as discussed below.

6.3 Chemical Sputtering

In knock-on and electronic sputtering of molecular material, the deposited energy will lead to broken bonds, formation of radicals, and preferential ejection. This can eventually lead to chemical reactions occurring, as the radical species bind efficiently to the sample. In addition, for electronic sputtering, an excited species can directly react with a neighbor, with again the possibility of new species forming. Such reactions can affect the erosion rate of the solid in two ways. First, the reacting species may release sufficient energy in an exothermic reaction to directly

cause ejection or to increase the local temperature enhancing sputtering (Johnson & Brown, 1982; David & Michl, 1989). Second, any newly formed species may have a lower or higher volatility than the molecules in the solid. This can change the effective cohesive energy, U, and, thereby, the sputtering yield. Such effects were treated for knock-on sputtering of refractory solids by Roth (1983).

When the new species are formed from radicals produced in the track of a single ion, the effect on the yield is independent of fluence. When a newly formed radical reacts with a background of previously produced radicals, the effect on the yield is fluence and temperature dependent (Reimann et al., 1984a). A typical reaction rate between two radical species would be written, $\kappa(T')N_iN_j$, where $\kappa(T')$ is the reaction rate constant and N_i and N_j are the local densities of the reacting species. This is one term of a set of rate equations which would include diffusion. T' is used to indicate that the reaction may be driven by the kinetic energy of one of the newly formed species, a 'hot atom' reaction (Matsuura et al., 1984; Adloff et al., 1992) or by the ambient temperature, T_a. In the latter case the ejection yield depends on the activation energy for the reaction, ΔE_a (Kelly, 1977; Johnson & Brown, 1982), so that the yield for a formed species would be proportional to $\exp(-\Delta E_a/kT_a)$ (Brown et al., 1982; Reimann et al., 1984a).

As a final issue, the implanted ion itself may be reactive: H, C, O, S, etc. In a refractory material with low sputtering yield, as for C^+ on a silicate grain or H^+ on graphite, more volatile species may form after a large fluence enhancing the sputtering yield: CO (Rocard & Bibring, 1982) and CH_4 (Roth, 1983) respectively. The second process is of interest in fusion devices, whereas the first process was of interest for solar wind sputtering of lunar soil at the time of the Apollo missions (Taylor, 1982). Such a process is also of interest at Europa, a moon of Jupiter where sulfur, ejected from the neighboring moon Io, is ionized, accelerated, and implanted into Europa's icy surface, producing an SO band seen in UV-reflectance (Sack et al., 1993). In the following we review first the experimental methods and then summarize the data available.

7 Experimental Methods

The study of sputtering of insulators involves a number of methods well known in other fields as well as some new techniques. In the standard setup shown in fig. 14, an insulating target is placed in a vacuum chamber with a pressure typically 10^{-8} torr or below. Beam particles (ions, electrons, or photons) impinge on the target causing a loss of material. Important properties to be measured are the sputtering yield, Y, the energy distribution dY/dE_1, angular and mass distributions of the ejected particles, the composition of the residual target, and the luminescence

from the target or from escaping particles. Measurements of the angular and mass distributions of the ejected particles, as well as systematic studies of the yields and energy distributions have been performed only in few cases.

Key parameters are the primary energy, E, the type of incident particle, and the angle of incidence, θ. However, based on the theoretical discussion, it is often advantageous to plot the results versus dE/dx or the corresponding stopping cross section, S. For experiments on frozen gases the thickness of the film and the temperature of the substrate are also important. For incident ions, varying the charge state and using molecular ions can be helpful, as discussed.

When irradiating films of frozen gases on a cryogenic substrate, the possibility of easily varying the thickness is a particular advantage. Because of the simplicity of producing low-temperature samples of condensed-gases in situ, systematic measurements have been carried out in a number of laboratories. Targets of sulfur, the only elemental room-temperature insulator studied (Chrisey et al., 1988; Torrisi et al., 1988), were also produced by in situ film deposition. This is in contrast to measurements on other room-temperature insulators, in which the samples have to be inserted into the vacuum system and cleaned by heating or sputtering prior to measurements.

7.1 Yield Measurements

The sputtering yield is measured in a variety of ways. For room-temperature insulators or refractory materials, the methods are similar to those applied to metals (Andersen & Bay, 1981), but typically with reduced beam currents to reduce sample heating and charging. Yields have been determined by weight-loss, film thickness change, profilometry of the sputtered volume, and interference micrographs (Bach, 1988). The only yield for electron-induced sputtering of alkali halides was determined by measuring the crater dimensions (Szymonski et al., 1985).

Because the yield can depend on the thickness of the target, integral and differential measurements of the yield can differ. In the former case, the yield is evaluated from the number of particles necessary to remove an insulating layer of known thickness completely. The erosion continues until a clear signal from the substrate is detected (Schou et al., 1984). The methods below are differential.

7.1.1 Mass Loss: Rutherford Backscattering

Rutherford backscattering (RBS) measures the absolute number of atoms per unit area (the column density) at any time, and, therefore, it can be used to determine both the sputtering yield (Brown et al., 1978, 1986; Ollerhead et al., 1980; Besenbacher et al., 1981) and the changing composition of the target (Brown et

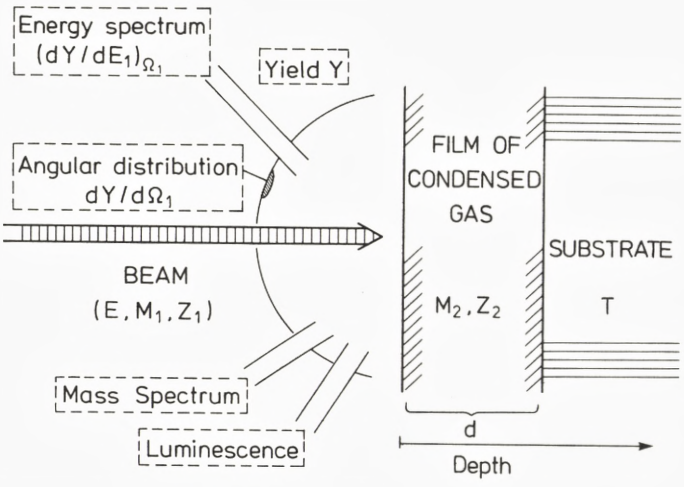

Figure 14. Schematic survey of the experimentally studied quantities in an erosion experiment with a frozen gas (From Schou, 1987).

al., 1984). A simultaneous monitoring of beam current, area of beam spot, and change in column density gives the yield, fig. 15. The precise determination of the change in column density may be carried out from the shift of the position of a thin heavy marker (typically a 50 Å thick gold layer deposited on beryllium) or from the reduction of the total number of film atoms detected in the backscattered peak. The ions responsible for probing the thickness can be different from those eroding the film. The agreement in the yield determined from the marker shift or the peak reduction is usually good, but the marker shift is generally used. Potential disadvantages are that the erosion produced by the probing beam, often 1 - 1.5 MeV He^+ ions, has to be subtracted, and species lighter than the probing beam can not be detected. Typically, the achievable sensitivity corresponds to the removal of a monolayer of argon from solid argon (Reimann, 1992).

Ion beam analysis of a foil on which sputtered atoms have been collected has been carried out for a few materials. This procedure requires a primary eroding beam and an analyzing beam, or the ability to change the beam setting from the target to the collector foils. Qui et al. (1982) used forward scattering of, typically, 4 MeV F^+ ions to study refractory solids.

7.1.2 Mass Loss: Energy Loss from Substrate Source

A method related to RBS is the determination of energy loss for helium ions originating from a thin radioactive layer deposited on the substrate. The column density

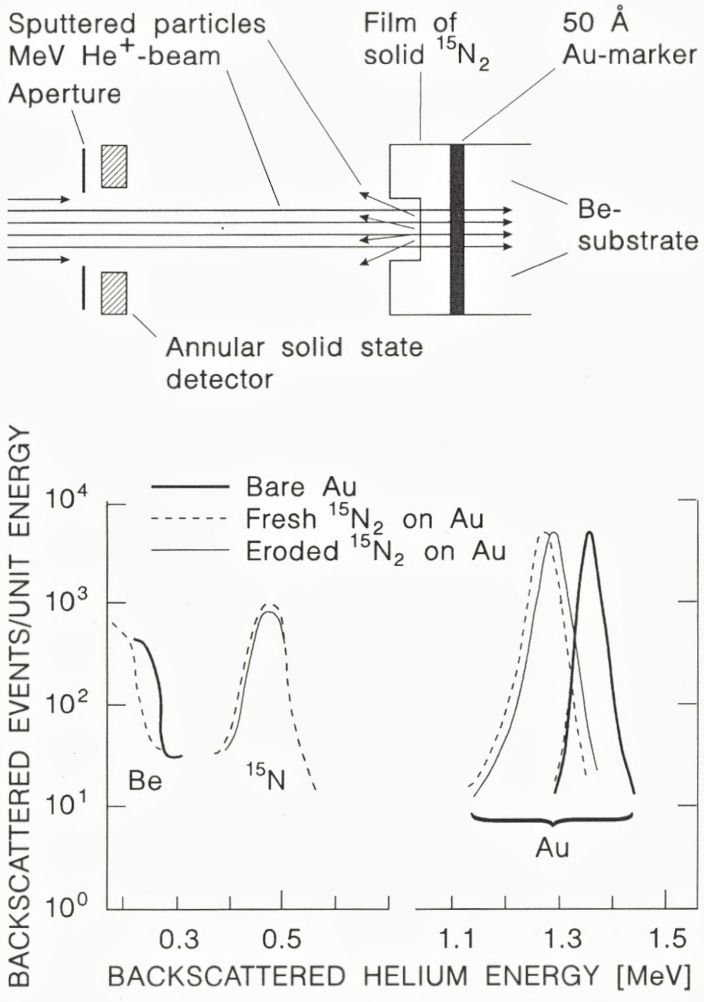

Figure 15. Schematic survey of the geometry (upper part) and the data curves (lower part) in an erosion experiment on solid $^{15}N_2$ with Rutherford Backscattering Spectrometry (RBS). (Modified from Brown et al., 1986).

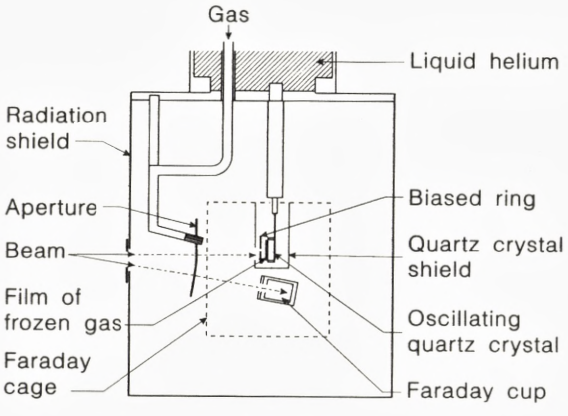

Figure 16. Schematic survey of the geometry for a typical erosion experiment with a frozen gas deposited on a quartz crystal (Modified from Schou et al., 1984).

can be evaluated from the energy loss of the emitted alpha particles traversing the film obtained from a solid state detector. Although care must be taken not to bombard the radioactive source, the method is simple and easy to apply, but because of the low dE/dx the sensitivity is less than in RBS experiments (Chrisey et al., 1988).

7.1.3 Mass Loss: Microbalance

The mass loss from a frozen-gas target by particle irradiation may be determined by a quartz crystal microbalance on which a cryogenic sample is deposited, fig. 16. This method has a high sensitivity and the mass loss is obtained from the linear change in frequency as the film is removed by sputtering (Schou et al., 1984; David & Michl, 1989). Two demands pose a problem for low-temperature erosion experiments with a quartz crystal microbalance: the crystal has to oscillate freely in a holder and the thermal conduction from the cryogenic area to the crystal electrode, on which the film is deposited, must be sufficiently good. The typical sensitivity corresponds to the removal of one monolayer of argon from solid argon. A reference quartz crystal can also be mounted in thermal contact with the target crystal (David & Michl, 1989), providing a large improvement in sensitivity, $\sim$ 0.1-10^{-3} monolayer of argon (Baragiola, 1993c). With a microbalance the control of film deposition is particularly easy. A complicating feature is the measurement of the primary current on a high-frequency electrode.

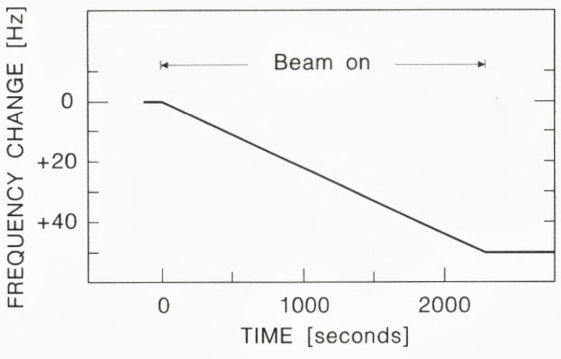

Figure 16, cont'd. Schematic survey of the frequency change curve for a typical erosion experiment with a frozen gas deposited on a quartz crystal (Modified from Schou et al., 1984).

7.1.4 Quadrupole Mass Spectrometry

A frequently used method for obtaining a relative yield is the detection of the sputtered species by a mass spectrometer. One of the first sputtering measurements of relevance to this chapter was carried out by Erents & McCracken (1973) with quadrupole mass spectrometry (QMS). The method is fast and can give absolute yields when calibrated. The spectrometer is directed toward the target, which is irradiated by a pulsed beam so that background subtraction is possible (Brown et al., 1986). An additional advantage is the ability to determine the composition of the ejecta. The relative sensitivity under typical beam currents is about 0.01 monolayers of argon (Reimann, 1992).

7.2 Energy Distributions

The energy distribution of the emitted particles can directly reflect the energetics of the ejection processes as discussed. For alkali halides this has also been decisive in identifying the erosion processes (Szymonski, 1993). The energy distributions of particles sputtered from insulating targets have almost exclusively been studied using time-of-flight (TOF). In general, the distribution is measured for a small solid angle around the target normal, whereas the angle of incidence differs between experiments [0° (Hudel et al., 1991), 45° (O'Shaughnessy et al., 1988a,b; Pedrys et al., 1988) or 60° (Haring et al., 1984a)]. A pulsed beam strikes the insulating target and generates a pulse of eroded particles that passes through a quadrupole equipped with an ionizer. The kinetic energy of each species can be determined from the time interval between the impact of the beam particles and the arrival of the sputtered particles, for energies from 10^{-3}eV up to about 10 eV. The problem

of obtaining good statistics for the rare ejection of particles with more than 1 eV was overcome using a correlation method (Overeijnder et al., 1978).

Mechanical TOF-spectrometers were used by Tombrello and coworkers (Griffith et al., 1980; Seiberling et al., 1980). The sputtered particles emitted normal to the target surface were collected on a rotating aluminum wheel and then exposed to neutron activation analysis. This gave accurate energy spectra for uranium atoms sputtered from room-temperature insulators, UF_4 and UO_2. A particularly refined setup that combines TOF-spectrometry and angular resolved spectrometry of metastable neutrals has been developed by Sanche and coworkers (Leclerc et al. 1990, 1992).

7.3 Mass and Luminescence Spectra

Measurements of the masses of emitted particles are useful for detecting clusters ejected from elemental targets and radicals, new chemical species, or clusters ejected from chemical compounds. The masses are typically determined using a QMS, with the beam pulsed or continuous.

Simultaneous measurements of luminescence and sputter ejecta have been important for identifying the energy release events for frozen gases and alkali halides (Reimann et al., 1984a, 1988; Szymonski, 1993). Occasionally, the change in luminescence intensity during particle irradiation has been utilized to estimate the erosion rate (Coletti & Debever, 1983) or to study the excited states of sputtered atoms (Kloiber et al., 1988) and molecules (Reimann et al., 1991).

7.4 Target Analysis

The particle or photon bombardment can cause preferential sputtering and modification of the target. It is sometimes possible to carry out an external macroscopic chemical analysis, if the amount of residual material is sufficient and is non-volatile. A common in situ analysis of atomic composition is Rutherford backscattering. For instance, absolute loss rates of carbon from frozen methane were obtained in this manner by Lanzerotti et al. (1987), whereas for the deuterium loss from CD_4 they used the $^3He(d,p)^4He$ nuclear reaction in the deuterated sample. A common in-situ analysis of molecular composition is infrared (IR) absorption spectroscopy (Benit et al., 1987; David et al., 1986; David & Michl, 1989). For instance, this has helped in the interpretation of the temperature dependence exhibited in water ice sputtering (Rocard et al., 1986; Spinella et al., 1991). In addition, mass spectrometers are used to monitor the change in character of the ejecta with irradiation time (SIMS or neutral SIMS), which is indicative of the changing target composition. This has also been used to monitor the change in water ice by loss of H_2 (D_2) and

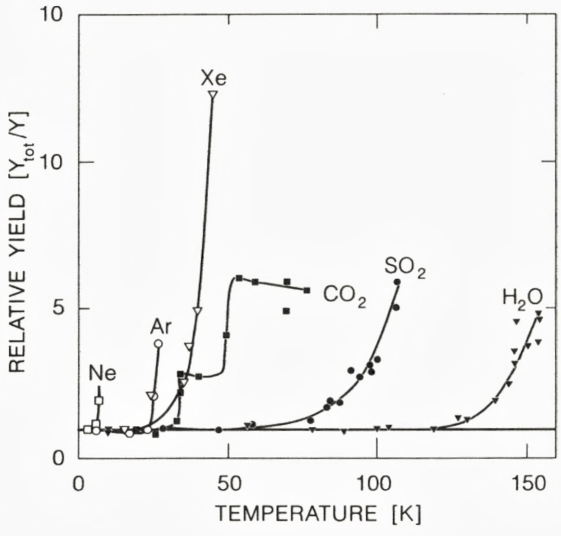

Figure 17. The relative yield Y_{tot}/Y is plotted versus the substrate temperature. Y_{tot}; total yield; Y, low-temperature yield. Ne-data, Schou et al. (1986); Ar-data, Besenbacher et al. (1981); Xe-data, Ollerhead et al. (1980); CO_2-data Brown et al. (1982); SO_2-data, Boring et al. (1984); H_2O, Brown et al. (1980a). From Schou (1987).

O_2 (Brown et al., 1982, 1984).

7.5 Selective State Excitation

Using laser or synchrotron light (Kloiber et al., 1988; Feulner et al., 1987; Menzel, 1990) selective excitation of the solid can be made to test particular electronic states that might lead to sputtering. Recently, Runne et al. (1993) selectively excited Kr atoms in the surface of solid argon to the $n = 1$ state, which can not migrate. In this way an excitation at the surface is known to decay at the point of absorption. Selective excitations of solids have been preformed with low energy electrons as well (Kloiber & Zimmerer, 1989; Hourmatallah et al., 1988; Leclerc et al., 1992).

8 Experimental Data

The solid inorganic insulators may be divided into the following classes according to their general properties and behavior during sputtering:

A) elemental solid insulators (e.g. deposited S_8)

B) oxides and related solid compounds (e.g. SiO_2, Al_2O_3)

C) frozen gases (e.g. N_2, Ar, H_2O)

D) alkali halides and related materials (e.g. $MgCl_2$)

The latter group is treated by Szymonski (1993). Whereas knock-on sputtering of insulators is similar to that of metals, electronic sputtering occurs in most insulators and only occurs in semiconductors and metals at extremely high excitation densities (Johnson, 1993; Brown, 1993). In addition, since frozen gases and elemental insulators are much more volatile than metals, beam-induced evaporation may play a larger role.

8.1 Beam-Induced Evaporation

The heating of the solid, externally or directly by a beam of high current, can lead to surface loss as discussed earlier. There is a threshold below which the yield is independent of the ambient temperature for a typical current density, whereas for higher temperatures or intensities the yield increases rapidly with temperature (Lanzerotti & Brown, 1983). For the rare-gas solids for a typical low ion current density the threshold temperature increases with increasing sublimation energy (Schou, 1987, 1991), as seen in fig. 17. This temperature, approximately $0.02U/k$, is somewhat below the melting temperature. In contrast to this, the increasing yield with temperature seen in fig. 17 for CO_2, SO_2, and H_2O (Brown et al, 1982; Boring et al., 1983) is due to formation of volatile products to be discussed; enhanced ejection due to heating occurs at much higher temperatures.

At high current densities the yield is beam current dependent (Besenbacher et al., 1981; Schou et al., 1984; Sigmund & Szymonski, 1984; Schou 1991). The erosion yield for electron-bombarded solid neon increased by more than two orders of magnitude as a result of a current density increase from 10 $\mu A/cm^2$ up to 35 $\mu A/cm^2$ (Schou et al., 1984). For the most volatile material which exists in equilibrium with laboratory vacuum, namely solid hydrogen, yield measurements could be carried out only for current densities below 0.2 $\mu A/cm^2$ (Stenum et al., 1991). Beam-induced evaporation is indicated by an enhancement in the energy spectrum at very low energies, eq. (19b) (Haring et al., 1984a; Ellegaard et al., 1993b). Pedrys et al. (1984) observed that ejection energies for F_2 emitted from electron-bombarded solid sulfur hexafluoride could be described by a Maxwell-Boltzmann function using a macroscopic target temperature. Sputtering of solid methane resulted in an energy spectrum for emitted hydrogen which could be similarly described (Pedrys et al., 1986). In contrast, for the ejected SF_6 and CH_4 molecules, the energy spectra were independent of the beam current since

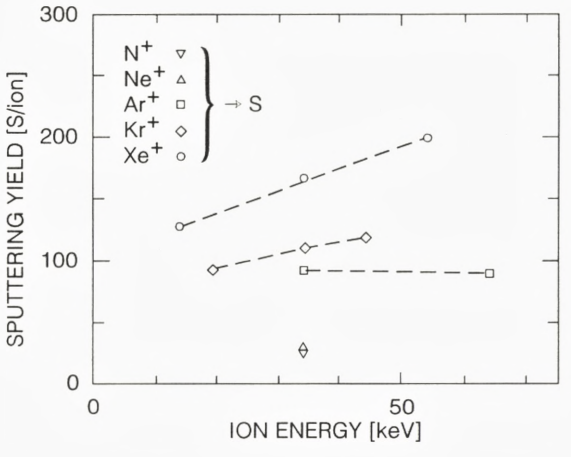

Figure 18. Sputtering yield for medium mass ions incident on sulfur. The yield is given in S-atoms per ion, but the ejected species are frequently polyatomic molecules. Data from Chrisey et al. (1988). Dashed curves to guide the eye only.

the molecular emission is determined by the energetic release processes. For solid sulfur, a strong beam-induced evaporation ($\sim 10^4 \mathrm{S/He^+}$) was seen if the target was not cooled (Fink et al., 1984). This yield is orders of magnitude larger than that at low temperatures (Torrisi et al., 1986).

The alkali halides show the remarkable feature that direct electronic sputtering takes place for the halide component alone. The surface becomes gradually enriched with the alkali atoms and the erosion may eventually cease, unless the temperature (for example, produced by a high beam current density) is high enough that the alkali atoms evaporate as fast as the halogen atoms are sputtered. At low temperatures the sputtering is controlled largely by the evaporation rate of the metal, which leads to a Maxwell-Boltzmann distribution for the ejecta (Overeijnder et al., 1978, Szymonski, 1980, 1993, Szymonski et al., 1990).

8.2 Knock-on Sputtering

Knock-on sputtering of insulators is similar to that of metals, as discussed earlier, except for the volatility and chemical composition. Low volatility means that many atoms are set in motion at each impact on the frozen gases. In addition, the molecular frozen gases show considerable chemical activity, and many refractory insulators are also multicomponent targets. For example, sputtering of the latter oxides resembles that of metallic alloys, although the anion may be chemically

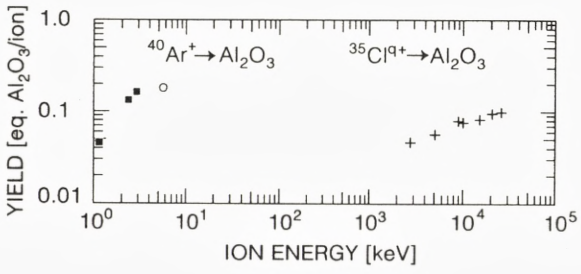

Figure 19. Knock-on and electronic sputtering yield for heavy ions incident on Al_2O_3, expressed as Al_2O_3 molecules/ion, even though the majority of the ejected particles may be atoms.+, electronic sputtering yield from Qui et al. (1982). Knockon sputtering yields, full squares from Davidse & Maissel (1966) and o from Bach (1988).

active in insulators.

8.2.1 Sulfur

Sulfur is the only elemental room-temperature insulator that has been investigated. It has been studied primarily because of its interest at Io (Johnson, 1990). The yield from low-temperature sulfur bombarded by medium mass ions in fig. 18 increases strongly with the mass of the primary ion, but the variation with ion energy is relatively small. The size of the experimental yield agrees roughly with that predicted by linear collision-cascade theory using an assumed average sublimation energy per atom, U, and an atomic interaction cross section, $\overline{\sigma}_d$, in eq. (6a) (Chrisey et al., 1988).

The sulfur atoms in the parent molecules, S_8 are bound much stronger to their neighbors (2.7 eV) than the unit species, S_8, is to the lattice (1.1 eV). Because of the size of S_8 and the strong S-S bond, the sulfur is ejected predominantly as diatomic molecules rather than as S_8 or other large molecules S_6 and S_7. The relative distribution of ejected masses depends very little on the incident ion mass. Chrisey et al. (1988) measured the energy distribution for S_1, S_2 and S_3 ejected as a result of 44 keV Ar^+ ion bombardment. The high-energy part of the tail for the two lightest species is consistent with knock-on sputtering (Urbassek & Hofer, 1993). The effective binding energy, U, inferred from the peak in the energy spectra, 100 and 50 meV for S_1 and S_2 respectively, is lower than that determined from the yield measurements. Even though the low-energy part of these spectra depends strongly on the background subtraction, one may interpret the spectra to be the result of linear collision-cascades in a damaged material of loosely bound sulfur fragments.

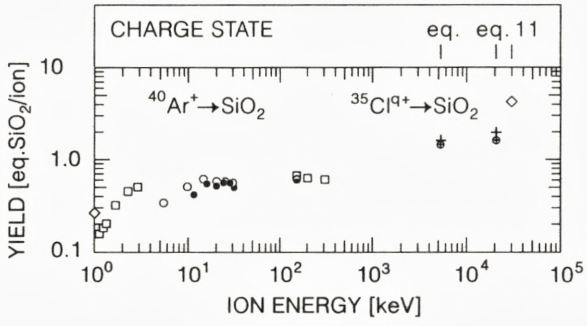

Figure 20. Knock-on and electronic sputtering yield for heavy ions incident on SiO_2. Knock-on yields: ◇, Cantagrel and Marchal (1973); ○, Bach et al. (1974); •, Edwin (1973); half-filled circles, Schroeder et al. (1971); □, Jacobsson and Holmén (1993). Electronic yields: +, fused and, ⊕, crystalline, Qui et al. (1983); ◇, Sugden et al. (1992). The ^{35}Cl charge states are indicated above the yield figure, 'eq.'means equilibrium charge state.

8.2.2 Refractory Materials

Oxides have been studied comprehensively within the last twenty years (Betz and Wehner, 1983). Oxygen is often sputtered preferentially as atoms or in molecular species. Therefore, an enrichment of the heaviest elements occurs in the surface region, which is partly compensated for by diffusion (Lam & Sigmund, 1993). The sputtering yield from oxides is comparable to that from metals except for MgO and Al_2O_3 (Betz & Wehner, 1983). For SiO_2, recent measurements by Jacobsson and Holmén (1993) demonstrate that the total yield does not deviate too much from the corresponding atomic yield from silicon. However, if metals are bombarded in an oxygen atmosphere, so that oygen atoms are continuously available, the yield of the metal atoms falls drastically as the oxygenation of the surface increases (Kelly, 1987).

Results for aluminum oxide bombarded by keV argon ions are shown in fig. 19. The total yield is given in equivalent Al_2O_3 molecules ejected, even though the ejection is primarily as atoms. This yield increases up to a plateau with a net ejection equivalent to about 0.2 Al_2O_3/ion at 5-10 keV . There are no data points above 10 keV, but the general trend should follow the nuclear stopping power until electronic sputtering becomes dominant. For silicon dioxide the energies 1-300 keV are fairly well investigated (fig. 20). These data show that there is a plateau from 5 to 300 keV similar to that at comparable velocities in fig. 1b for water.

Theoretical comparisons are difficult for the oxides since the magnitude of the effective surface barrier, U, is not known accurately. Kelly (1987) and Bach (1988) have used the atomization energy instead of the sublimation energy in order to

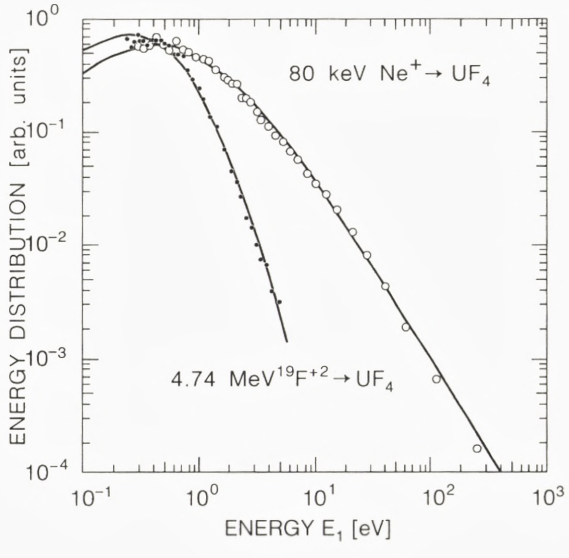

Figure 21. Energy spectra of sputtered U-atoms from UF_4 at medium mass ion bombardment (Griffith et al., 1980). The lines are a fit to $E/(E+U)^n$. For Ne^+ ion bombardment, $n = 2.6$ and $U = 12.0$ eV. For F^{+2} ion bombardment, $n = 6.1$ and $U = 0.71$ eV.

evaluate the yield, as discussed. This is the sum of the formation enthalpy for the oxide, the sublimation energy of the metal atom, and the dissociation energy for oxygen. Essentially, one divides the ejection process into subprocesses: the molecule is split into its gas-phase constituents, the metal atom is evaporated from the solid, and the oxygen molecule is dissociated. This gives an average value for U, although different values should be used for the ejected oxygen and metal atoms, because the forces at any surface site depend on the atom and on the atomic environment.

Sputtering of uranium atoms from uranium tetraflouride was studied by Griffith et al. (1980) with keV as well as MeV medium mass ions. The yield of uranium atoms, obtained from neutron activation analysis, was about 0.2 per ion for 100 keV-ions, which corresponds to a surface binding energy of 2.5 eV.

A study on low energy sputtering of tantalum oxide by argon and helium ions was recently reported (Baretzky et al., 1992). Preferential sputtering was shown to be governed by collision processes rather than by diffusion and segregation. Sputtering of the high T_c-superconductors has so far not been studied systematically, although the partial yields obviously play a key role in the thin-film deposition by sputtering. A complicating feature is the expected strong directional dependence

because of the anisotropy of the crystal structure (Geerk, 1993).

Energy spectra of metal atoms from oxygen-covered surfaces have been studied comprehensively (Betz, 1987; Dullni, 1984; Kelly, 1987). The energy distributions of the metal atoms are broadened compared with the emission from pure metal surfaces. Usually, this is characterized by a fitting parameter that replaces the sublimation energy in the energy distribution in eq. (8a). This parameter is often a factor of 2-3 larger than the sublimation energy. The relevance to regular oxides is not certain. The energy distribution of sputtered uranium atoms from uranium tetraflouride by 80 keV Ne-ions (Griffith et al., 1980) is typical of a linear collision-cascade (fig. 21). At high ejection energies (100 eV) the distribution shows a tail $E_1^{-1.6}$, close to the E_1^{-2}-tail in eq. (8a). The position of the maximum is at 0.35 eV, which is much lower than that inferred from the yield measurements by use of eqs. (4) and (6a).

8.2.3 Frozen Gases

Generally, the sputtering of the most volatile frozen gases shows the most pronounced deviation from the linear collision-cascade description. The energy spectra of the emitted particles, the energy dependence of the sputtering yield, and, in some cases, the dependence on incident angle have been studied.

Frozen gases often exhibit energy spectra with an E_1^{-2} high-energy tail, indicating that the linear collision-cascades dominate at an early stage of the sputtering process, as in eqs. (8a) and (8b). However, the maximum of the energy distribution, if seen, is usually substantially below one-half of the sublimation energy (Brown & Johnson, 1986), appropriate for eq. (8a). Even at low collisional excitation density, large λ_c, the effective surface binding energy deduced using eq. (8a) is below the sublimation energy (O'Shaughnessy et al., 1988a; Pedrys et al., 1985; Pedrys, 1990, 1993). At small λ_c the nonlinear behavior of the collision cascades enhances the low-energy ejecta, which is seen for solid xenon bombarded by xenon ions at 1-30 keV (Pedrys, 1990; O'Shaughnessy et al., 1988a).

The results for the total yields show the trend predicted from linear collision-cascade theory (eqs. (4) and (6a)) if the collisional excitation density, λ_c^{-1}, is small and/or the sublimation energy large. The best agreement for frozen gases is found for medium-mass ions incident on solid krypton and xenon (Stevanovic et al., 1984; Boring et al., 1987; O'Shaughnessy et al., 1988a). For the water ice results at low values of the stopping cross section S in fig. 1b (Christiansen et al., 1986; Bar-Nun et al., 1985), very rough agreement with the linear collision-cascade theory has been reported, even though the yield is controlled in part by formation and reaction of radicals, so that sputtering from this material is a complex process.

Generally, the agreement with the linear collision-cascade theory is fair for the

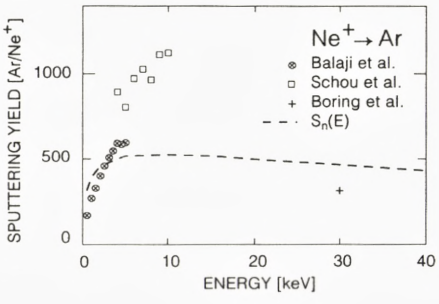

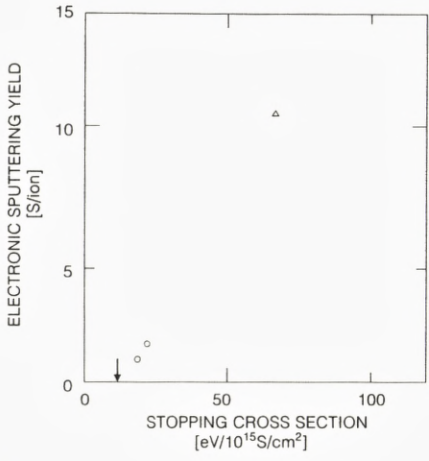

Figure 22. Sputtering yield for Ne^+ ions incident on solid Ar. ⊗, Balaji et al. (1990); □, Schou et al. (1992); +, Boring et al. (1987). Dashed line, the nuclear stopping cross section, calculated from Schou (1988) and normalized to the yield at $E = 2.75$ keV.
Figure 23. The electronic sputtering yield of sulfur as a function of the electronic stopping cross section, $(dE/dx)_e/N$, Δ, 1 MeV He^+ from Torrisi et al. (1986); ○, 49 keV and 33 keV H^+ from Chrisey et al. (1988). For MeV H^+, no sputtering was obtained; arrow indicates the rough threshold of dE/dx for which no erosion was measurable.

total yield up to much higher primary energies and for much higher collisional densities than for the energy distribution. The reason for the discrepancy is not known. It is possible that the energy distributions, which in all setups are measured for a limited solid angle around an exit angle perpendicular to the surface and for ions at non-normal incidence, may not be representative of all exit directions and of normal incidence. There is also a relatively low dE/dx threshold for nonlinear effects in the condensed gas solids, as discussed, and a linear region exhibiting spike effects can occur (Ellegaard et al., 1990, 1992). An example of a 'spike' regime, characterized by a strongly nonlinear dependence of the yield on the nuclear stopping power, is shown in fig. 22 for neon ions incident on solid argon. A similar trend is observed for neon ions on neon (Schou et al., 1992). Balaji et al. (1990) show that the yield for solid rare gases in general increases very strongly at low incident ion energies, whereas the point obtained by O'Shaughnessy et al. (1988a) shows that the yield decreases at high ion energies. The very large yield from such systems means that atoms are not individually ejected from an intact surface, as discussed.

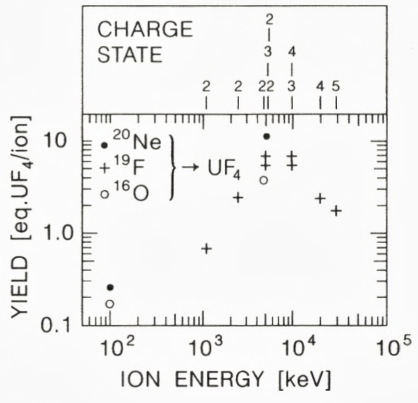

Figure 24. Knock-on and electronic sputtering yield from UF_4 in units of equivalent molecules per ion. Data points from Griffith et al. (1980). The charge state of the incident ion is shown above the yield figure.

9 Electronic Sputtering

9.1 Sulfur

As for knock-on sputtering, sulfur is the only elemental solid room-temperature insulator that has been investigated. Only, the three data points and a threshold value for the total yield shown in fig. 23 were obtained at low temperature (Torrisi et al., 1986; Chrisey et al., 1988). The trend observed for a number of other low-temperature frozen gases, to be discussed, suggested that this yield also is roughly quadratic in the stopping power above threshold, consistent with the thermal spike result in eq. (14), for the most common fragment, S_2 (Chrisey et al., 1988). The empirical efficiency for knock-on sputtering, Λ_c in eq.(4), is found to be about three times higher than that measured for electronic sputtering, Λ_e in eq. (20c). Such a difference is consistent with the results for other frozen gases.

An interesting feature of electronic sputtering of sulfur is the formation of a sputter-resistant residual layer. The material, which is primarily produced at low excitation densities, is probably polymerized sulfur. Because of its size, S_8 is not ejected efficiently by light ions so that the threshold seen in fig. 23 is associated with the competition between the formation and ejection of S_2, and the polymerization of sulfur which increases the effective U.

9.2 Refractory Materials

Electronic sputtering of refractory inorganic insulators occurs for high energy medium and heavy mass ions. Because the yields are small, sensitive methods are required so that these materials have not been studied as comprehensively as, for example, the alkali halides. The observation by Biersack & Santner (1976) that the sputtering yield of potassium chloride follows the electronic stopping power rather than the nuclear one stimulated the investigations of oxides, nitrides and other refractory materials (Betz & Wehner, 1983). Ion production by high-energy ions is summarized by Wien (1989, 1992) and Håkansson (1993). The luminescence spectra and defect formation are comparatively complex for these materials. It is known that luminescence and defect formation in silicon dioxide are correlated (Itoh et al., 1990), but the implications for sputtering of this material and other refractory materials are not clear.

Uranium tetrafluoride has been comprehensively studied. The yield was obtained for fluorine and chlorine ions from 1 to 30 MeV (Griffith et al., 1980; Meins et al., 1983) (fig. 24). The sputtered uranium atoms were detected by neutron activation analysis. Since there was no indication of preferential sputtering, the yield is given in equivalent molecules/ion. The yield as a function of incident ion energy follows the electronic stopping power (Seiberling et al., 1982), estimated from Ziegler's (1980) tables using Bragg's rule (Sigmund, 1975a). The yield decreased with stopping power above the peak much faster than linearly. At the stopping power peak $Y = 7$ molecules/ion for incident fluorine, an impressive value since that for knock-on sputtering is more than one order of magnitude lower (fig. 24).

Griffith et al. (1980) also investigated the effect of the primary ion type and charge state. For oxygen, fluorine, and neon ions, of the same charge state and energy per mass, shown in fig. 24, they found that the yield increased by a factor of 3, although the nuclear charge of the incident ion increased by only 25 percent. An increase of the charge state from 2 to 3 also led to a 30 percent enhancement of the yield. For a charge-equilibrated chlorine beam, the sputtering yield exceeded 100 molecules/ion (Meins et al., 1983). In contrast to this, the yields for bombardment of uranium tetrafluoride with 1 to 4 MeV helium ions were barely measurable, suggesting there is a threshold excitation density.

The energy distribution of uranium atoms emitted from uranium tetrafluoride during bombardment by 4.74 MeV F^{+2} had a maximum at about 0.3 eV (Griffith et al., 1980). Above this maximum the energy distribution decreased rapidly, exhibiting an asymptotic behavior close to E_1^{-5} in contrast to that for knock-on sputtering described earlier. Seiberling et al. (1980) interpreted this to be a thermal distribution with an effective temperature around 4100 K. A similar distribution induced by 13 MeV Cl-ions led to an effective temperature of $\sim$ 5200 K. The

authors argued that the trends may be described by a thermal spike model, eqs. (12)-(15), in which the lattice is heated by Coulomb repulsion, as discussed earlier. This group also obtained the only experimentally determined angular distribution for electronic sputtering. The data points for emitted uranium atoms from a film bombarded by 4.75 MeV $^{19}F^{+3}$-ions are well approximated by a cosine-function, consistent with the spike model.

The yield of uranium atoms from uranium dioxide under bombardment of 5 to 30 MeV chlorine ions with charge states from $q = 3$ to 6 was more than three orders of magnitude less than the corresponding one for uranium tetrafluoride (Meins et al., 1983).

Qui et al. (1982) measured the electronic sputtering yields from sapphire (Al_2O_3) and lithium niobate ($LiNbO_3$) with chlorine ions at energies between 3 and 25 MeV. The yield, determined by forward Rutherford scattering, varied from about 0.05 to 1.0 Al_2O_3/ion (fig. 19) and 0.06 to 0.12 $LiNbO_3$/ion. The data points lie on the low-energy side of the stopping power peak for both materials and vary nearly linearly with the electronic stopping power. Although they noted that lithium niobate is a much softer material than sapphire, and the latter has a higher thermal diffusivity than the former, these differences had no obvious influence on the yield.

Qui et al. (1983) also studied the sputtering of silicon and its compounds in the electronic stopping regime with chlorine ions at 5 and 20 MeV. Silicon showed a very low yield, probably without any electronic component. The yield from crystalline and fused silicon dioxide was measured for chlorine ions in the equilibrium charge state at 5 and 20 MeV (fig. 20). The average values for fused silicon dioxide were about ten percent larger than those for crystalline quartz, even though the authors consider this difference to be insignificant. They observed that a thickness of more than three monolayers of the oxide film is required for electronic sputtering. This effect has been confirmed by Sugden et al. (1992), who did not observe any electronic sputtering for a thin native oxide layer ~ 0.1 nm. According to the latter group the threshold thickness is about six monolayers. They also found that silicon dioxide is sputtered stoichiometrically, and the yield for perpendicular incidence, measured by a nuclear reaction technique, was almost twice as high as that measured by Qui et al. (1983), partly explained by a higher charge state. At 20 MeV the yield induced by equilibrium charge state chlorine, ($q = 11$) and angle of incidence of $\theta = 70°$, was about a factor of 2 larger than that for $q = 6$ (Sugden et al., 1992). They also found the yield varied with the angle of incidence as $(\cos\theta)^{-1.7}$. This is surprisingly similar to the result in eq. (16), also seen for frozen gases.

The processes that lead to electronic sputtering in these materials are not known, although trapping of excitons is accompanied by defect production (Gris-

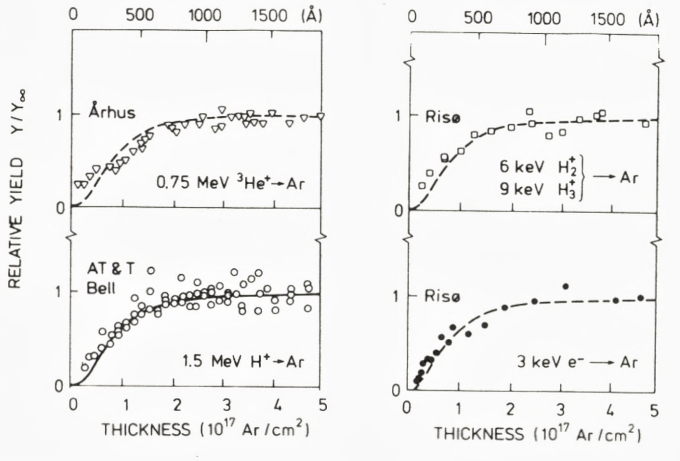

Figure 25. The thickness-dependence of electronic sputtering from solid argon for different projectiles. The relative yield is plotted versus thickness. All yields have been normalized to the thick-film yield $Y_\infty = 1$. Solid and dashed lines, eq. (25c) with $\ell_h = 210$ Å. Solid line from Reimann et al. (1984b) as reference. $^3He^+$, from Besenbacher et al. (1981); 3 keV e^-, from Ellegaard et al. (1988); hydrogen ions from Schou et al. (1987). (From Schou, 1987).

com, 1989). Fiori and Devine (1984) observed that laser irradiation created defects and oxygen deficiency in thin, amorphous silicon dioxide layers. Helium ions were more efficient in depleting the surface of oxygen than heavy-rare gas ions (Thomas & Hoffmann, 1985), and low energy neon ions are more efficient than neon neutrals of the same energy (Mizutani, 1991). Even though the low-energy results involve electronic excitations, the relaxation processes can be very different from those initiated by fast ions.

One oxide frequently studied is titanium oxide. Unfortunately, measurements have been made mainly for the emitted ions (Knotek & Feibelman, 1978; Kurtz, 1986; Kurtz et al., 1986). This desorption process has also been correlated with defect structures.

A strong yield dependence on the stopping power was observed for europium oxide bombarded by heavy rare gas and uranium ions with an energy between 0.5 and 1 MeV/amu (Guthier, 1986). The yield was roughly proportional to the stopping power cubed, which is suggestive either of threshold behavior for a thermal spike (fig. 3) or a hydrodynamic model, eq. (18b) (Wien, 1992; Reimann, 1993). Although obtained with unsatisfactory vacuum conditions, these yields represent the highest primary energy studied.

9.3 Frozen Gases

The group of the frozen gases is the most comprehensively studied for electronic sputtering:

A) the samples are relatively easy to handle and the yields are large,

B) the yield dependence on film thickness may be easily measured

C) for the elemental gases, the energy release processes in the gas phase are largely known,

D) many of the irradiated gases show strong luminescent features from which the excited states in the solid may be identified.

The group of frozen gases is divided into the rare gas solids, solid elemental molecular gases, and solid heteronuclear molecular gases. Early experiments suggested condensed gases were efficiently sputtered by electronic processes (Erents & McCracken, 1973, 1975), but systematic studies began in 1978.

9.3.1 Solid Rare Gases: Argon

Sputtering yields for the rare gas solids all exhibit a pronounced thickness dependence. This is suggested as being caused by transport of the deposited electronic energy either as mobile excitons or holes. In addition, the luminescence from these solids during charged-particle or photon bombardment is well known (Schwentner et al., 1985; Zimmerer, 1987), and many of the emitted bands can be assigned to identified excited states. Among the rare gas solids, argon has become the standard system.

The dependence of the yield on argon film thickness is shown in fig. 25, resembling that in fig. 10b. The figure includes data from three laboratories and four types of projectiles. The thickness dependences are similar, giving a characteristic diffusion length, ℓ_h in eq. (25c), of about 200 Å (Schou, 1987). This suggests that mobile excitons or holes generated within this depth are quenched at the substrate (Reimann et al., 1984b). Because the excitations are mobile they can also reach the surface and contribute to sputtering as described, eqs. (24) and (25b). Similar data for 0.2 keV electrons (Hudel et al., 1991) show a faster increase to saturation, indicating that the range of the electrons is smaller than the diffusion length.

The value $\ell_h = 210$ Å obtained by Reimann et al. (1984b) is used as a common reference in fig. 25, although reevaluation gave $\ell_h = 230$ Å (Reimann et al., 1988). The simultaneous measurements of the luminescence and sputtering yield as a function of argon film thickness were decisive for understanding the sputtering process. The similarity of the extracted diffusion lengths and the description of the two emission phenomena by the same diffusion equations was a strong argument

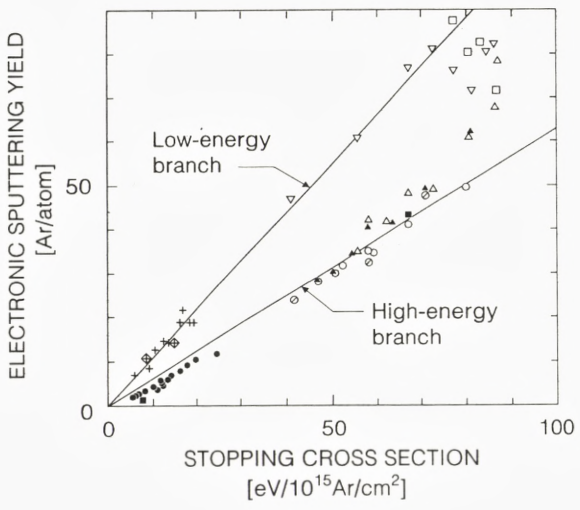

Figure 26. The electronic sputtering yield from solid Ar as a function of the electronic stopping cross section, $(dE/dx)_e/N$ for Ar. Data from Reimann et al. (1988); •, H^+ (QMS); ○, $^4He^+$ (QMS); ⊘, $^3He^+$ (QMS); filled squares, He^+, H^+ (RBS). Data from Besenbacher et al. (198l); filled triangles, $^3He^+$, $^4He^+$ (high velocity) (RBS); ▽, $^4He^+$ (low velocity) (RBS); □, He^{2+} (RBS). Data from Schou et al. (1988); +, H^+ , crossed diamond, He^+. The solid lines represent the high-energy and low-energy branches. Stopping cross section are from Andersen and Ziegler (1977) and Ziegler (1977).

that the same mobile excitations are responsible for photon emission and sputtering (Reimann et al., 1984b). Further, since impurities both trap and quench excitations (eq. (22a)) ℓ_h varied with oxygen impurity concentration (Reimann et al., 1988).

The agreement between diffusion lengths obtained by traditional optical methods (Schwentner et al., 1985; Zimmerer, 1987) and those obtained by particle bombardment is not good. The results produced with light MeV ion bombardment involve a constant energy deposition along the path of the ion through the thin film. Since this geometry requires few assumptions to interpret the data, these diffusion lengths appear to be firmly established. The data for low-energy ion or keV electron impact are more difficult to disentangle, since the profile of the deposited energy changes, because of either a varying stopping power for the ions or backscattering of the primary electrons.

Films which have been utilized to obtain fig. 25 are produced either using a jet of gas onto a cold target or emitting gas through the channels of a microchannel plate to obtain a more uniform solid. These are polycrystalline films with a considerable defect density (Zimmerer, 1987). In a few cases improved crystal quality has led

Table III

Diffusion Length in Solid Rare Gases at Charged-Particle Bombardment

Material	Ref.	Primary Particle	Length (Å)	Film growth temp. (K)
Ne	Schou et al. 86	2 keV e^-	230[1)]	6
	Hourmatallah et al. 88	24 eV e^-	252[1)]	8
Ar	Schou et al. 87	9 keV H_3^+	190	7
		6 keV H_2^+		
	Ellegaard et al. 88	2 keV e^-	200-300	7
	Besenbacher et al. 81	0.75 MeV $^3He^+$	270[2)]	8
	Hourmatallah et al. 88	24 eV e^-	310	10
	Reimann et al. 84	1.5 MeV H^+	190[3)]	12
		1.5 MeV He^+		
	Reimann et al. 88	1.5 MeV H^+	230[3)]	12
		1.5 MeV He^+		
	Hourmatallah et al. 88	24 eV e^-	383	17
	Hourmatallah et al. 88	24 eV e^-	436	22
	Hourmatallah et al. 88	24 eV e^-	845	25
Kr	Schou et al. 87	9 keV H_3^+	300	7
		6 keV H_2^+		
Xe	Ollerhead et al. 80	1 MeV He^+	500[4)]	25

Concerning the accuracy consult the references. 1) Absorbing-like boundary conditions for the surface. 2) Evaluated by Reimann et al. (1984b). 3) Same experimental points. Improved valuation in Reimann et al. (1988). 4) The length evaluated by Schou (1987).

to an enhanced diffusion length (Table III) (Hourmatallah et al., 1988); therefore, the measured diffusion length can depend on the fluence of the primary particle (Varding et al., 1993).

Three studies with photon irradiation have demonstrated that particle ejection takes place via exciton production. Feulner et al. (1987) and Kloiber & Zimmerer (1989, 1990) showed that selective photon excitation of the surface or bulk states induces sputtering. A strong enhancement of the yield for excitation energies above the energy gap was observed by Kloiber & Zimmerer (1989). The dominant mobile carrier of the excitation has not yet been identified, although it is thought to be an atomic hole or a free, highly excited exciton, as suggested by Reimann et al. (1984b) for MeV ion excitation of argon. The carrier can, of course, depend on the excitation process: e.g., ions produce excitons and holes with large wave numbers.

Yields for ion bombardment of thick solid argon films are shown in fig. 26. These have been obtained at three laboratories using several methods. For the two low-energy He-ions points the yields have been corrected for knock-on sputtering (Schou et al., 1988); otherwise, it is ignored. These yields lie on a common curve having two 'branches', and the data from different laboratories smoothly merge together. The branches roughly correspond to values on each side of the electronic stopping power peak (viz. fig. 1a). The yields on the low-energy side are ~1.7 times those on the high energy side at the same stopping power. Each branch may be approximated as a linear function of the electronic stopping cross section up to $\sim$ 70 eV/10^{15} Ar/cm^2. Using eq. (20c) and (21c) gives, $\overline{\Delta x_e} \approx 17$ and 29 ℓ respectively, or using $(dE/dx)_e$, $\Lambda_e \approx 2.4$ and 4.1 Å/eV respectively.

Differences in yield for the same value of the equilibrium stopping power, $(dE/dx)_e$, can occur for four reasons (Johnson & Brown, 1982):

(1) non-equilibrated charge states;

(2) a difference in the character of the excitations at different velocities (fig. 1a); and

(3) differences in the radial distribution of the deposited energy (fig. 6a), leading to increased excitation density at low velocity,

(4) difference in surface excitation density due to secondary excitation transport.

In the sputtering of refractory materials (Griffith et al., 1980) and solid oxygen (Gibbs et al., 1988), increasing ion charge state leads to an enhanced yield. The charge state and radial distribution are not expected to be as important for the solid rare gases as they are for other solids, since charge equilibration distances and mean radial distributions of secondaries are typically smaller than the diffusion length (Reimann et al., 1988). Therefore, the enhancement observed at low ion velocities is likely to be due to the changing character of the excitation spectrum, suggested

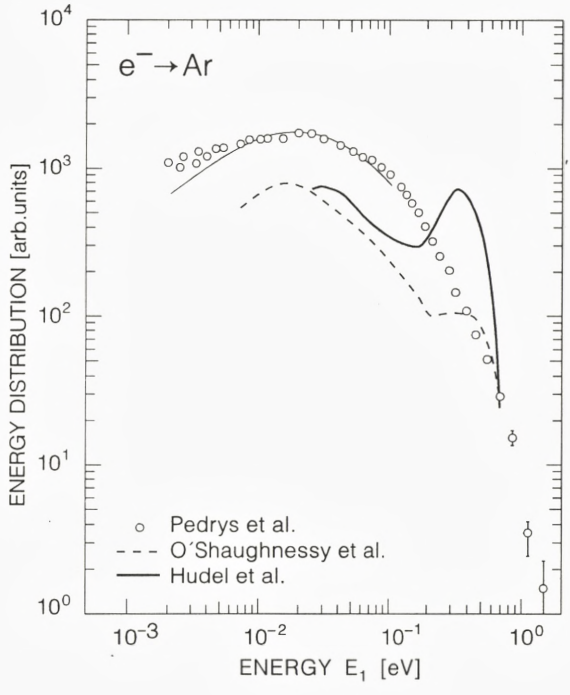

Figure 27. Energy spectra of Ar-atoms from electron-irradiated solid Ar. The three data sets have been place arbitarily relative to each other. The solid line through the points from Pedrys et al. (1988) is a fit with eq. (8a) for $U = 60$ meV. Pedrys et al. (1988), 0.5 keV e^-, $\theta = 45°$, $\theta_1 = 0°$. O'Shaughnessy et al. (1988), 2.5 keV e^-, $\theta = 45°$, $\theta_1 = 0°$. Hudel et al. (1991), 0.2 keV e^-, $\theta = 0°$, $\theta_1 = 0°$.

by figs. 1a and 7. However, Besenbacher et al. (1981) found, in the transition region, that the sputtering yield of argon is about 20 per cent larger for doubly charged helium ions than for singly charged ions, a change not unlike that for solid oxygen.

The dimerization process described earlier produces kinetic energy that ultimately leads to particle ejection. The mobile holes become trapped at the surface or in the bulk, forming Ar_2^+. The repulsive decay scheme then follows that described by Johnson & Inokuti (1983) (see fig. 8), although the recent observations of a resonant state which can lead to energy release is intriguing (Michaud et al., 1993). Since the mobile electrons are not trapped efficiently in argon (Sowada et al., 1982), the trapped holes will eventually capture an electron. The resulting repulsive dissociative recombination may liberate up to $\sim$ 1 eV to the two atoms (eq. (21c)). If this occurs in the surface layer, a ground state or excited atom is

ejected. If in the bulk, the electronically excited atom then can form a molecular exciton which decays radiatively to the repulsive ground-state, releasing ~ 1.1 eV. Since these energies are much larger than the cohesive energy of solid argon, a low energy collision cascade is generated [viz. eq. (27) and fig. 11] leading to ejection of ground state atoms. This relaxation sequence has been extensively discussed (Reimann et al. 1984b, 1988; Brown & Johnson, 1986; Schou, 1987, 1991). Quite remarkably, the luminescence and sputtering yields for fast penetrating ions are only slightly modified when an outside field is applied producing a large secondary electron yield (Grosjean & Baragiola, 1993).

The energy distributions of the ejected particles, combined with molecular dynamics calculations using the gas-phase ground-state pair potentials, have led to a definitive identification that the ground-state repulsion leads to ejection. The energy distributions shown in fig. 27 have either a peak around 0.5 eV (Hudel et al., 1991) or a shoulder (O'Shaughnessy et al., 1988b, Pedrys et al. 1988). Since the peak size depends on film purity, film structure, and, possibly, angle of detection, the conditions in each experiment are not completely comparable. The peak is due to the excimer emission, $Ar_2^* \ (^{1,3}\Sigma_u^+) \rightarrow Ar_2 \ (^1\Sigma_g^+) + \hbar\omega$, with the peak width determined by the ground vibrational state of Ar_2^* decaying to the repulsive part of the ground-state potential, as indicated in fig. 8 (O'Shaughnessy et al., 1988b). Therefore, the area under the peak was used to estimate the surface vs. the bulk trapping probability using eq. (23): i.e. $(\tau_h/\tau_h^s) \approx 4.7$ in the films studied (Boring et al., 1989). All three curves have a distinct low-energy peak due to low-energy, cascades following a repulsive decay below the surface [eq. (27) and fig. 11], again confirmed by molecular dynamics calculations (O'Shaughnessy et al., 1988b). A comparison to the linear collision cascade energy spectrum is made for one data set using an effective surface binding, $U = 60$ meV in eq. (8a).

Excited ejected atoms are clearly observed in the luminescence spectra as these exhibit narrow atomic lines. For photon and electron excitation at low kinetic energy, metastable neutrals $Ar^* \ ^3P_0$ and $^3P_2$ were detected by Arakawa et al. (1989), Arakawa & Sakurai (1990), Kloiber & Zimmerer (1990), and Leclerc et al. (1990, 1992). The maximum value kinetic energy, ~ 40 meV, originates from the repulsive interaction associated with cavity formation occurring around the atomic exciton (figs. 8 and 9b). This ejection process occurs in addition to dimer decay, as suggested by Coletti et al. (1984) and as corroborated by molecular dynamics calculations (Cui et al., 1989a, Reimann et al. 1990, 1991). The measurements of the energy distribution of metastable neutrals ejected by 200 eV electrons showed the low-energy peak around 40 meV and a high-energy feature (Arakawa et al., 1989). The studies with 14.5 eV electrons have resolved the low-energy peak into three components (Leclerc et al., 1992) which are characterized by the numbers of nearest neighbors in accordance with the studies of molecular dynamics (Cui et al.,

1989a). The high-energy peak had a maximum around 0.35 eV and a full-width of half maximum of 0.19 eV (Leclerc et al., 1992). This peak, partly embedded in the ground state peak in fig. 27, suggests that about 0.7 eV, on the average, is liberated by the upper state transition in fig. 8, Eq. (21c), a dissociative recombination predicted by Johnson & Inokuti (1983). Therefore, a dominant solid-state, electron-hole recombination pathway has been identified from particle ejection studies.

The well known W-band in the luminescence spectrum was shown to be a surface feature as adsorbed atoms could quench it but not the M-band (Roick et al., 1984). It was later shown to be due to luminescence from ejected electronically-excited dimers in high vibrational states (Reimann et al., 1988, 1990, 1991). The kinetic energy of these excited dimers is low, about 60 meV, suggesting they originate from cavity ejection (Cui et al., 1989b). However, a distribution of vibrational states is seen, including the ejection of Ar_2^* in low vibrational states but with higher kinetic energy, $\sim$ 100 meV. Because of the inefficiency of transfer of vibrational energy into lattice motion, the origin of more energetic dimers in low vibrational states is not clear. Three-body interactions involving an energetic, excited argon atom from a dissociative recombination, or recombination involving Ar_3^+, might be precursors of energetic-relaxed excimers Ar_2^* (Reimann et al., 1991, 1992).

For photon and electron excitation, thresholds are exhibited for ion emission (Dujardin et al., 1990; Baba et al., 1991; Schwabenthan et al., 1991; Menzel, 1990). Again, gas phase cross sections are instructive. For example, simultaneous excitation of two 3p-excitons in adjacent atoms was used to explain a threshold around 24 eV in the emission of Ar^+ and Ar_2^+ induced by low-energy electrons (Baba et al., 1991).

9.3.2 Solid Rare Gases: Neon, Krypton and Xenon

Solid neon is much more volatile than argon, whereas the heavy rare gas solids are correspondingly less volatile. The sublimation energy varies from 20 meV for neon up to 164 meV for xenon (Table I). The atomic excitons are important primarily for solid neon and argon, and formation and vibrational relaxation of the molecular excitons occurs more efficiently with increasing atomic number (Zimmerer, 1979, 1987). The luminescence in neon originates from atomic rather than molecular excitons, and the molecular excitons have not yet been observed in the vibrational ground state. Although the energy release following emission from the molecular exciton in the vibrational ground state decreases with increasing atomic number, the exciton in neon decays from a vibrationally excited state. Therefore, the average energy release is $\sim$ 200 meV, compared with $\sim$ 1.1 eV for solid argon.

The electron-induced sputtering yield from solid neon is almost an order of magnitude larger than that from argon consistent with the small sublimation energy

(Table I) (Schou et al., 1986). It appears that the net conversion of electronic energy into atomic motion from all channels is about as efficient for solid neon as for argon based on low energy keV hydrogen ion bombardment of neon. The diffusion length of excitons in solid neon irradiated by electrons from 0.8 to 3 keV was determined to be $\sim$ 230 Å (Schou et al., 1986)[5] consistent with $\sim$ 250 Å using 24 eV-electrons (Hourmatallah et al., 1988, see Table III).

Neon atoms are also ejected due to VUV-photon irradiation. Mass spectroscopy studies (Kloiber & Zimmerer, 1989) and luminescence studies (Coletti & Debever, 1983) were used to show that neutral desorption occurs for incident electrons with energies below the band gap. The results from Kloiber et al. (1988) and Kloiber & Zimmerer (1989) demonstrate that the excitation of the $n' = 1$ excitons leads to a yield that is almost as large as that from photons just above the energy gap. These experiments did not provide any clear evidence on the type of the mobile excitation, an atomic hole or a highly excited free exciton. Ellegaard et al. (1986a) noted the absence of a thickness dependence during bombardment by keV hydrogen ions. Comparing the ionization cross sections (Rudd et al., 1985) to stopping cross sections, they conclude these ions largely produce excitations below the ionization threshold of neon, implying the mobile excitation is an atomic hole.

Although the yield of excited neutrals is about one-tenth of the total yield (Kloiber et al., 1988), a rich structure is exhibited. For instance, exciton trapping below the surface can lead to ejection of the excited species as well as ejection of ground state atoms (Coletti et al., 1985; Hourmatallah et al., 1988; Laasch et al., 1990). This occurs because the sublimation energy is low but lattice distortion energy is large and differs for trapping at the surface or in the bulk, as indicated by the shifts in the luminescence spectra. The distribution of kinetic energy of the emitted $^3P_2$ and $^3P_0$ atoms was measured by Kloiber & Zimmerer (1990) and Weibel et al. (1993). The most probable value of the energy of these atoms ranged from 0.16 eV up to 0.25 eV depending on the excitation energy (Fugol' et al., 1988; Belov et al., 1989; Kloiber & Zimmerer, 1990). According to Fugol' et al. (1988) the trapping of a $3p$-exciton leads to an energy release of 0.8 eV which is responsible for the ejection of the $3p$- atoms. A diffusion length before trapping of the order of a few hundred Å is again extracted from these luminescence data.

Charged-particle bombardment of solid krypton has been studied systematically for keV hydrogen ions (Schou et al., 1987). The diffusion length is $\sim$ 300 Å, slightly larger than that for argon, consistent with theory (Fugol', 1988). The yield is smaller than that for argon, in agreement with the larger sublimation energy of solid krypton, eqs. (20c) and (27).

The energy release following M-band emission is about 0.8 eV and the fraction

[5]The data points from Børgesen et al. (1982) were not corrected for energy-dependent beam broadening.

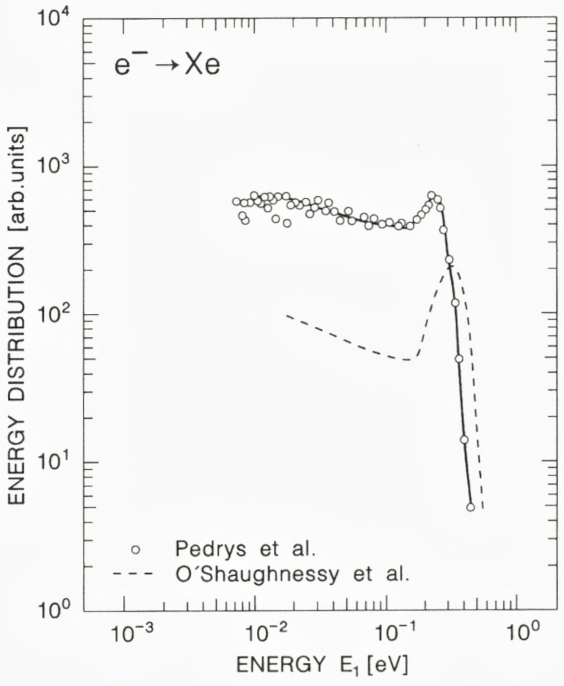

Figure 28. Energy spectra of Xe-atoms, see fig. 27. The line through the data points of Pedrys et al. (1988) has been drawn merely to guide the eye.

of the ejecta associated with surface trapped species was shown to be larger than that for solid argon (Boring et al., 1989) with (τ_h/τ_h^s) in eq. (23) about 6.5 for the films studied. Arakawa et al. (1989) observed excited neutrals with energy up to more than 0.7 eV, presumably from dissociative recombination, and Mann et al. (1992) observed metastable neutrals under bombardment with eV electrons. Low energy metastable krypton atoms resulting from trapping at the surface were not seen (Arakawa et al., 1989), consistent with molecular dynamics calculations (Buller & Johnson, 1991), since the cavity-forming, repulsive interaction is not as strong as in argon (Kloiber and Zimmerer, 1989). The total yield of the metastable atoms increased with thickness up to about 100 atomic layers consistent with the diffusion length determined from the total yield due to hydrogen ion bombardment. Because the metastable neutrals originate via recombination (fig. 8), the atomic hole is the dominant mobile excitation.

For solid krypton irradiated by photons, there is a substantial sputtering for photon energies that coincide with the lowest excitonic levels, but ejection also

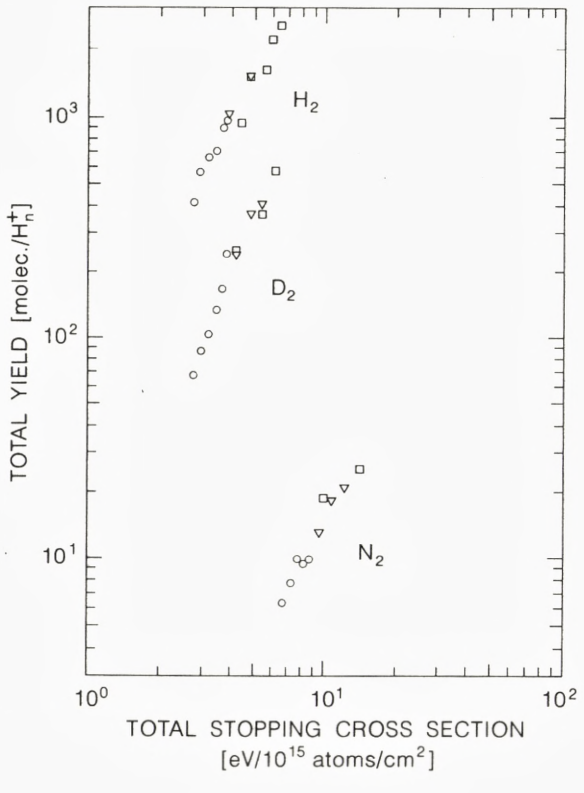

Figure 29. The yield as a function of the sum of the stopping cross sections of the atoms in the hydrogen ions. ○, H+; ▽, H_2^+; □, H_3^+. Nitrogen data from Ellegaard et al. (1993a), deuterium data from Stenum et al. (1990), hydrogen data from Stenum et al. (1991) and Schou (unpublished).

occurs for photon energies above the band gap (Feulner et al., 1987; Kloiber & Zimmerer, 1989, 1990). In particular, the yield increases strongly for photon energies above the threshold for electron-electron scattering.

Electronic sputtering yields for solid xenon by light ions, 0.2 MeV - 2 MeV, were originally interpreted as thermal spike sputtering (Ollerhead et al., 1980). However, the few data are consistent with a yield versus stopping power, $(dE/dx)_e$, with two branches which depend linearly on the stopping power (Schou, 1987). The ratio of the yield divided by the electronic stopping cross section, Y/S_e, is about a factor of five lower for xenon than argon, because of the higher sublimation energy and the smaller energy release after M-band emission. This energy is clearly indicated by the peak at ~ 0.3 eV in the energy distribution of emitted xenon atoms from electron-bombarded xenon (fig. 28). Since this energy is comparable to the

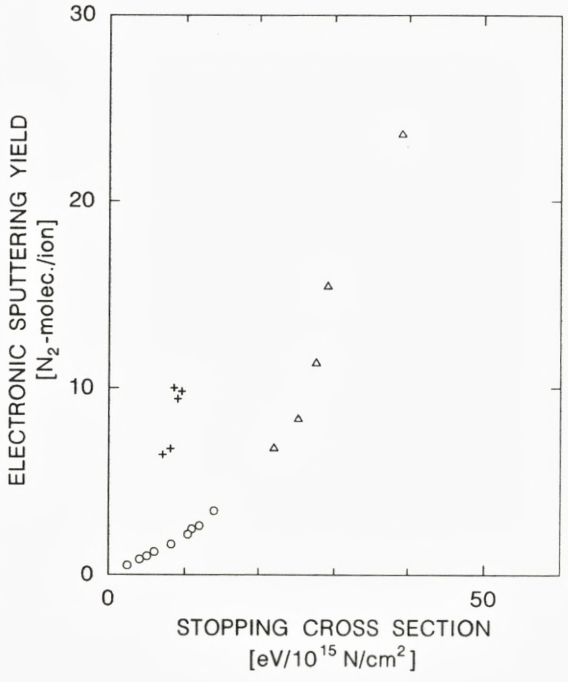

Figure 30. The electronic sputtering yield from solid N_2 as a function of the electronic stopping cross section, $(dE/dx)_e/N$, for N_2. Data from Johnson et al. (1991), ○, H^+; Δ, He^+. Data from Ellegaard et al. (1993a), + , H^+.

sublimation energy, no clear low-energy peak due to decay below surface is seen in the xenon spectra for incident keV electrons (O'Shaughnessy et al., 1988b; Pedrys et al., 1989). Here enhanced surface trapping of excitons dominates sputtering, with (τ_h/τ_h^s) in eq. (23) about 3.9 for the films studied (Boring et al., 1989), but no metastables have been observed (Mann et al., 1992).

The yield due to 1 MeV He^+-ions was measured as a function of xenon film thickness (Ollerhead et al., 1980). This gives a rough estimate of the diffusion length of $\ell_h = 580$ Å (Schou, 1987), consistent with the expected trend with the atomic number. The existing measurements do not indicate the predominant mobile excitation. Photon-induced ejection from solid xenon occured for excitation energies at the excitonic levels as well as for energies above the band gap (Kloiber & Zimmerer, 1989, 1990). However, the relative yield decreases with increasing photon energy up to the largest energies studied, around 17 eV.

9.3.3 Solid Elemental Molecular Gases

In addition to frozen S_8, sputtering has been investigated for solid nitrogen, oxygen and hydrogen and its isotopes. The yields for the latter are shown in fig. 29. Like the rare gas solids these van der Waals solids have low cohesive energies, but the sputtering yield does not appear to be controlled by significant exciton mobility. No photon-induced neutral particle emission has been studied, in contrast to the many contributions on photon-stimulated ion emission (e.g., Rocker et al., 1990; Hellner et al., 1990).

Deexcitation processes in solid nitrogen are fairly well known and the optical emission from electronically excited states has been studied (Oehler et al., 1977; Coletti & Bonnot, 1977; Poltoratskii & Fugol', 1979; Zumofen et al., 1984; M. Kühle et al., 1985; Pan et al., 1987). The dominant emission process seen in the luminescence spectrum, $[N(^2D) \rightarrow N(^4S)]$, gives the green line and clearly indicates that dissociation can drive sputtering (Rook et al., 1985), leaving stable radicals in solid nitrogen. The sputtering yield for light ions is shown in fig. 30 versus the stopping cross section exhibiting two branches. The increase in the yield for the low-energy ions over that for the MeV-ions with equal stopping powers is more pronounced than for light ion bombardment of solid argon, probably due to the lack of significant excitation transport. In contrast to argon, these results exhibit both a clear linear and quadratic dependence on the stopping cross section. The electron-induced yield points, not shown in the figure, comprise a curve that lies slightly above the linear part of the lower branch below $S_e = 10$ eV/(10^{15} atoms/cm^2) in fig. 30. Using MeV H^+ and He^+, Brown et al. (1986) mapped the transition from the linear dependence, first observed using keV electrons (Ellegaard et al., 1986b), to the quadratic dependence, first observed using MeV He^+ ions (Rook et al., 1985).

Sputtering is produced by energy deposited in the first four to five monolayers (Banerjee et al., 1991b) for solids without significant excitation transport. Therefore, electronic sputtering by an incident molecular ion is determined by the total stopping power of the constituent atoms in a bombarding molecule (fig. 29). This gives a yield in the quadratic regime for incident H_2^+ which is four times the yield due to an H^+ at the same velocity, in contrast to the results for solid argon (Brown et al., 1982).

Since the excited state mobility is only a few monolayers (Johnson et al., 1991), the changing dependence of the yield seen in fig. 30 can be a result of the increasing excitation density, λ_e^{-1}, going from isolated relaxation processes to closely spaced processes (fig. 3 and eqs. (20c) and (14)). The yields in the transition region can be explained by assuming the electronic relaxation processes do not change with excitation density, but the energy release from individual events acts additively:

overlapping spikes (Johnson et al., 1991). Using the yields in the linear regime and molecular dynamics estimates of $\Delta\overline{x}$ in eq. (27) then $f_e \approx 0.1$, corresponding to energy release $\Delta E \approx$ 2eV - 3eV.

The energy distributions of particles emitted from solid nitrogen have been measured for keV electrons (Pedrys et al., 1988, 1993a; Hudel et al., 1992) for hydrogen ions (Ellegaard et al., 1993a) and for helium ions (Ellegaard et al., 1993b). The dominant particle in the emission flux is the parent molecule, N_2, but atoms and polyatomic molecules with up to four atoms have also been observed. The fraction of monatomic neutrals is considerable, but the polyatomic molecules comprise less than one percent of the diatomic ejecta. The spectrum of the diatomic molecules has no pronounced features, but exhibits a maximum around 20 meV, decreasing steeply at higher energies.

The most obvious recombination process for an intrinsically molecular species is that which is dominant in the gas phase, $N_2^+ + e \rightarrow N + N^*$, (Fox & Dalgarno, 1983). This is clear from the green luminescent feature associated with the $N(^2D)$ radical in solid nitrogen (Rook et al., 1985). For outer shell ionization, such processes deposit a few eV (Oehler et al., 1977), consistent with the energy release extracted from the yield data in the linear regime. However, since there was no distinct high-energy tail of N-atoms in the energy distribution of electron-irradiated solid nitrogen, Pedrys et al. (1993a) suggested that the dimerization process identified in solid argon might also occur efficiently in solid nitrogen,

$$N_2^+ + N_2 + e \rightarrow (N_2)_2^+ + e \rightarrow N_2^* + N_2, \quad \Delta E \approx 1 - 3.7\,\mathrm{eV}.$$

In fact, the interaction between an excited and ground state molecule leading to dimerization has been identified in the luminescence spectrum of a number of materials.

The electronic sputtering yield of solid oxygen has a dependence on $(dE/dx)_e$ which is similar to that of nitrogen, fig. 30. However, there are some differences between these materials which effect the size of the sputtering yield (Rook et al., 1985; Ellegaard et al., 1986; Brown et al., 1986; Schou, 1991). Solid oxygen is known not to luminesce as efficiently and is more active chemically following irradiation. Therefore, the conversion of excitation energy into motion is more efficient than in nitrogen, since other parameters such as the sublimation energy, the number density and the W-value are similar (see Table I). The yield data indicate that $f_e \approx 0.2$ and $\Delta E \approx 4 - 6$ eV (Johnson et al., 1991), of the order of twice that for N_2.

The electron-induced kinetic energy distributions of emitted O_2 (Hudel et al., 1992; Pedrys et al., 1993b) also resembles that for nitrogen, except that the distribution falls off more steeply above 1 eV and the maximum is slightly higher. The energy distribution of oxygen molecules from bombardment by keV hydro-

gen ions is similar to that obtained from electron bombardment (Ellegaard et al., 1993a). Ozone formation can play an important role by quenching the excited radicals created by dissociative excitation or recombination (David & Michl, 1989). Since there is no activation threshold, the reaction does not depend on background temperature. By this process 1.1-6 eV may be eventually liberated, depending on whether the oxygen atom is in the ground or an excited state (Pedrys et al., 1993a). However, the contribution of this energy to the yield is unknown, as is the contribution from processes such as attachment (Sanche, 1984).

The influence of the initial charge state has been investigated. The yield induced by charge-equilibrated 2 MeV He ions with the charge state $q = 1.75$ is a factor of 1.2 larger than that of singly charged ions (Gibbs et al., 1988). This result is, surprisingly, similar to that for argon. These authors also found that the yield $Y(\theta)$ as a function of angle of incidence behaves similarly for the singly charged and the charge-equilibrated ions, and closely fits the thermal spike expression in eq. (16) (fig. 4). These measurements demonstrate that hole production by charge-exchange at the surface is not a dominant channel for electronic sputtering of oxygen.

Electronic sputtering of solid hydrogenic targets deviates in several respects from that of the less volatile solid nitrogen and oxygen. The sublimation energy is extremely low, ranging from 8.7 meV/molecule for hydrogen up to 14.8 meV/molecule for solid tritium. The yield for very thin films of hydrogen or its isotopes is found to be strongly enhanced on all substrates. Even though this effect has been observed during electron as well as ion bombardment (Erents & McCracken, 1973; Børgesen & Sørensen, 1982; Stenum et al., 1990), the origin of the enhancement is not known. A similar enhancement is seen in most condensed gas films at the few monolayer level (Rook et al., 1985; Hudel et al., 1991).

Very few studies of luminescence from solid hydrogen isotopes exist. A relatively strong continuum with a maximum around 800 nm, probably generated by association of neutral atoms, was observed by Forrest et al. (1992). In contrast, very weak features were observed in the visible or ultraviolet region (Schou, 1991; Stenum et al., 1993) suggesting non-radiative relaxations dominate. This combined with the low sublimation energy leads to high sputtering yields. Using 10 keV protons, the yield ranges from about 200 molecules for deuterium and up to about 800 molecules for solid hydrogen per proton (Stenum et al., 1991).

For incident molecular and atomic hydrogen ions the dependence of the yield on the sum of the stopping powers is roughly quadratic for the most volatile molecules, hydrogen and hydrogen deuteride, and cubic for the least volatile molecule, deuterium (Stenum et al., 1991). This nonlinearity shows up also in the dependence on the cohesive energy, U. Sputtering of solid hydrogen is electronic at these velocities since incident deuterium and hydrogen ions of equal velocity produce equivalent sputtering yields and the nuclear stopping power has a different dependence on the

ion energy than does the yield.

Sputtering of solid deuterium by keV electrons deviates strongly from that produced by ions in that the yield decreases, passes through a minimum and then increases with increasing thickness (Erents & McCracken, 1973; Børgesen & Sørensen, 1982; Schou et al., 1984; Ellegaard, 1986). The minimum is typically located at thicknesses that exceed the electron range. The enhancement for thick films was suggested to be due to charging (Schou, 1991). For the solid hydrogen isotopes, the relaxation events determining sputtering are uncertain, although transitions from the repulsive triplet ($b^3\Sigma_u^+$) state to the ground state are a possibility, liberating up to 7 eV (Celiberto et al., 1989).

9.3.4 Solid Heteronuclear Molecular Gases: Water Ice

Electronic sputtering of water ice has been extensively studied because of its importance in the outer solar system and the interstellar medium (Johnson, 1990; Greenberg & Pirronello, 1991). This link to astrophysical and planetary problems was the reason that water ice was the first material for which electronic sputtering was studied systematically (Brown et al., 1978, 1980a, 1980b). These early experiments showed that electronic sputtering was a general process, occurring for materials other than alkali halides. The yield data from water ice during hydrogen ion and medium light ion bombardment versus energy, E, are shown in fig. 1b. The knock-on contribution dominates at low energies, whereas for energies above about 1 keV/amu the dependence clearly resembles that of the electronic stopping power. The measured yields induced by hydrogen and helium ions are large in view of the large sublimation energy, $U = 0.53$ eV. Whereas the yield is about 20 H_2O/He^+ for ion energies close to the stopping power peak, the yield from solid nitrogen for the same dE/dx is only a factor 2 larger although the sublimation energy is almost an order of magnitude smaller.

The yields for hydrogen and helium ion bombardment also exhibit higher yields for the same stopping power below the stopping power peak than those above the peak (Brown et al., 1980b). This effect was in part attributed to the use of the equilibrium charge state stopping power, as discussed earlier, rather than the actual stopping power for the non-equilibrated ions (Johnson and Brown, 1982). The yield as a function of the stopping power at high velocities is well approximated by a quadratic function down to below 10^{-14}eVcm$^2/H_2O$. The yield induced by high-energy fluorine ions also correlated with the electronic stopping power, and reducing the incident charge state reduced the yield (Cooper & Tombrello, 1984).

The temperature dependence of the yield of emitted species, fig. 31, has been critical for understanding the sputtering of water ice. The RBS-measurements of the sputtering of water ice by 1.5 MeV He^+-ions from Brown et al. (1980a)

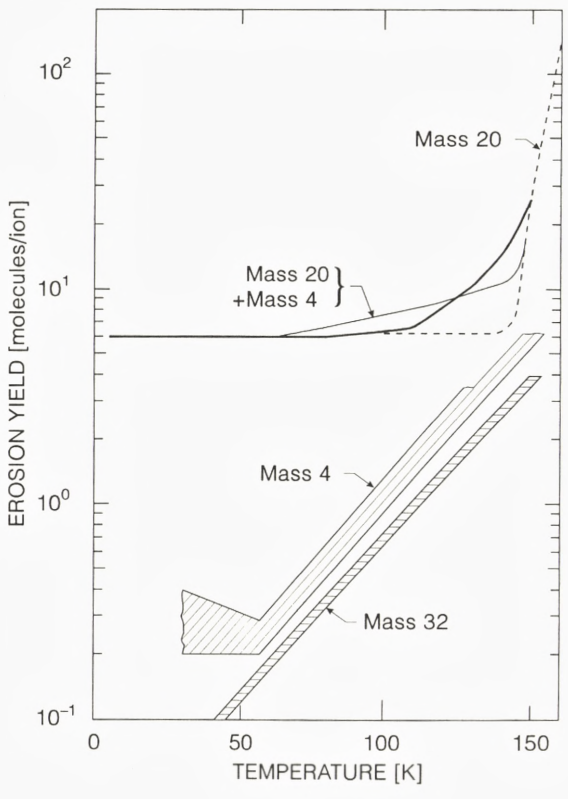

Figure 31. The temperature dependence of partial and total yields. Total and partial erosion yield from solid D_2O bombarded by 1.5 MeV He^+ ions. Details of normalization procedure described in the text or by Brown et al. (1984) Thick solid line, absolute yield of D_2O (RBS); thin solid line, sum of partial yields of D_2O and D_2 (QMS); dashed line, D_2O (QMS); hatched area for D_2 and O_2 includes the scattering of the data points (QMS).

showed that the total yield was independent of temperature at low temperatures and increases with increasing temperature above $\sim$ 120 K. The existence of a temperature independent yield was confirmed by Cooper and Tombrello (1984) and Bar-nun et al. (1985). The onset of the temperature dependent contribution depends on the ion energy, implying that the temperature independent and temperature dependent contributions depend differently on the electronic stopping power, $(dE/dx)_e$ (Brown et al., 1980a). The surface composition, however, appears to remain roughly stoichiometric, a 2:1 ratio of hydrogen to oxygen atoms.

Heavy water, D_2O, was used to obtain a substantial improvement in the signal-

to-background ratio of the measurements of the ejected species in fig. 31 (Brown et al., 1984). Primarily D_2O, D_2 and O_2 were seen. The mass spectra were normalized to the RBS yield at low temperatures, whereas the sum of deuterium and heavy water molecules has been adjusted to the RBS-yield at 150 K. The oxygen yield has been normalized to a value one-half of that for the deuterium molecules, so that the stoichiometry is preserved. The yield of oxygen and deuterium molecules varies with temperature even at temperatures below the liquid nitrogen temperature. Using IR spectroscopy Rocard et al. (1986) and Benit et al. (1987) observed the disappearance of water molecules due to heavy ion bombardment at liquid-nitrogen temperature. They suggested that at very high excitation densities erosion may be affected by hydrogen atom migration to the surface.

The ejecta reflect considerable chemical activity in the irradiated solid. Although D_2 can be formed by direct excitation, oxygen molecules are not present in the film, but have to be formed before the ejection (Reimann et al., 1984a). The ejected flux determined by Haring et al. (1984c) also contained a number of radicals up to mass 37 even for hydrogen and helium ion bombardment. For 1.5 MeV Ne^+-ions Benit and Brown (1990) demonstrated using hydrogen and oxygen isotopes that new molecules are formed that involve considerable diffusion before particle ejection.

Energy spectra for oxygen molecules sputtered from water ice by He^+-ions at 6 keV (Haring et al., 1984b) and 0.5 keV incident electrons (Pedrys et al. 1993b) exhibit a maximum at an ejection energy of $\sim$ 10 meV. However, there is no clear indication of an E_1^{-2}-tail above 0.1 eV. For emitted D_2O ice at 12 K energies observed from 0.1 eV up to 1 eV suggest the existence of an E_1^{-2}-tail for 1.5 MeV He^+-ion bombardment (Brown et al., 1984).

Experiments in radiation chemistry demonstrate that irradiation of water by light MeV ions or keV electrons primarily leads to the production of electron-hole pairs and excited water molecules. The excited molecules dissociate to H + OH or H_2 + O, and the charged species, e and H_2O^+, recombine and dissociate releasing $\sim$ 1-2 eV (Spinks & Woods, 1990; Turner et al., 1983, 1988; Dixon, 1970). Certain electronic relaxation processes have been identified from luminescence measurements from water ice irradiated by MeV electrons (Quickenden et al., 1991; Vernon et al., 1991; Trotman et al., 1986). A feature at 385 nm is associated with dissociative excitation of water. This leads to OH and H with up to 2 eV, with H receiving (17/18) of the energy. Because the products are radicals their binding to the solid is increased over that of H_2O. Therefore, the yield of OH is small, but H atoms are ejected from the surface. By a three-body reaction, the association of H and OH to either H_2 or H_2O can gradually release approximately 5 eV.

Although the net energy released in a single excitation can be larger than the sublimation energy, 0.53 eV for water molecules in ice, most of the energy is trans-

ferred to the lightest species, H_2 or H, so that ejection of an H_2O in a single event is unlikely (Johnson, 1990). Therefore, the quadratic dependence seen for low temperature ice (< 77 K) at very low stopping powers, $(dE/dx)_e$, is sensible. Since the average bond energies of the hydrogen and oxygen molecules to the surface are small, such species can diffuse to the surface and are easily ejected. For this reason yields at higher temperatures should be linear after a threshold fluence (Brown et al., 1980a). For 1.5 MeV He^+-ion bombardment, two ion-electron pairs are produced per Å along the track, and the quadratic dependence of the yield on the stopping power persists, consistent with the other molecular condensed gases.

The total yield did not depend on film thickness for thicknesses between 0.8 and $90 \times 10^{17} H_2O/cm^2$ at 77 K (Brown et al., 1980b) and at 10 K (Cooper and Tombrello, 1984). The yield of deuterium as well as oxygen molecules increased with film thickness during 1.5 MeV neon-ion bombardment (Reimann et al., 1984a), suggestive either of diffusion along the track (Benit et al., 1987; Rochard et al., 1986) or that the thickness may affect the storage time of the radicals prior to reaction.

The temperature dependence of the yield of a newly formed species is determined by the mobility of the radicals and the energy barrier for the reaction. At the lowest temperatures (below 20 K), the hydrogen atoms are fairly immobile, but around 30 K the mobility increases (Hudson & Moore, 1992). The hydroxyl radical is immobile up to liquid-nitrogen temperature, but the radicals become increasingly mobile from 90 K up to the temperature 140 K, around which they disappear (Spinks & Woods, 1990). The electrons can be trapped at low temperatures and become mobile with increasing temperature. The trapping mechanism depends on the crystal and defect structure of the ice (Buxton et al., 1977).

The diffusion of radicals and the reactions are activated processes. The temperature dependent part of the yield of water molecules suggests an activation energy of 50 meV at low temperatures for 0.9 MeV proton bombardment and an activation energy of 300 meV at temperatures between 120 and 160 K, for 1.5 MeV He^+-ion bombardment (Brown et al., 1980a). The temperature dependence of the molecular-oxygen-yield transient leads to activation energies around 50 and 70 meV under 1.5 MeV neon ion bombardment (Reimann et al., 1984a).

The net erosion of water ice can be influenced by the morphology of the ice. Hudson & Moore (1992) recently found that a transition from amorphous to crystalline ice, induced by irradiation with 0.7 MeV protons, is accompanied by a sudden release of hydrogen and water molecules as well as hydroxyl radicals. Beam-induced amorphorization of crystalline water ice also occurs for light ion and electron bombardment (Strazzulla et al., 1992). Sample structure clearly influences electronic sputtering via the mobility of the radicals, but details are not understood yet.

9.3.5 Other Solid Heteronuclear Molecular Gases

Electronic excitation of the solid heteronuclear molecular gases results in sputtering in a manner similar to that for water ice. The solids are modified and decomposed during light-ion or electron bombardment. Chemical compounds that initially were not present in the solid may be generated (de Vries et al., 1984) and those with lower binding energy are easily released. Conversely, higher binding energy products remain, so that involatile residues also form. The details of the processes that lead to particle ejection are largely unknown, but repulsive relaxation (dissociative recombination) can provide energetic fragments and chemical activity both of which can heat the lattice and lead to sputtering. Generally, luminescence studies from these solids have not yet been particularly helpful because sputtering involves prompt processes ($< 10^{-11}$ sec) whereas luminescence is delayed ($> 10^{-9}$ sec).

Solid carbon monoxide is the only heteronuclear diatomic species that has been studied systematically. This solid is perhaps the simplest non-elemental insulator, since many of the molecular properties are similar to those of solid nitrogen and oxygen. The electronic sputtering yield for MeV ion incidence was measured by Brown et al. (1984) and later extended to keV ion bombardment by Chrisey et al. (1990). The yield is quadratic in the stopping power for MeV ion bombardment and significantly exceeds that for solid nitrogen and oxygen, even though the sublimation energy is comparable (Table I). Even at the lowest values of the stopping power there is no evidence of a linear regime (Chrisey et al., 1990). Adsorbed CO is known to efficiently lose O in a single excitation (Leung et al., 1977); therefore, single events can lead to sputter loss of neutrals or even negative ions (Sanche, 1984). However, the size of the yield suggests that these events are dominated by quadratic processes. Although, the yield for helium ions below the stopping power peak lies somewhat above those from energies above the stopping power peak, this is not the case for the low-energy hydrogen points which apparently are similar above and below the electronic stopping power maximum.

The sputtering yields due to 2 keV-electron bombardment (Schou et al., 1985) and relative yields for 1 to 3.5 keV electrons (Brown et al., 1984) were normalized to the MeV ion data and were found to follow the high-energy ion branch very closely (Chrisey et al., 1990). This agreement requires that the surface value of the deposited energy is $\sim 1.6(dE/dx)_e$, because of backscattered primaries (Ellegaard et al., 1986b). Even though this choice is standard for materials of atomic numbers from 6 up to 10 (Valkealahti et al., 1989), agreement between ion and electron data only occurs for carbon monoxide. For solid nitrogen the yields induced by electrons and high-energy ions disagree by a factor of 2 for the same value of the energy deposited at the surface.

Energy distributions for species sputtered from solid carbon monoxide during

ion bombardment have been determined by Haring et al. (1984b) and Chrisey et al. (1990). The latter group compared the spectrum of emitted CO induced by argon ion bombardment with that induced by helium bombardment. Even though the first type of ion produces dominantly knock-on sputtering and the second type electronic sputtering, the spectra were similar. Both showed a pronounced E_1^{-2}-tail up to almost 1 eV, and a low-energy peak around 15 meV.

The processes that convert excitational energy into kinetic energy are less established than those for the elemental molecular gases. Dissociation of an excited or ionized carbon monoxide molecule and dissociative recombination of a molecular ion are seen in radiation chemistry. These processes typically release about 1 eV, sufficient to initiate displacement cascades since $U = 0.08$ eV (Chrisey et al., 1990). Reactions among fragments may be important as well since the yield is quadratic even at low stopping powers: e.g., C_2 and O_2 form as well as CO_2, C_2O, and O_3 (Haring et al., 1984b; Pedrys et al., 1985; Chrisey et al., 1990). The reactions lead to the production of a non-volatile residue (Haring et al., 1984c; Schou et al., 1985; Chrisey et al., 1990). For MeV He^+ RBS analysis indicates that the stoichiometric composition is approximately C_3O (probably polymerized) corresponding to $\sim$ 2-5 percent of the original film, (Chrisey et al., 1990).

Electronic sputtering of solid sulfur dioxide has been studied by Lanzerotti et al. (1982), Boring et al. (1984), and Moore (1984) because of its interest at Io. The yield for MeV protons and helium ions is roughly quadratic in stopping power. No thickness dependence was observed between thicknesses 3.9 to 4.9 $\times$ 10^{17} SO_2/cm^2, but mass 80 (either S_2O or SO_3) was observed to be fluence dependent (Boring et al., 1983). Large yields were found by Lepoire et al. (1983) for fluorine ion bombardment up to 8000 SO_2/F, for energies between 1.6 MeV and 25 MeV and charge states from 2 to 5. Their yield for 1.5 MeV He^+-ion at 30° is about three times larger than that obtained by Boring et al. (1984) at 0°. Based on eq.(16) a factor of $\sim$ 1.3 is expected ignoring charge-state equilibrium effects. The yield for the fluorine ion bombardment varies faster than the stopping power squared. A residue is observed which is enriched in oxygen, but had a low sputtering yield (Lepoire et al., 1983; Moore, 1984). However, details of the sputtering process are not understood.

Methane, though not inorganic has erosion properties related to the other condensed gases. It is a simple hydrocarbon and is found in condensed form in fractional concentrations on Pluto and Triton. Light-ion bombardment leads immediately to modification of the solid, so the yield depends on the fluence in addition to the usual parameters (Lanzerotti et al., 1987). At low fluence the yield is around 100 molecules for 900 keV-helium ion. The decomposition of the methane leads to emission of hydrogen, so that the sample progresses from an initially pure methane film towards a carbon-rich polymer (Lanzerotti et al., 1987). These authors ob-

served that the bond breaking starts immediately under keV proton and helium ion bombardment of deuterated methane, but the yield of the deuterium molecules remains small until a fluence threshold has been reached. Above this threshold the yield of deuterium increases by an order of magnitude, until it decreases as the film is depleted in deuterium. At these temperatures (12-28 K) the diffusivity of deuterium is low, so the threshold is a percolation threshold for which a sufficient fraction of the methane is made porous. This is consistent with finding that the hydrogen (deuterium) emission was accompanied by an enhanced light scattering (Strazzulla et al., 1988) and the net loss is proportional to film thickness for these ions which penetrate to the substrate (Lanzerotti et al., 1987). The chemical modification of the methane by light ion bombardment has been studied by several groups. Large hydrocarbon ions are observed in the sputtered flux (Pedrys et al., 1986) as well as high mass neutrals (Foti et al., 1987). Benit et al. (1987) observed the formation of new carbon-hydrogen bonds with infrared absorption spectroscopy.

The energy distribution of methane molecules emitted during 6-8 keV hydrogen or helium ion bombardment falls off steeply above 0.1 eV for large fluences. Pedrys et al. (1986) approximated the spectra by a Maxwell-Boltzmann distribution with a temperature of 203 K. Although formation of hydrogen and hydrocarbon polymer can provide the energy, the processes that lead to particle ejection are not known.

Ariyansinghe et al. (1989) studied C_2H_2 and C_2H_4 and Foti et al. (1987) studied benzene, C_2H_6. The results showed largely the same trends as for methane: hydrogen depletion and formation of an involatile residue. A heavy residue was generated in C_2H_2, but not in C_2H_6 in which the bonds are saturated, when low energy ions are used.

One of the most complicated solidified gases that has been sputtered is frozen sulfur hexafluoride (Pedrys et al., 1984). The sputtered flux during keV electron bombardment consisted of sulfur flourides, which at high fluences exhibit energy distributions which fall off steeply above 0.1 eV. Only the distribution of SF_5^+, which originates in part from post ionized sulfur hexafluoride, shows a distribution with an E_1^{-2}-tail. The distribution of diatomic fluorine molecules can be approximated with a Maxwell-Boltzmann distribution corresponding to the actual target temperature. As with $H_2(D_2)$ in methane, the diatomic molecules are, apparently, formed and ejected in events uncorrelated with the ejection of the sulfur fluorides.

10 Summary

Results for knock-on sputtering of inorganic insulators by incident ions and electronic sputtering by incident ions, electrons and photons were summarized. Knock-

on sputtering of room-temperature insulators, with surface binding energies for constituent atoms comparable to that of metals, can be roughly treated on the basis of standard sputtering theory at low fluences. However, the molecular character of room-temperature insulators adds a complication, especially at high fluences. There is some analogy for these with the sputtering of metallic alloys, except that efficient molecular ejection can occur, which is not understood quantitatively. Unfortunately, sputtering data are available for only one room-temperature elemental insulator, sulfur. The most important new studies for knock-on sputtering are for the volatile, frozen gases, for which nonlinear effects are observed in the yield and/or the ejected particle energy spectra even at relatively low excitation densities. Although this has been known for some time the nonlinear effects are not understood quantitatively.

The most exciting results and ideas described in this review concern electronic sputtering, since the relaxation processes which follow the electronic excitation of a solid can be studied via detecting the sputtered species. In this manner a clear picture has emerged of the electronic relaxation processes which lead to sputtering in the rare-gas solids. The physics of the sputtering of solid argon is the best known for these materials, although there are a number of important outstanding questions regarding differences in the yield above and below the stopping power maximum, on the mechanism for dimer ejection and vibrational cooling, and on the relationship of the large secondary electron yields to sputtering and luminescence. Certain aspects of nonradiative electronic relaxation in a few molecular solids have also emerged, particularly for solid nitrogen and oxygen. However, the details of the decay processes leading to sputtering of these materials are not well understood, and often quite complicated chemical processes can affect sputtering of the heteronuclear molecular condensed gases.

An essential parameter in electronic sputtering of inorganic insulators is the excitation density, which determines the nature of the transport and ejection processes. At low excitation densities, excitonic processes occur which ultimately lead to particle ejection in the condensed gases: migration of excitons, trapping, and relaxation and energy transfer to target atoms. There are, however, very few studies of these processes as a function of sample crystal quality or impurity content. For high excitation densities, the volatile solids exhibit nonlinear yields and even refractory solids may be sputtered electronically. Although these are not understood quantitatively, the magnitude of the stopping power and the surface binding energy control the electronic sputtering yield, as is the case for knock-on sputtering. In addition, for high velocity ions, the W-value is important. Therefore, most experimental results can be analyzed using the quantity $f_e \ell (dE/dx)_e / U$, where f_e is the fraction of the electronic energy released in energetic non-radiative processes. Here, $f_e \approx \Delta E/W$, is of the order 0.1-0.3 in a number of condensed gases for fast

light ions, and f_e appears to increase with decreasing ion velocity The increasing ability to carry out detailed experiments, combined with molecular dynamics calculations, will allow one to obtain a high level of detail about the electronic relaxation processes which lead to sputtering of a number of low-temperature, molecular condensed gases.

Acknowledgements

The authors would like to thank G. Zimmerer, C. Reimann, R.A. Baragiola, H.H. Andersen, and P. Sigmund and one anonymous referee for extensive comments on the manuscript.

References

Adloff JP, Gaspar PP, Imamura M, Maddock AG, Matsuura T, Sano H and Yoshihara Y, 1992: *Handbook of Hot Atom Chemistry*, Kodanska, Tokyo

Allison SK, 1958: Rev. Mod. Phys. **30**, 1137

Andersen HH, 1984: in *Ion Implantation and Beam Processing*, eds. Williams JM and Poate JM, Academic, Australia, 127

Andersen HH and Bay HL, 1974: J. Appl. Phys. **45**, 953

Andersen HH and Ziegler JF, 1977: *Hydrogen Stopping Powers and Ranges in All Elements*, Pergamon, NY

Andersen HH and Bay HL, 1981: in *Sputtering by Particle Bombardment I*, ed. Behrisch, R, Springer, NY, 145

Andersen N and Sigmund P, 1974: Mat. Fys. Medd. **39**, no. 3

Arakawa I, Takahashi M and Takeuchi K, 1989: J. Vac. Science Techn. **A7**, 2090

Arakawa I and Sakurai M, 1990: in *Desorption Induced by Electronic Transitions, DIET IV*, eds. Betz G and Varga P, Springer, NY, 246

Ariyasinghe WM, McElroy RD and Powers D, 1989: Nucl. Instrum. Methods B **44**, 61

Baba Y, Dujardin J, Feulner P and Menzel D, 1991: Phys. Rev. Lett. **66**, 3269

Bach H, Kitzmann I and Schröder H, 1974: Rad. Effects **21**, 31

Bach H, 1988: J. Non-Cryst. Solids **102**, 36

Balaji V, David DE, Magnera TF, Michl J and Urbassek HM, 1990: Nucl. Instrum. Methods B **46**, 435

Banerjee S, Johnson RE, Cui ST and Cummings PT, 1991a: Phys. Rev. B **43**, 12707

Banerjee S, Liu M and Johnson RE, 1991b: Surf. Sci. Lett. **255**, L504

Baragiola RA, 1993a: in *Low Energy Ion-Surface Interactions*, ed. Rabalais JW, Wiley, NY

Baragiola RA, 1993b: *Ionization of Solids by Heavy Particles*, Plenum, NY

Bargiola RA, 1993c: Unpublished communication

Baretzky B, Møller W and Taglauer E, 1992: Vac. **43**, 1207

Bar-nun A, Herman G, Rappaport ML and Mekler Yu 1985: Surf. Sci. **150**, 143

Belov AG, Svishchev VN and Fugol' Ya, I, 1989: Sov. J. Low Temp. Phys. **15**, 34

Benit J and Brown WL, 1990: Nucl. Instrum. Methods B **46**, 448

Benit J, Bibring J-P, Della-Negra S, Le Beyec Y, Mendenhall M, Rocard F and Standing K, 1987: Nucl. Instrum. Methods B **19-20**, 838

Benit J, Bibring J-P and Rocard F, 1988: Nucl. Instrum. Methods B **32**, 349

Benvenuti C, Calder R and Gröbner O, 1987: Vacuum 37, 699: Erratum Vacuum **38**, 145
Besenbacher F, Bøttiger J, Graversen O, Hansen JL and Sørensen H, 1981: Nucl. Instrum. Methods **191**, 221
Betz G and Wehner GK, 1983: in: *Sputtering by Particle Bombardment II*, ed. Behrisch R., Springer, 11
Betz G, 1987: Nucl. Instrum. Methods B **27**, 104
Biersack JP and Santner E, 1976: Nucl. Instrum. Methods **132**, 229
Bitensky IS and Parilis ES, 1987: Nucl. Instrum. Methods B **21**, 26
Bitensky IS, Goldenburg AM and Parilis ES, 1990: in *Ion Formation from Organic Solids V (IFOSV)*, eds Hedin A et al. Wiley, Chichester, 205
Boring JW, Johnson RE, Reimann CT, Garret JW, Brown WL and Macantonio KJ, 1983: Nucl. Instrum. Methods **218**, 707
Boring JW, Garrett JW, Cummings TA, Johnson RE and Brown WL, 1984: Nucl. Instrum. Methods B **1**, 321
Boring JW, O'Shaughnessy DJ and Phipps JA, 1987: Nucl. Instrum. Methods B **18**, 613
Boring JW, Johnson RE and O'Shaughnessy DJ, 1989: Phys. Rev. B **39**, 268
Boursey E, Castex MC and Chandrasekharan V 1977: Phys. Rev. B **16**, 2858
Brandt W and Ritchie RH, 1974: in *Physical Mechanisms in Radiation Biology*, eds. Cooper RD and Wood RW, US Dept. of Commerce, Wash. D.C., 20
Brown WL, 1993: in *Ionization in Solids by Secondary Electrons* ed. Baragiola RA, Plenum, N.Y. 395
Brown WL, 1984: in *Ion Implantation and Beam Processing*, eds. Williams, JM and Poate MJ, Academic, Australia (Acad. Press. N.Y.) 99
Brown WL, Lanzerotti LJ, Poate JM and Augustyniak WM, 1978: Phys. Rev. Lett. **40**, 1027
Brown WL, Augustyniak WM, Lanzerotti LJ, Johnson RE and Evatt R, 1980a: Phys. Rev. Lett. **45**, 1632
Brown WL, Augustynik WM, Brody E, Cooper B, Lanzerotti LJ, Ramirez A, Evatt R and Johnson RE 1980b: Nucl. Instrum. Methods **170**, 321
Brown WL, Augustyniak WM, Marcantonio KJ, Simmons EH, Boring JW, Johnson RE and Reimann CT, 1982: Nucl. Instrum. Methods B **1**, 307
Brown WL, Augustyuniak WM, Marcantonio KJ, Simmons EH, Boring JW, Johnson RE and Reimann CT, 1984: Nucl. Instrum. Methods B **1**, 307
Brown WL and Johnson RE, 1986: Nucl. Instrum. Methods B **13**, 295
Brown WL, Lanzerotti LJ, Marcantonio KJ, Johnson RE and Reimann CT: 1986: Nucl. Instrum Methods B **14**, 392
Buller WT and Johnson RE, 1991: Phys. Rev. B **43**, 6118
Buxton GV, Gillis HA and Klassen NV, 1977: Can. J. Phys. **55**, 2385
Børgesen P and Sørensen H, 1982: Phys. Lett. **90 A**, 319
Børgesen P, Schou J, Sørensen H and Claussen C, 1982: Appl. Phys. A **29**, 57
Bøttiger J, L'Ecuyer J, Matsunami N and Ollerhead R, 1980: Rad. Effects **49**, 119
Cantagrel M and Marchal M, 1973: J. Mat. Science **8**, 1711
Carter G., 1983: Nucl. Instrum. Methods **209/210**, 1
Celiberto R, Cacciatore M and Capitelli M, 1989: Chem. Phys. **133**, 369
Chrisey DB, Boring JW, Phipps JA, Johnson RE and Brown WL 1986: Nucl. Instrum. Methods **13**, 360
Chrisey DB, Boring JW, Johnson RE and Phipps JA, 1988: Surf. Sci. **195**, 594
Chrisey DB, Brown WL and Boring JW, 1990: Surf. Sci. **225**, 130
Christiansen JW, Carpini D Delli and Tsong IST, 1986: Nucl. Instrum. Methods B **15**, 218
Claussen C, 1982: Nucl. Instrum. Methods **194**, 567
Coletti F and Bonnot AM, 1977: Chem. Phys. Lett. **45**, 580

Coletti F and Debever JM, 1983: Solid State Comm. **47**, 47
Coletti F, Debever JM and Zimmerer G, 1984: J. Physique Lett. **45**, L 467
Coletti F, Debever JM and Zimmerer G, 1985: J. Chem. Phys. **83**, 49
Cooper BH and Tombrello TA, 1984: Rad. Effects **80**, 203
Cui ST, Johnson RE and Cummings PT, 1988: Surf. Sci. **207**, l86
Cui ST and Johnson RE, 1989: Int. J. Quant. Chem: Quant. Chem. Symp. 23, 575; Errata, 1991: I.J.Q.C. **41**, 383
Cui ST, Johnson RE and Cummings PT, 1989a: Phys. Rev. B **39**, 9580
Cui ST, Johnson RE, Reimann CT, Boring JW, 1989b: Phys. Rev B **39**, 12345
David DE, Magnera TF, Tian R, Stulik D and Michl J, 1986: Nucl. Instrum. Methods B **14**, 378
David DE and Michl J, 1989: Prog. Solid St. Chem. **19**, 283
Davidse PD and Maissel LI, 1966: J. Vac. Sci. Techn. **4**, 33
DIET I, 1983: Springer Ser. in Chem. Phys. **24**, eds. Tolk NH et al. Springer, Berlin
DIET II, 1985: Springer Ser. in Surf. Science **4**, eds. Brenig W and Menzel D, Springer, Berlin
DIET III, 1988: Springer Ser. in Surf. Science **13**, eds. Stulen RH and Knotek ML, Springer, Berlin
DIET IV, 1990: Springer Ser. in Surf. Science **19**, eds. Betz G and Varga P, Springer, Berlin
DIET V, 1993: Springer Ser. in Surf. Science **31**, eds. Burns AR et al. Springer, Berlin
Dixon RS, 1970: Rad. Res. Rev. **2**, 237
Doke T, Hitachi A, Kubota S, Nakamoto A and Takahashi T, 1976: Nucl. Instrum. Methods **134**, 353
DuBois RD, Toburen LH and Rudd ME, 1984: Phys. Rev. A **29**, 70
Dubus A, Devooght J and Dehaes JC, 1987: Phys. Rev. B **36**, 5110
Dujardin G, Hellner L, Besnard-Ramage MJ and Azria R, 1990: Phys. Rev. Lett. **64**, 1289
Dullni E, 1984: Nucl. Instrum. Methods B **2**, 610
Edwin RP, 1973: J. Phys. **D6**, 833
Ellegaard O, 1986: PH.D. Thesis Risø-M-2617, Risø National Laboratory
Ellegaard O, Schou J and Sørensen H, 1986a: Nucl. Instrum. Methods B **13**, 567
Ellegaard O, Schou J, Sørensen H, 1986b: Surf. Sci. **167**, 474
Ellegaard O, Pedrys R, Schou J, Sørensen H and Børgesen P,1988: Appl. Phys. A **46**, 305
Ellegaard O, Schou J and Sørensen H, 1990: Europhys. Lett. **12**, 459
Ellegaard O, Schou J, Stenum B, Sørensen H and Pedrys R, 1992: Nucl. Instrum. Methods B **62**, 44
Ellegaard O, Schou J, Stenum B, Sørensen H, Pedrys R, Oostra DJ, Haring A and De Vries AE, 1993a: to be published
Ellegaard O, Schou J, Sørensen H, Pedrys R and Warczak B, 1993b: Nucl. Instrum. Methods B **78**, 192
Erents SK and McCracken GM, 1973: J. Appl. Phys. **44**, 3139
Erents SK and McCracken GM, 1975: in *Atomic Collisions in Solids* eds. S. Datz and C.D. Moak Plenum, N.Y. 625
Falcone G and Sigmund P, 1981: Appl. Phys. **25**, 307
Falcone G, 1990 Riv. di Nuov. Cimento **13**, 1
Fano U, 1963: Ann. Rev Nucl. Sci. **13**, 1
Fenyö D, 1993: Phys. Rev. B (in press)
Fenyö D, Sundqvist BUR, Karlsson BR and Johnson RE, 1990: Phys. Rev. B **42**, 1895
Fenyö D and Johnson RE, 1992: Phys. Rev. B **46**, 5090
Feulner P, Müller T, Puschmann A and Menzel D, 1987: Phys. Rev. Lett. **59**, 791
Fiori C and Devine RAB, 1984: Phys. Rev. Lett. **52**, 2081
Fink D, Biersack JP, Städele M, Tjan K, Haring R and de Vries AE, 1984: Nucl. Instrum. Methods **B 1**, 275

Fleischer RL, Price PB and Walker RM, 1975: *Nuclear Tracks in Solids*, Univ. of Calif. Press, Berkeley
Forrest JA, Brooks RL, Hunt JL, Stenum B, Schou J, Sørensen H, Gürtler P, Magnotta F, Mapoles ER, Souers PC and Collins GW, 1992: Phys. Rev. B **46**, 13820
Foti G, Calcagno L, Zhou FZ and Strazzulla G, 1987: Nucl. Instrum. Methods B **24-25**, 552
Fox JL and Dalgarno A, 1983: J. Geophys. Res. **88**, 9027
Fugol' I Ya, 1978: Adv. Phys. **27**, 1
Fugol' I Ya, 1988: Adv. Phys. **37**, 1
Fugol' I Ya, Belov AG and Svishchev VN, 1988: Solid State Comm. **66**, 503
Garrison BJ, 1983: Int. J. Mass. Spec. and Ion Physics **53**, 243
Garrison BJ and Johnson RE, 1984: Surface Science **148**, 388
Geerk J, 1993: Private communication
Geerk J, Linker G and Meyer O, 1989: Mat. Science Rep. **4**, 19
Gibbs KM, Brown WL and Johnson RE, 1988: Phys. Rev. B **38**, 11001
Greenberg JM and Pirronello V, 1991: eds. *Chemistry in Space*, NATO-ASI series C Vol. 323
Griffith JW, Weller RA, Sieberling LE and Tombrello TA, 1980: Rad. Effect **51**, 223
Griscom DL, 1989: Phys. Rev. B **40**, 4224
Grosjean DE and Baragiola RA, 1993: in *Ionization of Solids by Heavy Particles*, ed. Baragiola RA, Plenum, N.Y., 381
Guthier W, 1986: Proc. in Physics **9**, Springer, 17
Håkansson P, 1993: Mat. Fys. Medd. Dan. Vid. Selsk. **43**, 593
Haff PK, 1976: Appl. Phys. Lett. **29**, 473
Haff PK and Switkowski ZE, 1976: Appl. Phys. Lett. **29**, 549
Haring RA, Pedrys R, Haring A and de Vries AE, 1984a: Nucl. Instrum. Methods B **4**, 40
Haring RA, Pedrys R, Oostra DJ, Haring A and de Vries AE, 1984b: Nucl. Instrum. Methods B **5**, 483
Haring RA, Pedrys R, Oostra DJ, Haring A and de Vries AE, 1984c: Nucl. Instrum. Methods B **5**, 476
Harper J, 1990: *Plasma-Surface Interactions and Processing of Materials*, eds. Auciello O et al. NATO ASI Series-No. E 176, Kluwer Academic, Dordrecht, 251
Hellner L, Besnard-Ramage MJ, Dujardin G and Azria R, 1990: in: *Desorption Induced by Electronic Transitions, DIET IV*, eds. Betz G. and Varga P. Springer, 240
Herzberg G, 1950: *Spectra of Diatomic Molecules*, Van Nostrand-Reinhold, Princeton
Hoover WG, 1986: *Molecular Dynamics*, Springer-Verlag, Berlin
Houpert C, Stader F, Groult D and Toulemonde M, 1989: Nucl. Instrum. Methods B **39**, 120
Hourmatallah A, Coletti F and Debever JM, 1988: J. Phys. C. **21**, 1307
Hudel E., Steinacker E and Feulner P, 1991: Phys. Rev. B **44**, 8972
Hudel E, Steinacker E and Feulner P, 1992: Surf. Sci. **273**, 405
Hudson RL and Moore MH, 1992: J. Phys. Chem. **96**, 6500
ICRU, 1979: *Average Energy Required to Produce an Ion-Pair*, Internat. Commission on Radiation Units and Measurements Report **31**
Inokuti M, 1971: Rev. Modern Phys. **43**, 297
Inokuti M, 1991: Appl. Radiat. Inst. **42**, 979
Itoh N, 1987: Nucl. Instrum. Methods B **27**, 155
Itoh N, Nakayama T and Tombrello TA, 1985: Phys. Lett. **108A**, 480
Itoh C, Suzuki T and Itoh N, 1990: Phys. Rev. B **41**, 3794
Jacobsson H and Holmén G, 1993: Nucl. Instrum. Methods B **82**, 291
Johnson RE, 1970: J. Phys. B **3**, 539
Johnson RE, 1982: *Introduction to Atomic and Molecular Collisions*, Plenum, N.Y.
Johnson RE, 1987: Int. J. Mass Spec. Ion Proc. **78**, 357

Johnson RE, 1989: J. de Physique Coll. **C2**, 251
Johnson RE, 1990: *Energetic Charged Particle Interactions with Atmospheres and Surfaces*, Springer-Verlag, Berlin
Johnson RE 1993: in *Ionization of Solids by Heavy Particles*, ed. Baragiola RA, Plenum, N.Y. 419
Johnson RE and Evatt R, 1980: Radiat. Effects. **52**, 187
Johnson RE and Brown WL, 1982: Nucl. Instrum. Methods **198**, 103
Johnson RE and Brown WL, 1983: Nucl. Instrum. Methods **209/210**, 469
Johnson RE and Inokuti M, 1983: Nucl. Instrum. Methods **206**, 289
Johnson RE, Sundqvist BUR, Hedin A and Fenyö D, 1989: Phys. Rev. B. **40**, 49
Johnson RE, Pospieszalska M and Brown WL, 1991: Phys. Rev. B **44**, 7263
Johnson RE and Sundqvist BUR, 1992: Phys. Today, **45(3)**, 28
Kaiser RI, Mahfouz RM and Roessler K, 1992: Nucl. Instrum. Methods B **65**, 468
Kelly R, 1977: Rad. Effects. **32**, 91
Kelly R, 1979: Surf. Sci. **90**, 280
Kelly R, 1984a: Rad. Effects. **80**, 273
Kelly R, 1984b: in *Ion Bombardment Modification of Surfaces*, eds. Aucello O. and Kelly R., Elsevier, N.Y. 27
Kelly R, 1987: Nucl. Instrum. Methods B **18**, 388
Kelly R, 1990: Nucl. Instrum. Methods B **46**, 441
Klaumünzer S, Hou M-D and Schumacher G, 1986: Phys. Rev. Lett. **57**, 850
Kloiber T, Lasch W, Zimmerer G, Coletti F and Debever JM, 1988: Europhys. Lett. **7**, 77
Kloiber T and Zimmerer G, 1989: Rad. Eff. Def. Solids **109**, 219
Kloiber T and Zimmerer G, 1990: Phys. Scr. **41**, 962
Knotek ML and Feibelman PJ, 1978: Phys. Rev. Lett. **110**, 964
Kühle H, Bahrdt J, Fröhling R, Schwentner N and Wilcke H, 1985: Phys. Rev. B **31**, 4854
Kurtz RL, 1986: Surf. Sci. **177**, 526
Kurtz RL, Stockbauer R and Madey TE, 1986: Nucl. Instrum. Methods B **13**, 518
Laasch W, Hagedorn H, Kloiber T and Zimmerer G 1990: Phys. Stat. Sol. **b 158**, 753
Lam NQ, 1990: Scan. Micr. Suppl. **4**, 311
Lanzerotti LJ and Brown WL, 1983: J. Geophys. Res. **88**, 989
Lanzerotti LJ, Brown WL, Augustyniak WM and Johnson RE, 1982: Astrophys. J **259**, 920
Lanzerotti LJ, Brown WL, Marcantonio KJ, 1987: Astrophys. J. **313**, 910
Leclerc G, Bass AD, Michaud M and Sanche L, 1990: J. Elec. Spec. Rel. Phen. **52**, 725
Leclerc G, Bass AD, Mann A and Sanche L, 1992: Phys. Rev. B **46**, 4865
Lepoire DJ, Cooper BH, Melcher CL and Tombrello TA, 1983: Rad. Effects **71**, 245
Leung C, Steinbrüchel Ch and Gomer R, 1977: Appl. Phys. **14**, 79
Lindhard J. and Winther Aa, 1964: Mat. Fys. Medd. **34** no. 4
Liu M and Johnson RE, 1993: submitted
Mann A, Leclerc G and Sanche L, 1992: Phys. Rev. B **46**, 9683
Matsunami N, 1990: Nucl. Instrum. Methods B **46**, 452
Matsuura T, 1984: *Hot Atom Chemistry*, Elsevier, Amsterdam.
Maynard G and Deutsch C, 1987: Lecture Notes in Physics **269** ed. by Hilf ER et al., Springer, 94
McClanahan ED and Laegreid N, 1991: *Sputtering by Particle Bombardment III*, eds. Behrisch R and Wittmaack K, Springer, Berlin-Heidelberg, 339
Meins CK, Griffith JE, Qiu Y, Mendenhall MH, Seiberling LE and Tombrello TA, 1983: **71**, l3
Menzel D, 1990: Appl. Phys. A **51**, 163
Menzel D and Gomer R, 1964: J. Chem. Phys. **42**, 886
Michaud M, Cloutier P and Sanche L, 1993: Phys. Rev. B **47**, 4131

Miller JH and Green AES, 1973: Rad. Res. **54**, 354
Mizutani 1991: Jap. J. Appl. Phys. **30**, L628
Moore MH, 1984: Icarus **59**, 114
Mozumder A, 1969: Adv. Radiat. Chem **1**, 1
Nieschler E, Nees B, Bischof N, Fröhlich H, Tiereth W and Voit H, 1984: Rad. Effects **83**, 121
Oehler O, Smith DA and Dressler K, 1977: J. Chem. Phys. **66**, 2097
Ollerhead RW, Bøttiger J, Davies JA, L'Ecuyer J, Haugen HK and Matsunami N, 1980: Rad. Eff. **49**, 203
Oliva A, Kelly R and Falcone G, 1987: Nucl. Instrum. Methods B **19/20**, 101
Oliva-Florio A, Alonso EV, Baragiola RA, Ferron J and Jakas MM, 1979: Rad. Eff. Lett **50**, 3
O'Shaughnessy DJ, Boring JW, Phipps JA and Johnson RE, 1988a: Surf. Sci. **203**, 227
O'Shaughnessy DJ, Boring JW, Cui S and Johnson RE, 1988b: Phys. Rev. Lett. **61**, 1635
Overeijnder H, Szymonski M, Haring A and de Vries AE, 1978: Rad. Eff. **36**, 63
Pan SL, Zumofen G and Dressler K, 1987: J. Chem. Phys. **87**, 3482
Paretzke HG, Turner JE, Hamm RN, Wright HA and Ritchie RH, 1986: J. Chem. Phys. **84**, 3182
Pedrys R, 1990: Nucl. Instrum. Methods B **48**, 525
Pedrys R, 1993: Unpublished communication
Pedrys R, Haring RA, Haring A and de Vries AE 1984: Nucl. Instrum. Methods B **2**, 573
Pedrys R, Oostra DJ and de Vries AE, 1985: in *Desorption Induced by Electornic Transitions, DIET II*, eds. Brenig W and Menzel D, Springer, Berlin, 190
Pedrys R, Oostra DJ, Haring RA, Calcagno T, Haring A and de Vries AE, 1986: Nucl. Instrum. Methods B **17**, 15
Pedrys R, Oostra DJ, Haring A, de Vries AE and Schou J, 1988: Nucl. Instrum. Methods B **33**, 840
Pedrys R, Oostra DJ, Haring A, de Vries AE and Schou J, 1989: Rad. Eff. Def. Solids **109**, 239
Pedrys R, Warczak B and Schou J, 1993a: to be published
Pedrys R, Warczak B, Schou J and Ellegaard O, 1993b: to be published
Platzmann RL, 1961: Int. J. Appl. Rad. Inst. **10**, 116
Poltorataskii YuB and Fugol' Ya, I, 1979: Sov. J. Low Temp. **5**, 439
Qui Y, Griffith JE and Tombrello TA, 1982: Rad. Eff. **64**, 111
Qui Y, Griffith JE, Meng WJ and Tombrello TA, 1983: Rad. Effect. **70**, 231
Quickenden TI, Matich AJ, Bakker MG, Freeman CG and Sangster DF, 1991: J. Chem. Phys. **95**, 8843
Redhead PA, 1964: Can. J. Phys. **42**, 886
Reimann CT, 1992: Unpublished communication
Reimann CT, 1993: Mat. Fys. Medd. Dan. Vid. Selsk. **43**, 351
Reimann CT, Boring JW, Johnson RE, Garret JW, Farmer KR, Brown WL, Marcantonio KJ and Augustyniak WM, 1984a: Surf. Sci. **147**, 227
Reimann CT, Johnson RE and Brown WL, 1984b: Phys. Rev. Lett. **53**, 600
Reimann CT, Brown WL and Johnson RE, 1988: Phys. Rev. B **37**, 1455
Reimann CT, Brown WL, Nowakowski MJ, Cui ST and Johnson RE, 1990: in *Desorption Induced by Electronic Transitions DIET IV*, eds. Betz G and Varga P, Springer-Verlag, Berlin, 226
Reimann CT, Brown WL, Grosjean DE, Nowakowski MJ, Buller WT, Cui ST and Johnson RE, 1991: Nucl. Instrum. Methods B **58**, 404
Reimann CT, Brown WL, Grosjean DE and Nowakowski MJ, 1992: Phys. Rev. B **45**, 43
Ritchie RH and Claussen C, 1982: Nucl. Instrum. Methods **198**, 133
Ritchie RH, Gras-Marti A and Ashley JC, 1989: in *Proc. 12th Werner Brandt Workshop*, ed. Ritchie RH, Oak Ridge Nat. Lab, Oak Ridge, Tenn, 595

Robinson MT, 1989: in *Sputtering by Particle Bombardment I*, ed. Behrisch R, Springer-Verlag, Berlin, 73
Rocard F and Bibring JP, 1982: Phys. Rev. Lett. **38**, 1763
Rocard F, Benit J, Bibring JP, Ledu D and Meunier R, 1986: Rad. Effects **99**, 97
Rocker G, Feulner P, Scheuerer R, Zhu L and Menzel D, 1990: Phys. Scr. **41**, 1014
Roessler K, 1992: Nucl. Instrum. Methods B **65**, 55
Roick E, Gaethke R, Gürtler P, Woodruff TO and Zimmerer G, 1984: J. Phys. **C17**, 945
Rook FL, Johnson RE and Brown WL, 1985: Surf. Sci. **164**, 625
Roth J, 1983: In *Sputtering by Particle Bombardment II*, ed. Behrisch R, Springer, NY, 1991
Rudd ME, Kim YK, Madison DH and Gallagher JW, 1985: Rev. Mod. Phys. **57**, 965
Rudd ME, Kim YK, Madison DH and Gay TS, 1992: Rev. Mod. Phys. **64**, 441 73
Runne M, Becker J, Laasch W, Varding D, Zimmerer G, Liu M and Johnson RE, 1993: Nucl. Instrum. Methods B **82**, 301
Sack N, Johnson RE, Boring JW and Baragiola RA, 1993: Icarus **100**, 534
Sanche L, 1984: Phys. Rev. Lett. **53**, 1638
Sanche L, 1990: J.Phys. B **23**,1597
Schou J, 1980: Phys. Rev. B **22**, 2141
Schou J, 1987: Nucl. Instrum. Methods B **27**, 188
Schou J, 1988: Scan. Micr. **2**, 607
Schou J, 1989: in *Structure-Property Relationships in Surface-Modified Ceramics*, eds. McHargue C et al. (Kluwer Academics) 61
Schou J, 1991: Dr. Scient. thesis, Risø-report R-591 (EN), Risø National Laboratory
Schou J.: 1993: Unpublished communication
Schou J, Sørensen H and Børgesen P, 1984: Nucl. Instrum. Methods B **5**, 44
Schou J, Ellegaard O, Børgesen P and Sørensen H, 1985: in *Desorption Induced by Electronic Transitions, DIET II*, eds. Brenig W and Menzel D, Springer, Verlag, Berlin, 170
Schou J, Børgesen P, Ellegaard O, Sørensen H and Claussen C, 1986: Phys. Rev. B **34**, 93
Schou J, Pedrys R, Ellegaard O and Sørensen H, 1987: Nucl. Instrum. Methods B **18**, 609
Schou J, Ellegaard O, Sørensen H and Pedrys R, 1988: Nucl. Instrum. Methods B **337**, 808
Schou J, Ellegaard O, Pedrys R and Sørensen H, 1992: Nucl. Instrum. Methods B **65**, 173
Schriver KE, Hahn MY and Whetten RI, 1987: Phys. Rev. Lett. **59**, 1986
Schroeder JB, Dieselman HD and Douglass JW, 1971: Appl. Opt. **10**, 295
Schwabentahn P, Scheurer R, Hudel E and Feulner P, 1992: Sol. State. Comm **80**, 773
Schwentner N, Koch EE and Jortner J, 1985: *Electronic Excitations in Condensed Rare Gases*, (Springer)
Seiberling LE, Griffith JE and Tombrello TA, 1980: Rad. Eff. **52**, 201
Seiberling LE, Meins CK, Cooper BM, Griffith JE, Mendenhall MH and Tombrello TA, 1982: Nucl. Instrum. Methods **198**, 17
Shiea JT and Summer J, 1991: in *Methods and Mechanisms for Producing Ions from Large Molecular*, eds. Standing K and Ens W, Plenum, N.Y. 147
Sigmund P, 1969: Phys. Rev. **184**, 383
Sigmund P, 1972: Rev. Roum. Phys. **17**, 969 and 1079
Sigmund P, 1975a: in *Radiation Damage Processes in Materials*, ed. Dupuy CHS, (Noordhoff, Leyden) 3
Sigmund P, 1975b: Appl. Phys. Letts. **27**, 52
Sigmund P, 1977: in *Inelastic Ion-Surface Collisions*, eds. Tolk NH et al. Academic, NY, 121
Sigmund P, 1981: in *Sputtering by Particle Bombardment I*, ed. Behrisch R, (Springer Verlag), 9
Sigmund P, 1987: Nucl. Instrum. Methods B **27**, 1
Sigmund P and Claussen C, 1981: J. Appl. Phys. **52**, 990
Sigmund P and Szymonski M, 1984: Appl. Phys. A **33**, 141

Sigmund P, Robinson MT, Baskes M, Hautala M, Cui FZ, Eckstein W, Yamamura Y, Hosaka S, Ishitani T, Shulga VI, Harrison Jr DE, Charakov IR, Karpuzov DS, Kawatoh E, Shimizu R, Valkealahti S, Nieminen RM, Betz G, Husinsky W, Shapiro MH, Vicanek M and Urbassek HM, 1989: Nucl. Instrum. Methods B **36**, 110

Sigmund P and Oliva A, 1993: Nucl. Instrum. Methods B **82**, 269

Sigmund P and Lam NQ, 1993: Mat. Fys. Medd. Dan. Vid. Selsk. **43**, 255

Sonntag B, 1977: in *Rare Gas Solids II*, ed. Klein ML and Venables JA, Academic Press, Inc. N.Y., 1021

Sowada V, Warman JM and Deltas MP, 1982: Phys. Rev. B **25**, 3434

Spinella F, Baratta GA and Strazzulla G, 1991: Rev. Sci. Instr. **62**, 1743

Spinks JWT and Woods RJ, 1990: *Introduction to Radiation Chemistry*, John Wiley, NY

Srdoč D, Inokuti M and Krajear-Bronić I, 1993: in *Atomic and Molecular Data for Radiotherapy (IAEA CRP)* in press

Stenum B, Ellegaard O, Schou J and Sørensen H, 1990: Nucl. Instrum. Methods B **48**, 530

Stenum B, Schou J, Ellegaard O, Sørensen H and Pedrys R, 1991: Phys. Rev. Lett. **67**, 2842

Stenum B, Schou J, Sørensen H and Gürtler P, 1993: J. Chem. Phys. **98**, 126

Stevanovic DV, Thompson DA and Davies JA 1984: Nucl. Instrum. Methods **B1**, 315

Strazzulla G, Torrisi L and Foti G, 1988: Europhys. Lett. **7**, 413

Strazzulla G, Baratta GA, Leto G and Foti G, 1992: Europhys. Lett. **18**, 517

Sugden S, Sofield CJ and Murrell MP, 1992: Nucl. Instrum. Methods B **67**, 569

Szymonski M, 1980: in *Symposium on Sputtering*, eds. Varga P et al. Techn. Univ. Wien, Austria, 761

Szymonski M, Ruthowski J, Poradzisz A, Postawa Z and Jørgensen B, 1985: in *Desorption Induced by Electronic Transitons, DIET II*, eds, Brenig W and Menzel D, Springer-Verlag, Berlin, 160

Szymonski M, Czuba P, Dohnalik T, Jozefowski L, Karawajczyk A, Kolodziej J, Lesniak R and Postawa Z, 1990: Nucl. Instrum. Methods B **48**, 534

Szymonski M, 1993: Mat. Fys. Medd. Dan. Vid. Selsk. **43**, 495

Tarrio C and Schnatterly SE, 1992: J. Phys. Chem. Solids **53**, 1013

Taylor SR, 1982: it Planetary Science: A Lunar Perspective, Lunar and Planet. Inst., Houston

Thomas JH, III and Hoffmann S, 1985: J. Vac. Sci. Techn. **A 3**, 1921

Torrisi L, Coffa S, Foti G and Strazzulla G, 1986: Rad. Effects **100**, 61

Torrisi L, Coffa C, Foti G, Johnson RE, Chrisey DB and Boring JW, 1988: Phys. Rev. B **38**, 1516

Townsend PC, 1983: in *Sputtering by Particle Bombardment, II*, ed. Behrisch R, Springer-Verlag, Berlin, 147

Trotman SM, Quickenden TI and Sangster DF, 1986: J. Chem. Phys. **85**, 2555

Turner JE, Magee JL, Wright HA, Chatterjee A, Hamm RN and Ritchie RH, 1983: Rad. Res. **96**, 437

Turner JE, Hamm RN, Wright HA, Ritchie RH, Magee JL, Chatterjee A and Bolch WE, 1988: Rad. Phys. Chem. **32**, 503

Urbassek HM and Sigmund P, 1984: Appl. Phys. A **35**, 19

Urbassek HM and Michl J, 1987: Nucl. Instrum. Methods B **22**, 480

Urbassek HM and Waldeer T, 1991: Phys. Rev. Lett. **67**,105

Urbassek HM and Hofer WO, 1993: Mat. Fys. Medd. Dan. Vid. Selsk. **43**, 97

Urbassek HM, Kafemann H and Johnson RE, 1993: Phys. Rev. B in press

Valkealahti S, Schou J and Nieminen RM, 1989: J. Appl. Phys. **65**, 2258

Varding D, Becker J, Frankenstein L, Peters B, Runne M, Schröder A and Zimmerer G, 1993: Fiz. Nizh. Temp. **19**, 600

Varga P, Diebold U and Wutte D, 1991: Nucl. Instrum. Methods B **58**, 417

Varma MN and Baum JW, 1980: Radiat. Res. **81**,335
Vernon CF, Matich AJ, Quickenden TI and Sangster DF, 1991: J. Phys. Chem. **95**, 7313
Vicanek M, Jimenz Rodriguez JJ and Sigmund P, 1989: Nucl. Instrum. Methods B **36**, 124
Vineyard GH, 1976: Rad. Effects. **29**, 245
de Vries AE, Haring RA, Haring A, Klein FS, Kummel AC and Saris FW, 1984: J. Phys. Chem. **88**, 4510
Watson CC and Tombrello TA, 1985: Rad. Effects. **89**, 263
Watson WD, 1976: Rev. Mod. Phys. **48**, 513
Weibel DE, Herayama T and Arakawa I, 1993: Surf. Sci. **283**, 204
Weller RA and Weller MR, 1982: Nucl. Instrum. Methods **194**, 573
Wien K, 1989: Rad. Eff. Def. Solids **109**, 137
Wien K, 1992: Nucl. Instrum. Methods B **65**, 149
Wien K, Becker O, Guthier W, Della Negra S, LeBeyec Y, Monart B, Standing KG, Maynard G and Deutsch C, 1987: Int. J. Mass Spectrom Ion Proc. **78**, 273
Williams P and Sundqvist BUR, 1987: Phys. Rev. Lett. **58**, 1031
Yamamura Y, 1982: Nucl. Instrum. Methods **194**, 515
Zel'dovich YaB and Raizer YuP, 1967: *Physics of Shock Waves and High Temperature Hydrodynamic Phenomena* Vol. I & II, eds. Hayes WP and Probstein RP, Academic Press, N.Y.
Ziegler JF, 1980: *Handbook of Stopping Cross Section for Energetic Ions in All Elements*, Pergamon, New York
Ziegler JF, Biersack JP and Littmark U, 1985: *The Stopping and Range of Ions in Solids*, Pergamon, New York
Zimmerer G, 1979: J. Lum. **18-19**, 875
Zimmerer G, 1987: in *Excited State Spectroscopy in Solids*, ed. M. Manfredi (XCVI Corso, Soc. Italiana di Fisica, Bologna, Italy) eds. Grassano UM and Terzi N, North-Holland, Amsterdam, The Netherlands, 37
Zumofen G, Sedlacek J, Taubenberger R, Pan SL, Oehler O and Dressler K, 1984: J. Chem. Phys. **81**, 2305